Technische Universität München

Max-Planck-Institut für Biochemie

Structural and Functional Analysis of the Natural JNK1 Inhibitor Quercetagetin

Structure of the Stapled p53 Peptide Bound to HDM2

Sohee Baek

Vollständiger Abdruck der von der Fakultät für Chemie der Technischen Universität München zur Erlangung des akademischen Grades eines

Doktors der Naturwissenschaften

genehmigten Dissertation.

Vorsitzender:	Univ.-Prof. Dr. M. Groll
Prüfer der Dissertation:	1. apl. Prof. Dr. Dr. h.c. R. Huber (i. R.)
	2. Univ.-Prof. Dr. S. Weinkauf

Die Dissertation wurde am 03. 01. 2014 bei der Technischen Universität München eingereicht und durch die Fakultät für Chemie am 10. 02. 2014 angenommen.

Acknowledgement

First of all, I would like to express my heartfelt gratitude to Prof. Huber for giving me a great opportunity to study under his supervision and being my mentor as well.

I am also deeply grateful to my supervisors Dr. Ki Won Lee at Seoul National University and Dr. Martin Augustin at Proteros for all their help including scientific guidance, inspiration, valuable advices and financial support during my PhD study.

I would like to extend my thanks to Dr. Tad A. Holak and Dr. Grzegorz Popowicz for their support, discussion and interest in my work.

My thanks to Monika Schneider for helping me to study at MPIB in many ways.

In particular, thanks so much to all my (former) lab mates: Elena Lesca, Elisabeth V. Schneider, Marcelino Castro, Kaja Kowalska, Linda Wolf, Arkadiusz Sikora for giving warm air in the lab.

I would like to thank to all my Korean friends in both Munich and Korea for providing a non-scientific buffer that boosted up my energy during my Munich life.

Special thanks to my soul mate, Jin Kim for sharing everything that we felt in life.

Especially, I am deeply indebted to my mother and Sungchul for all their love, care, support, encouragement and considerable understanding.

I am thankful to the God Almighty.

Most of the work described has been published:

Baek, S., Kang, N. J., Popowicz, G. M., Arciniega, M., Jung, S. K., Byun, S., Song, N. R., Heo, Y. S., Kim, B.Y., Lee, H. J., Holak, T. A., Augustin, M., Bode, A. M., Huber, R., Dong, Z., Lee, K. W. (2013). **Structural and Functional Analysis of the Natural JNK1 Inhibitor Quercetagetin**, *J. Mol. Biol*. **425**, 411-423.

Baek, S., Kutchukian, P. S., Verdine, G. L., Huber, R., Holak, T. A., Lee, K. W., Popowicz, G. M. (2012). **Structure of the Stapled p53 Peptide Bound to Mdm2**, *J. Am. Chem. Soc*. **134**, 103-106.

List of Abbrevations

Å	angstrom, 1 x 10^{-10}m
AP-1	activator protein 1
ATF1	cyclic AMP-dependent transcription factor
ATP	adenosintriphosphate
CCP4	Collaborative Computational Project, number 4
CDK	cyclin-dependent kinase
CML	chronic myelogenous leukaemia
COX-2	cyclooxygenase-2
CTD	C-terminal domain
DNA	deoxyribonucleic acid
DTT	1,4-dithiothreitol
E. coli	Escherichia coli
EGFR	epidermal growth factor receptor;
ERK	extracellular signal-regulated kinase
GIST	gastrointestinal stromal tumours
HEPES	4-(2-hydroxyethyl)-1-piperazineethanesulfonic acid
HTS	high-throughput screening
IMAP	immobilized metal ion affinity-based fluorescence polarization
IKK	IκB kinase
IPTG	isopropyl- β -D-thiogalactopyranoside
JNK	c-Jun N-terminal kinase
MAPK	mitogen activated protein kinases
MAP2K	mitogen activated protein kinases kinase
MAP3K	mitogen activated protein kinases kinase kinase
MDM2	murine double minute 2
MDMX	murine double minute X
NF-κB	nuclear factor-kappaB
NMR	nuclear magnetic resonance
PBS	phosphate buffered saline
PCR	polymerase chain reaction
PDB	Protein Data Bank
PEG	polyethylene glycol
PI3-K	phosphatidylinositol 3-kinase
PKA	protein kinase A
PKC	protein kinase C
PMSF	phenylmethylsulfonyl fluoride

PTEN	phosphatase and tensin homolog
RB	retinoblastoma tumor suppressor protein
RSK	ribosomal s6 kinase
RMSD	root mean square deviation
SDS	sodium dodecyl sulfate
SDS-PAGE	sodium dodecyl sulfate polyacrylamide gel electrophoresis
SLS	Swiss Light Source
STAT3	signal transducer and activator of transcription 3
TRIS	tris(hydroxymethyl)aminomethane
TPA	12-O-Tetradecanoylphorbol-13-acetate
UV	ultraviolet
VEGF	vascular endothelial growth factor
v/v	volume/volume
w/v	weight/volume

Table of Contents

Part II. Structure of the stapled p53 peptide bound to HDM2

Part I

Structural and Functional Analysis of the Natural JNK1 Inhibitor Quercetagetin

Summary

c-Jun NH2-terminal kinases (JNKs) and phosphatidylinositol 3-kinase (PI3-K) play critical roles in chronic diseases such as cancer, type II diabetes, and obesity. I describe here the binding of quercetagetin (3,3′,4′,5,6,7-hydroxyflavone), related flavonoids and SP600125 to JNK1 and PI3-K by ATP-competitive and immobilized metal ion affinity-based fluorescence polarization assays and measure the effect of quercetagetin on JNK1 and PI3-K activities. Quercetagetin attenuates the phosphorylation of c-Jun and AKT, suppresses AP-1 and NF-κB promoter activities, and also reduces cell transformation. It attenuates tumor incidence and reduces tumor volumes in a two-stage skin carcinogenesis mouse model. The crystal structure of JNK1 in complex with quercetagetin is presented in this thesis. In comparison with a previously determined JNK1-structure, the interaction between Lys55, Asp169, and Glu73 of JNK1 and the catechol moiety of quercetagetin reorients the N-terminal lobe of JNK1, thereby improving compatibility of the ligand with its binding site. The results of a docking study suggest a binding mode of PI3-K with the hydroxyl groups of the catechol moiety forming hydrogen bonds with the side chains of Asp964 and Asp841 in the p110γ catalytic subunit. These interactions could contribute to the high inhibitory activity of quercetagetin against PI3-K.

Teil I

Strukturelle und funktionelle Sudien des natürlichen JNK1 Inhibitors Quercetagetin

Zusammenfassung

Die Familien der c-Jun NH2-terminalen Kinasen (JNKs) und Phosphatidylinositol 3-kinasen (PI3-K) spielen eine wichtige Rolle bei unterschiedlichen Erkrankungen wie beispielsweises Krebs, Diabetes Mellitus Typ 2 und Adipositas. In der vorliegenden Arbeit beschreibe ich die Bindung von Quercetagetin (3,3′,4′,5,6,7-hydroxyflavone), verwandten Flavonoiden, und SP600125 an JNK1 und PI3-K mittels ATP-kompetitiver und Fluoreszenz Polarisations-basierten Techniken. Weiterhin zeige ich den Effekt der Bindung von Quercetagetin auf die Kinase-Aktivität von JNK1 und PI3-K. Quercetagetin erniedrigt die Phosphorylierung von c-Jun und AKT, unterdrückt die Promotoraktivität von AP-1 und NF-κB, und vermindert ebenso eine maligne Transformation. In einem zweistufigen Mausmodell zur Kanzerogenese der Haut wird durch Quercetagetin die Tumorinzidenz abgeschwächt sowie das Tumorvolumen vermindert. In dieser Doktorarbeit wurde die Kristallstrukur von JNK1 in Komplex mit Quercetagetin gelöst. Die Interaktion zwischen den JNK1 -Aminosäuren Lys55, Asp169 und Glu73 mit Quercetagetin führt im Vergleich zu vorher ermittelten JNK1-Strukturen zu einer Umlagerung der N-terminalen JNK1 Kinasedomäne, wodurch die Interaktionsfläche zwischen JNK1 und Querctagetin optimiert wird. Einer theoretischen Docking-Studie zufolge erfolgt die Bindung von Quercetagetin an PI3-K hingegen über Wasserstoffbrücken zwischen den Hydroxyl-Gruppen mit den Seitenketten von Asp964 und Asp841 in der katalytischen Untereinheit p110γ. Diese Interaktionen könnten das höhere inhibitorische Potential Quercetagetins auf die Kinaseaktivität von PI3-K erklären.

1. Introduction

1.1 Protein kinase signal transduction pathways

Protein kinases are enzymes that modify other proteins by chemically transferring phosphate groups from ATP and covalently adding them to threonine, serine, tyrosine and histidine, which is called phosphorylation. Phosphorylation is one of the most ubiquitous post-translational modifications and is known to alter target protein activity and/or function. The human genome appears to encode 538 distinct protein kinase genes (constituting approximately 2% of all eukaryotic genes), which are classified into about 20 known families (Manning et al., 2002; Rubin et al., 2000). Protein kinases are key regulators of most aspects of cell life since they play an important role in most of cellular signaling pathways (Zhang et al., 2009).

1.2 Signaling cascades as potential therapeutic targets

A consensus is arising that kinase regulation is an important treatment for a diversity of diseases (Cohen, 2002). The phosphorylation of a protein kinase by its upstream kinase regulates downstream functions and activities. Disrupting a pathway via complete inhibition of a kinase involved in this pathway is a fascinating proposition. So a major drug development issue is to identify appropriate targets within signaling cascades for therapeutic intervention. There are diverse signaling pathways, and especially the MAP-kinase pathway has been identified as an important pathway involved in the development of cancer and it is therefore targeted by a great number of drug candidates (Figure 1).

1.2.1 MAP Kinase signaling pathway

MAP kinases (mitogen activated protein kinases, MAPKs) function as serine/threonine protein kinases. MAP kinase cascades are composed of three kinases: MAP kinase kinase kinase (MAPKKK, MAP3K), MAP kinase kinase (MAPKK, MAP2K, also called as MEK), MAP kinase (Widmann et al., 1999; Kyriakis and Avruch, 2001). Tremendous efforts from many researchers over the past decade have contributed to the elucidation of the MAPKs signaling mechanism and their involvement in a variety of cellular functions such as cell differentiation, cell proliferation, cell migration and cell death (Bode

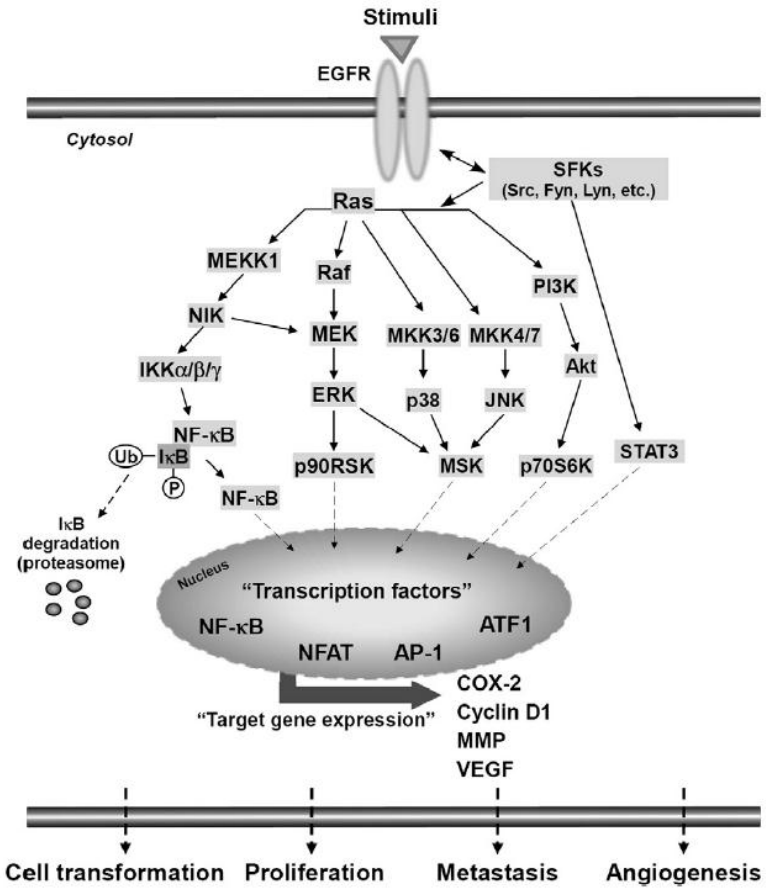

Figure 1 General scheme of signaling cascades in carcinogenesis. If cellular receptors recognize the oncogenic stimuli, SFKs are activated. This event leads to the phosphorylation of downstream kinases, such as Ras or STAT3. Activated Ras phosphorylates the MAPK upstream proteins, including Raf and MKKs, to trigger downstream signaling effectors. The signaling cascades result in MAPKs phosphorylation and activation. MAPK pathways lead to expression of oncogenic proteins. Besides MAPKs, PI3-K is also activated by Ras, Src and Fyn. Activated PI3-K leads to activation of Akt, and consequently turns on downstream signals to induce oncogenic gene expression. Along with MAPK and PI3-K pathways, IKK activates NF-κB by the phosphorylation and degradation of IκB protein. Activated NF-κB goes into the nucleus, and activates the expression of specific target genes in carcinogenesis. These signaling cascades result in cell transformation, proliferation, metastasis and angiogenesis. AP-1, activator protein 1; ATF1, Cyclic AMP-dependent transcription factor; EGFR, epidermal growth factor receptor; ERK, extracellular signal-regulated kinase; IKK, IκB kinase; IκB, inhibitor kappaB; JNK, c-Jun N-terminal kinases; MEK, mitogen-activated protein-ERK kinase; MEKK1, MEK kinase 1; MKK, mitogen-activated protein kinase kinase; MMP, matrix metallopeptidase; MSK, mitogen- and stress-activated protein kinase; NFAT, Nuclear factor of activated T-cells; NF-κB, nuclear factor-kappaB; NIK, NF-κB-inducing kinase; PI3-K, phosphatidylinositol 3-kinase; RSK, ribosomal s6 kinase; S6K, s6 kinase; SFK, Src family

kinase; STAT3, signal transducer and activator of transcription 3; VEGF, vascular endothelial growth factor. Figure adapted from Kang et al., 2011.

and Dong, 2003). This three step cascade is found in all eukaryotic organisms and is highly conserved in signaling pathways (Waskiewicz and Cooper; 1995). MAPKs are modulated by phosphorylation cascades, resulting in sequential stimulation. This signaling cascade is initiated by a set of extracellular signals including growth factor, UV, TPA or small GTP-binding protein or other kinases (e.g. PKC) serving for the cascade and stimulate MAPKKK. A MAPKKK activated in series lead to phosphorylation of MAPKK at two specific serine residues; dual phosphorylated MAPKK which is also known as dual specificity enzyme, in turn activates specific hydroxyl side chains of threonine and tyrosine residues in MAPK as substrate (Marshall, 1994; Cobb and Goldsmith, 1996). MAPK exert major effects on both transcription factors and other protein kinases, highlighting the prominence of these MAPKs for different drug therapies. Up to date, three distinct groups of MAPKs have been identified: Extracellular signal-regulated kinases (ERKs), c-Jun N-terminal kinases (JNKs) and p38 kinases (Bode and Dong, 2003).

1.2.2 JNK signaling pathway

C-Jun NH2-terminal kinases (JNKs) are a group of serine/threonine protein kinases known as members of the mitogen-activated protein kinase family which also includes the extracellular signal regulated kinases (ERKs) and p38 kinases (Hibi et al., 1993; Davis, 2000). JNKs are encoded by three genes: JNK1, JNK2 and JNK3 that are generated by alternative splicing to create up to 10 isoforms ranging from 46 kDa to 55 kDa (Gupta et al., 1996; Davis, 2000; Barr et al., 2001). JNK1 and JNK2 are ubiquitously found in all cells and tissue type, whereas JNK2 is primarily expressed in brain, heart, and testis (Martin et al., 1996; Davis, 2000; Chang and Karin, 2001; Shaulian and Karin, 2002; Lin, 2003). JNKs were originally discovered by their ability to specifically bind and phosphorylate Ser63 and Ser73 within the N-terminal transactivation domain of the transcription factor c-Jun, which regulates the activity of the transcription factor (Hibi et al., 1993; Kallunki et al., 1996). It has subsequently been found that JNKs also regulate the activity of transcription factors, such as ATF2, Elk-1, p53, SMAD4, NF-Atcl, HSF-1, STAT3, c-Myc (Davis, 2000; Chang and Karin, 2001; Lin,

2003; Karin, 1995; IP and Davis, 1998) and non-transcription factors including members of the Bcl-2 family other than c-Jun (Yamamoto et al., 1999; Maundrell et al., 1997; Yu et al., 2004). JNKs are predominantly responsive to a variety of inflammatory signals or stress stimuli, such as UV radiation, cytokines, growth factor deprivation, DNA-damaging agent and heat shock (Wagner and Nebreda, 2009; Tournier, 2000; Weston and Davis, 2002). In response to stresses such as oxidative stress and UVB radiation, JNKs bind to and regulate p53 (Wu, 2004). Various transmitted signals activate MAP3Ks, which in turn phosphorylate and activate MAP2Ks (MKK4 and MKK7) that subsequently phosphorylate JNKs by dual phosphorylation on TPY (Thr-Pro-Tyr) motif (i.e. in the activation loop at residues Thr183-Pro-Tyr185) (Davis, 2000; Weston and Davis, 2002). Then JNKs trigger the activation of a large number of downstream targets that regulate cellular functions implicated in cancer and other diseases (Bogoyevitch et al., 2006). JNKs can be deactivated by a specialized group of MAPK phosphatases, such as MKP1 and MKP5 (Karin and Gallagher, 2005).

1.3 Structural organization of MAPK family

On the basis of sequence and structure, the members of MAPK family all contain the same catalytic scaffold as the several hundred protein kinases do and show the typical kinase fold. The conserved core consists of two lobes: the smaller N-terminal lobe, or N-lobe and the larger C-terminal lobe, or C-lobe. The N-lobe is mainly composed of β-strands, connecting loops and one functionally important α helix, called helix αC. The lager C-lobe is primarily comprised of α-helices. These two lobes, connected by a small linker known as hinge, serve as a cleft for ATP (Figure 3).

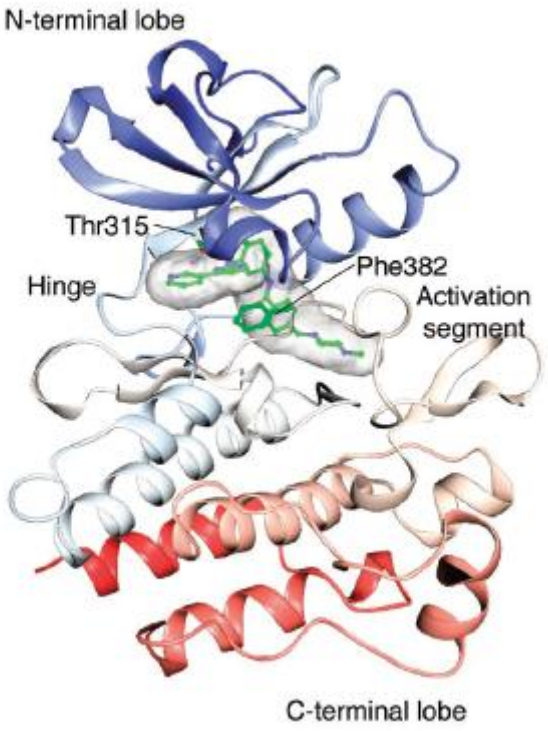

Figure 3 The structure of the catalytic domain of cAbl in complex with Gleevec (Nagar et al., 2002). The N-terminal lobe consists of a β sheet and one conserved α helix (helix αC). The C-terminal lobe is largely helical and contains a segment, the activation segment, which includes residues that in many kinases are phosphorylated for activity (Johnson et al., 1996). The hinge region connects the two lobes. The protein structure is color ramped so that residues close to the N-terminus are blue, and those close to the C-terminus are red. Gleevec is shown bound to the ATP-binding site, from which it extends under the αC helix. Thr315, the "gatekeeper" residue, and Phe382, the conserved phenylalanine that marks the beginning of the activation segment, are labeled. Figure adapted from Noble et al., 2004.

ATP bound in this cleft poses beneath a highly conserved phosphate binding loop located between the β2 and β3 strands. This loop contains a glycine-rich sequence (GXGXΦG) where Φ is often tyrosine or phenylalanine as a lid on top of the ATP for the phosphoryl transfer. There are two general conformations in protein kinases: an active state and an inactive state that toggle between open and closed conformation as the kinase undergoes the catalytic cycle. The αC helix, which is the only conserved helix in the N-lobe, plays an important role in catalysis as a mediator of conformational changes. The catalytically active conformation typically associates with changes in the orientation of the αC helix and the activation segment. One of the main features is a lysine-glutamate ion pair. The

glutamate (E91 in PKA) is absolutely conserved in the middle of αC helix and forms an ion pair (a salt bridge) with a conserved lysine (K72 in PKA) that coordinates the α- and β-phosphates of ATP to facilitate catalysis in the active conformation of the kinase (Huse and Kuriyan, 2002; Zheng et al., 1993). The αC helix also makes crucial contacts with the conserved Asp-Phe-Gly (DFG) motif at the N-terminal region of the activation loop or T-loop which starts with conserved amino acid sequence "DFG" and ends with "APE". A centrally located T-loop spans both N- and C-terminal lobes and key residues within this loop are phosphorylated when the kinase is in the active state that enables substrate binding and catalysis (Hubbard, 1997). Similarly, the phosphorylation of a residue in the MAPK T-loop leads to a rearrangement of the loop that changes the flexibility around the ATP binding site and increases the activity of the kinase (Adams, 2003; Lew, 2003; Lee, 2005). In the MAPKs, dual phosphorylation on Thr and Tyr residues within a conserved Thr-X-Tyr (TXY) activation motif located in the T-loop is required for achieving full activity (Robbins and Cobb, 1992). Phosphorylation of Thr183 and Tyr185 results in more than 1000-fold activation of ERK1 and ERK2 (Ahn et al., 1991; Payne et al., 1991; Robbins and Cobb, 1992; Robbins et al., 1993) and the activity is lost by the action of serine/threonine phosphatases, tyrosine phosphatases (Anderson et al., 1990; Boulton and Cobb, 1991), or dual specificity phosphatases (Sun et al., 1993; Zheng and Guan, 1993). All MAPKs contain this signature sequence "TXY", the intervening residue X is glutamate in ERK, glycine in p38, and proline in JNK (Robbins et al., 1993; Ahn et al., 1991; Payne et al., 1991). The crystal structure of ERK2 offered the first example of why the unique dual-phosphorylation is required for the activation (Zhang et al., 1994). ERK2 is phosphorylated on residues Thr183 and Tyr185 within the loop. Tyr185 is buried in a hydrophobic pocket while Thr183 is exposed at the surface of the loop, thereby enabling access for MEK1. pThr183 makes contacts that extend to the αC helix, leading to closure of the N-lobe and C-lobe and activation of the kinase (Canagarajah et al., 1997).

1.4 Kinase inhibitors as therapeutic agents

The deregulation of protein kinase signaling pathways causes a wide range of diseases including cancer, inflammation, diabetes, congestive heart failure and neurological damage. Considering their widespread roles in such a great variety of diseases, protein kinases have emerged as attractive targets

for drug discovery (especially in the cancer field) and have demonstrated clinical impact by the vast amount of research that has been performed over many years (Sawyers, 2003). More than 10,000 patent applications for kinase inhibitors have been submitted in the United States alone since 2001. It is estimated that approximately 30% of the drug discovery efforts in the pharmaceutical industry are headed for exploring and validating kinase inhibitors and more than 50 compounds are in clinical trials, thus representing an important and emerging class of therapeutic agents (Cohen, 1999b). As of now, more than 10 FDA-approved kinase inhibitors have been used as drugs to treat human diseases since the late 1990s (Kontzias et al., 2012) (Table1). The tremendous potential of kinase inhibitors came with the success of imatinib (Gleevec; Novartis), first approved for use by the U.S. Food and Drug Administration (FDA) in 2001, which is used in treating CML (chronic myelogenous leukaemia) as an inhibitor of the Bcr-Abl kinase (Druker et al., 2001). Further studies have shown that Imatinib has also been used successfully for patients with GIST (gastrointestinal stromal tumours) (Demetri et al., 2002). The clinical success of Imatinib has further led to extensive efforts to understand the full range of kinases present in human for the development of therapeutic kinase inhibitors, particularly as anticancer drugs (Futreal et al., 2004).

Agent	Targets for therapeutic activity	US FDA-approved indication
Direct kinase inhibitors by competing for the ATP-binding pocket		
Imatinib	BCR–ABL, PDGFR and KIT	CML and GIST
Dasatinib	BCR–ABL	CML
Nilotinib	BCR–ABL	CML
Gefitinib	EGFR	Non-small cell lung cancer
Erlotinib	EGFR	Non-small cell lung cancer and pancreatic cancer
Lapatinib	EGFR and ERBB2	Breast cancer
Sunitinib	VEGFR2, PDGFR and KIT	Renal cell carcinoma, GIST, pancreatic cancer
Sorafenib	VEGFR2 and PDGFR	Renal cell carcinoma and hepatocellular carcinoma
Pazopanib	VEGFR2, PDGFR and KIT	Renal cell carcinoma
Crizotinib	ALK/c-MET	Non-small cell lung cancer
Vemurafenib	BRAF	Melanoma
Vandetanib	VEGFR-2, EGFR, RET and ErbB-1	Medullary thyroid cancer
Ruxolitinib	JAK1/JAK2	Myelofibrosis
Indirect kinase inhibitors by binding to FK506 binding protein 12 (FKBP12)		
Sirolimus	mTOR	Solid organ and bone marrow transplantation
Everolimus	mTOR	Renal cell carcinoma, Subependymal Giant Cell Astrocytoma (SEGA) associated with Tuberous Sclerosis (TS) and Progressive Neuroendocrine Tumors of Pancreatic Origin (PNET)
Temsirolimus	mTOR	Renal cell carcinoma
Monoclonal antibodies binding to receptor tyrosine kinases		
Trastuzumab	ERBB2	Breast cancer
Cetuximab	EGFR	Colorectal cancer, and squamous carcinoma of head and neck
Panitumumab	EGFR	Colorectal cancer
Bevacizumab	VEGF	Colorectal cancer, non-small cell lung cancer, breast cancers, glioblastoma and renal cell carcinoma

Table 1 US FDA-approved kinase inhibitors. Table adapted from Kontzias et al., 2012.

1.4.1 JNKs are prominent members of MAPKs

Because it is well known that JNKs are deeply involved in pathologic conditions including diabetes, neurodegenerative disorders, arthritis, atherosclerosis and cancer (Hirosumi et al., 2002; Borsello and Forloni, 2007; Kaneto et al., 2005; Thalhamer et al., 2008; Chen et al., 2001), it is not surprising that much efforts towards inhibitors against JNKs are underway. Although some debate exists regarding the roles of JNKs in cancer, they are up-regulated in several types of cancer, such as liver and prostate cancers. JNKs are best known for their role in the activation of the c-Jun/activator protein-1 (AP-1) transcription–factor complex (Adler et al., 1992). AP-1 activation is required for neoplastic transformation and for skin tumor formation in mice. Phophorylation of c-Jun by JNKs activity has been shown to play an important role in Ras-induced tumorigenesis and Ras, in cooperation with c-Jun, has been found essential in cellular transformation (Smeal et al, 1991, Kennedy and Davis, 2003). Tumor formation is inhibited in c-Jun-knock out mice. Recent study suggested that the interaction of the tumor suppressor p16INK4a with JNK1 can occur at the same site where c-Jun binds, and that it interferes with the phosphorylation and activation of c-Jun in response to UV exposure (Tournier et al., 2000). Additionally, JNKs are crucial mediators of obesity and insulin resistance in type II diabetes. JNK1 phosphorylates IRS-1 that downregulates insulin signaling and JNK1 knockout mice show less increase in diet-induced obesity (Aguirre et al., 2000, 2002; Hirosumi et al., 2002; Sabio and Davis, 2010). Besides the function in metabolic diseases, several studies have shown that JNKs are causally linked to aberrant neurodegeneration, particularly in Alzheimer's and Parkinson's diseases (Kyriakis and Avruch, 2001; Zhang and Zhang, 2005; Hunot et al., 2004; Borsello and Forloni, 2007). In concert with JNK2, JNK1 has also been implicated in autoimmune disorders such as asthma and rheumatic diseases (Han et al., 2002; Wong, 2005; Pelaia et al., 2005; Blease et al., 2003; Chialda et al., 2005). These links between abnormal JNK signaling and a lot of pathologic conditions contribute to develop small molecule JNK inhibitors, suggesting inhibition of JNKs might provide clinical benefits in these devastating diseases.

To date, several crystal structures of JNKs in complex with synthetic inhibitors have been solved (Figure 4). The synthetic small molecule JNK inhibitors shown in Figure 4 include examples from the

diaryl-imidazoles (as reported by scientists at Merck, Scapin et al., 2003), (benzoylaminomethyl) thiophene sulfonamides (Serono, Ruckle et al., 2004), dihydro-pyrrolo-imidazoles (Eisai, Graczyk et al., 2005), (benzothiazol-2-yl) acetonitrile (known as AS601245; Serono, Gaillard et al., 2005), anilinoindazoles and anilino-bipyridines (Astra Zeneca, Swahn et al., 2005; Swahn et al., 2006), as well as pyrazoloquinolinones, aminopyridines, pyridine carboxamides and anilino-pyrimidines (Abbott, Liu et al., 2006; Szczepankiewicz et al., 2006; Zhao et al., 2006; Liu et al., 2007). Especially, the diaryl-imidazoles (known as SP 600125) are most frequently used as reversible and ATP competitive inhibitors in JNK signaling with high potency in the range of 50-100 nM and selectivity (Bennett et al, 2001; Maroney et al., 2001). The interaction between SP600125 and JNK3 have been revealed by the co-crystal structure (Figure 5). The residues I70, V79, V196, L206 and Q155 on JNK3 produce a narrow ATP-binding pocket which allows the accommodation of planar SP600125 (Scapin et al., 2003).

However, to date, no inhibitors for JNKs have been approved to be effective for use in humans yet.

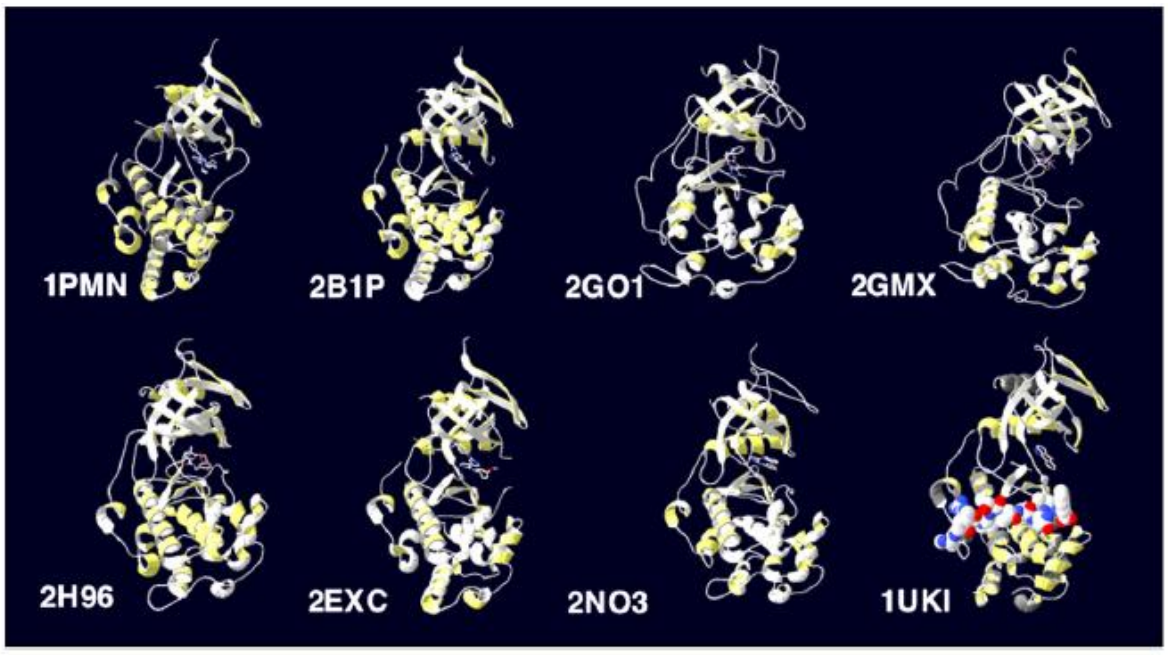

Figure 4 Structures of complexes of JNK with ATP-competitive inhibitors or the JNK-inhibitory peptide derived from JIP. Crystal structures have been recorded in the PDB for JNK in the presence of a number of different ATP-competitive inhibitors. These include 1PMN: diaryl-imidazoles (Merck, Scapin et al., 2003), 2B1P: anilinoindazoles (Astra Zeneca, Swahn et al., 2005), 2GO1: pyrazoloquinolinones, 2GMX:

aminopyridines and 2H96: pyridine carboxamides (Abbott, Szczepankiewicz et al., 2006; Zhao et al., 2006; Liu et al., 2006), 2EXC: anilino-bipyridines (Astra Zeneca, Swahn et al., 2006) and ZNO3: anilino-pyrimidines (Abbott, Liu et al., 2007). The complex of JNK1 with SP600125 and the JNK inhibitory peptide derived from JIP1 is also indicated in 1UKI. Figure adapted from Bogoyevitch and Arthur; 2008

1.4.2 Natural product inhibitors of MAPKs

Small-molecule kinase inhibitors are being intensively highlighted as new anticancer therapeutics. A vast amount of research has been carried out over the past few decades and tremendous advances have been made in drug discovery. In addition, natural products derived from plants have received attention more and more for the discovery of novel therapeutic agents to treat human diseases (Newman, 2008; Newman et al., 2003). Traditionally, natural products have been promising resources for a multitude of disease indications. In fact, more than half of current therapeutics are either from natural products or their derivatives. Many researchers have made efforts to identify novel natural products, in particular, flavonoids which play a highly significant role in various oncogenic signaling pathways (Table 2).

Group	Polyphenol	Source	Chemical structure	Direct binding protein	Reference
Flavonols	5-Deoxykaempferol	Woundwort (*Anthyllis vulneraria*)	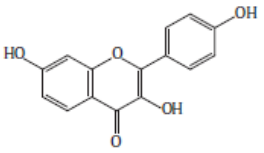	RSK2, PI3-K, Src	Lee et al., 2010e
	Kaempferol	Tea, broccoli, delphinium, witch-hazel, grapefruit, brussel sprouts, apples	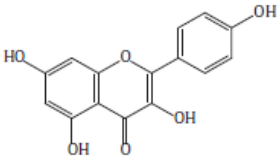	RSK2, PI3-K, Src	Cho et al., 2009; Lee et al., 2010d; Lee et al., 2010f
	Quercetin	Black/green tea, capers, lovage, apples, onion, red grapes, citrus fruit, tomato, broccoli, berries	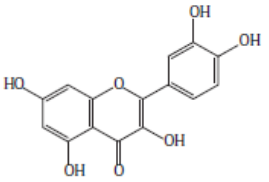	Raf-1, MEK1, PI3-K	Lee et al., 2008b; Hwang et al., 2009a
	Myricetin	Onions, berries, grapes	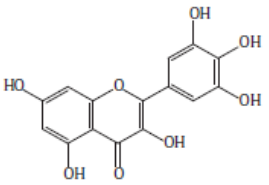	Raf-1, Fyn, MEK1, MKK4, JAK1, PI3-K	Lee et al., 2007; Jung et al., 2008; Kim et al., 2009a; Kumamoto et al., 2009; Jung et al., 2010a; Jung et al., 2010b
	Fisetin	*Acacia greggii*, *Acacia berlandieri*, parrot tree, cypress	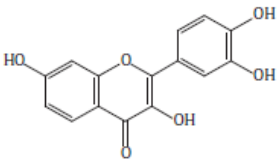	CDK6	Lu et al., 2005; Chen et al., 2010
Flavones	Luteolin	Onions, broccoli, celery	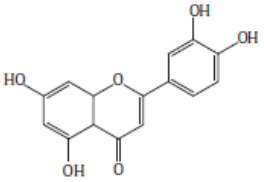	PKCε, Src	Byun et al., 2010

Table 2 Direct binding proteins with polyphenols in carcinogenesis. Table partly adapted from Kang et al., 2011.

Flavonoids have been known for some time for their general chemopreventive effects in human health, which might be explained partially by the identification of the molecular targets and their mechanism of action (Edwards et al., 1990; Holder et al., 2007). Recent studies demonstrate that flavonoids can directly target signaling cascades involved in carcinogenesis. 5-deoxykaempferol (5-DK) is a natural compound found in Anthyllis vulneraria. 5-DK had a chemopreventive effect on UVB-induced skin carcinogenesis such as UVB-induced expression of COX-2 and VEGF in mouse skin by targeting

multiple signaling molecules (Lee et al., 2010e). Moreover, Kaempferol, which has been isolated from tea, broccoli cabbage, propolis and grapefruit, is an antioxidant showing anti-inflammatory effects. Kaempferol regulated RSK2-mediated cancer signaling by directly binding to RSK2 (Cho et al., 2009). Quercetin is well known to be a potent anti-carcinogenic agent found in many plants and foods, such as red wine, onions, green tea, apples and berries. Its content in red wine is more than 30 times that of resveratrol (Waterhouse, 2002). It has been demonstrated that quercetin inhibited TPA-induced cell transformation and MEK1 and Raf-1 kinase (Lee et al., 2008b). The inhibitory effects of these flavonoids as direct inhibitors against protein kinases strongly support the hypothesis that the development of natural products, in particular flavonoids can be regarded as a rational approach for the treatment of carcinogenesis.

Although some debate exists regarding the lack of specificity of natural products, it can actually be an advantage because of its two distinct features, less toxicity and a multi-signaling inhibitory effect (Kang et al., 2011). Generally, most of the current synthetic kinase inhibitors target a specific kinase of interest with high selectivity. However quite a few synthetic inhibitors were shown to have high toxicity or adverse side effects in clinical trials. Conversely, natural products including flavonoids are relatively less toxic since they are usually consumed for long periods of time as ingredients in food and drinks. In addition, a single natural product can directly bind and regulate many signal regulatory molecules as shown in Table 2. So this can prove advantageous as it can yield opportunities to use a single natural product as a multiple signaling inhibitor for the treatment of several clinical indications that are correlated with various kinases. These aforementioned facts indicate that natural products can be considered as novel therapeutic agents with effectiveness for overcoming the difficulty of synthetic inhibitors.

1.5 Crosstalk between PI3K and JNK MAP kinase

The phosphatidylinositol 3-kinases (PI3Ks) signaling pathway has been identified as a key regulatory player in many essential cellular processes that link cell survival, proliferation and differentiation, death, vesicle trafficking and motility (Engelman et al., 2006; Martin, 1998; Vivanco and Sawyers,

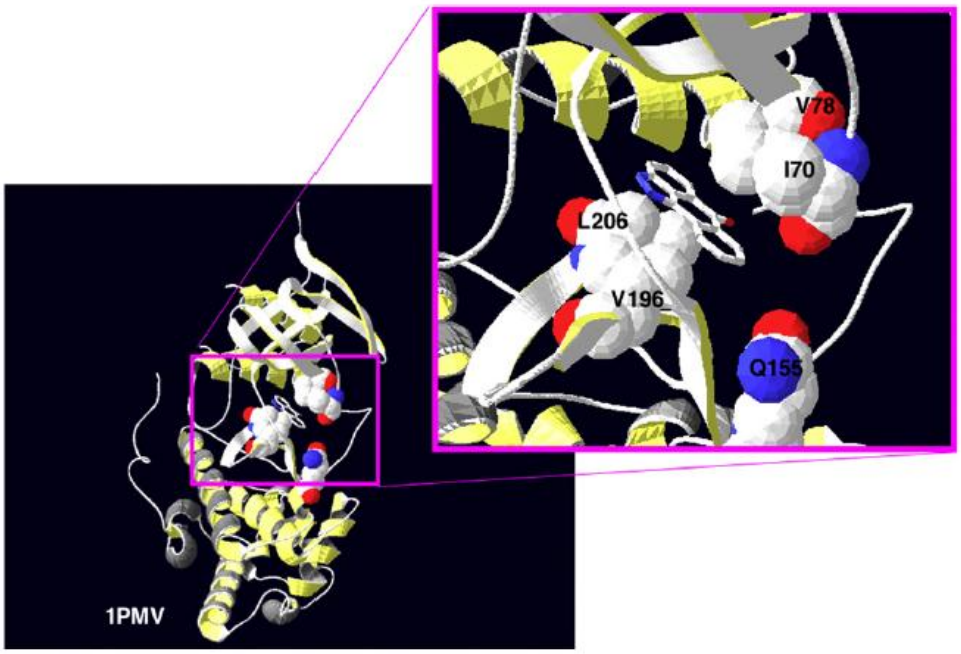

Figure 5 Structure of the JNK complex with the ATP-competitive inhibitor SP600125. SP600125 has been co-crystallised with JNK3, and the resulting structure has been recorded in the Protein DataBase (PDB) as 1PMV (Scapin et al., 2003). Here, the residues in JNK3 not conserved in p38-2, namely I70, V79, V196, L206 and Q155, are highlighted. Although these residues were predicted to most likely contribute to the specificity of SP600125 towards JNK1/2/3 over the p38 MAPKs (Scapin et al., 2003), subsequent mutagenesis studies further work is required to evaluate which residues make major contributions to binding (Fricker et al., 2005). Figure adapted from Bogoyevitch and Arthur; 2008.

2002; Bader et al., 2005). PI3Ks are divided into three distant subclasses: Class I, Class II and Class III, which are classified according to their primary structure and substrate specificity (Engelman et al., 2006; Fruman et al., 1998; Katso et al., 2001; Leevers et al., 1999; Vanhaesebroeck et al., 2010). Among them, the most extensively studied is the class I enzyme that is activated directly via cell surface receptors. PI3K can be stimulated by various growth factors and cytokines, thereby activating a serine/threonine protein kinase known as AKT (also called as protein kinase B, PKB). There have been a large number of studies on the PI3K pathway which implicate that this pathway is activated in a broad range of human cancers including skin cancer, in inflammation as well as cardiovascular and metabolic diseases (Cantley, 2002). Indeed, many findings have demonstrated that the tumor suppressor PTEN (phosphatase and tensin homologue) is the most pivotal negative regulator of PI3K

signaling pathway (Cully et al., 2006; Cantley and Neel, 1999) and mutation of PTEN, which is the second most commonly found tumor suppressor followed by p53 in human cancers, results in unrestrained PI3K signaling pathway, leading to cancer (Cully et al., 2006). PTEN functionally acts as a tumor suppressor by antagonizing PI3K action through its phosphatase activity. Moreover, PTEN also regulates JNK activity and function. Vivanco et al. recently showed, using a fascinating screening technique, that JNK pathway activation is a major consequence of PTEN loss, suggesting that PI3-K promotes cancer progression by inducing the parallel activation of AKT and JNKs (Vivanco et al., 2007). PTEN deficiency sensitizes cells to JNK inhibition and negative feedback regulation of PI3-K was impaired in PTEN-null cells. Similarly, another group has revealed that inhibition of PI3K triggered increase in JNK phosphorylation and islet cell death, which could be reversed by SP600125, the specific JNK inhibitor (Aikin et al., 2004).

Taken together, dual JNKs and PI3-K inhibition might be a novel and effective therapeutic approach in patients, preventing feedback and cross talk.

2. Materials and Methods

2.1 Materials

2.1.1 Chemicals, enzymes, primers and equipments

All chemicals were purchased from Merck, Sigma-Aldrich or Carl Roth unless otherwise stated. (>99% pure) Oligonucleotides for PCR were synthesized by Metabion Enzymes used for PCR and cloning were from Fermentas, New England Biolabs, Stratagene and Takara. All cloning vectors used here were purchased from Novagen. All chromatographic materials and columns were obtained from GE Healthcare (AKTA system).

2.2 Methods

2.2.1 Cloning and protein expression

The C-terminal truncated form of human JNK1α1 (residues 1-364) was generated by a standard PCR-based cloning strategy. The PCR product was inserted into the pET21b expression vector with a 6His-tag at the C-terminus and this plasmid was transformed into E. coli BL21-CodonPlus (DE3)-RIL expression cells (Stratagene).

2.2.2 Protein purification

All purification steps were performed at 4°C. The transformant cells were grown in LB medium at 37 °C up to an OD_{600} of 0.6. Protein expression was induced by adding 1 mM IPTG, and the cells were grown for 15 h. Cells were harvested by centrifugation; resuspended in buffer A containing 50 mM Hepes (pH 7.2), 10% glycerol, 100 mM NaCl, 2 mM β- mercaptoethanol and protease inhibitors (0.1 mM phenylmethylsulfonyl fluoride, 1 μg/mL leupeptin, and 1 μg/ mL pepstatin), and frozen quickly by immersion in liquid nitrogen. For purification, cells were thawed, sonicated, and centrifuged to remove insoluble debris. The supernatant was passed through a 10-mL Ni-NTA Superflow column. The column was washed with resuspension buffer A and then washed again with buffer A plus 10 mM

imidazole. The protein was eluted with buffer A plus 250 mM imidazole. The eluted protein was dialyzed against buffer B (20 mM Hepes, pH 7.0, 10% glycerol, 50 mM NaCl, and 2 mM DTT) and applied to an SP Sepharose cation-exchange column. The column was washed with seven column volumes of buffer B and bound protein was then eluted with a 10-column-volume linear gradient of 50-400 mM NaCl. The eluted protein from the SP-Sepharose column was concentrated and passed over a gel-filtration column (Superdex 200) preequilibrated with buffer C (25 mM Hepes, pH 7.0, 5% glycerol, 50 mM NaCl, and 10 mM DTT). Peak fractions were concentrated to 10 mg/mL as measured by the Bradford method. Purity was judged to be 98% by Coomassie Blue-stained SDS-PAGE.

2.2.3 Crystallization and data collection

Before the crystallization trial, the purified protein was mixed with a peptide fragment of JIP1 (pepJIP1: synthesized from the core facility of MPI-Biochemistry) with the amino acid sequence "RPKRPTTLNLF" at a molar ratio of 1:5 and incubated on ice for 3 h to allow complex formation. To obtain the JNK1-pepJIP1-quercetagetin ternary complex, the JNK1-pepJIP1 complex was mixed with a 10-fold excess of quercetagetin and concentrated it to approximately 10 mg/mL. Crystallization was achieved at 4 °C by vapor diffusion using the sitting drop method and a protein-to-well solution ratio of 1:1 with well solution containing 2.1 M $(NH_4)_2SO_4$ and 0.1 M 2-[bis (2-hydroxyethyl) amino]-2-(hydroxymethyl) propane-1,3-diol (pH 5.5). Single crystals grew within 1 week to an average size of 0.3 mm × 0.1 mm × 0.1 mm. Crystals were transferred to cryoprotectant solution containing well solution plus 25% (v/v) ethylene glycol for a few seconds and then flash-frozen in liquid nitrogen. Data sets were collected at 100 K on the PXII beamline at the Swiss Light Source synchrotron (Paul Scherrer Institute, Switzerland) and processed using XDS and XSCALE software.

2.2.4 Structure determination and refinement

The structures of the JNK1-pepJIP1-quercetagetin ternary complex were solved with the molecular replacement program Phaser using the N- and C-terminal domains of the structure of the binary complex JNK1-pepJIP1 separately (PDB ID: 1UKH). The crystals, which belonged to space group $P2_12_12_1$, were isomorphous to the 1UKH unit cells and did not contain interpretable ligand density.

The other space group, I422, contained an interpretable ligand density in the ATP-binding site. The model was subsequently improved by rigid-body refinement of the individual domains and restrained refinement using Refmac and rebuilt using Coot and X-fit. Water molecules were added by ARP/wARP.

2.2.5 IMAP assay

An IMAP assay was carried out in accordance with the instructions provided by Molecular Devices. The IMAP reaction was carried out with recombinant JNK1 in 384-well black plates containing serially diluted test compounds. The reaction contained 7.46 μM ATP, 100 nM JNK1, 400 nM fluorescein-isothiocyanate-labeled JNK1 substrate peptide (LVEPLTPSGEAPNQK-5FAM-COOH), 20 mM Mops (pH 6.5), 1 mM DTT, 10 mM $MgCl_2$, and 0.01% Brij35. It was incubated for 1 h at room temperature with the addition of IMAP Binding Buffer (a 1:1200 dilution of IMAP Progressive Binding Reagent in 65% IMAP Progressive Binding Buffer A/45% IMAP Progressive Binding Buffer B). Then, the plate was read using a PHERAstar Plus microplate reader from BMG Labtech. The excitation and emission wavelengths were 485 nm with a bandwidth of 20 nm and 530 nm with a bandwidth of 25 nm, respectively.

2.2.6 Docking simulations

To further evaluate the binding affinity of quercetagetin in comparison with other flavonoids, we performed a series of docking simulations. A set of five inhibitors (flavonoids: quercetagetin, quercetin, myricetin, kaempferol and the commercially available inhibitor SP600126) was docked in the ATP-binding sites of two JNK1 structures: (1) JNK1 in complex with quercetagetin and (2) the apoprotein structure (PDB ID 1UKH). A 25-Å simulation box was defined around the binding pocket. The geometric center of the docking box was chosen to coincide with the molecule's center of mass. The docking procedure consisted of three stages: (1) inhibitor–receptor pose generation, (2) pose minimization, and (3) scoring of the final pose. After the first stage, 400 poses were selected for energy minimization (100 steps of Steepest Descent). The XPscoring function of Glide version 5.6 was used to evaluate the final pose. No constraints were imposed on the system.

2.2.7 Molecular modeling and docking

Insight II (Accelrys, Inc., San Diego, CA) was used for docking studies and structure analysis with the crystal coordinates of PI3-K in complex with quercetin (PDB ID: 1E8W). Docking was subsequently performed using the XP-scoring function of Glide version 5.6 (Schrödinger, LLC, New York, NY, 2010). No constraints were imposed on the system. For each ligand, 400 poses were selected for energy minimization (100 steps Steepest Descent) and scoring.

2.2.8 In vitro JNK1 kinase assay

The in vitro kinase assay was conducted in accordance with the instructions provided by Upstate Biotechnology. Briefly, each reaction contained 20 μL of assay dilution buffer [20 mmol/L Mops (pH 7.2), 25 mM β-glycerophosphate, 5 mM ethylene glycol bis (β-aminoethyl ether) N, N′-tetraacetic acid, 1 mM sodium orthovanadate (Na_3VO_4), and 1 mM DTT] and a magnesium-ATP cocktail buffer. For JNK1, the activating transcription factor 2 substrate peptide was included at a concentration of 3 μM. Active JNK1 protein (20 ng) and 10 μL of diluted [γ-32P] ATP solution were incubated at 30 °C for 10 min with the above assay buffer and substrate peptide, and then 15-μL aliquots were transferred onto p81 paper and washed three times with 0.75% phosphoric acid (5 min per wash) and once with acetone (5 min). The incorporation of radioactivity was determined using a scintillation counter (LS6500, Beckman Coulter). Each experiment was performed in triplicate.

2.2.9 In vitro PI3-K kinase assay

Active PI3-K protein (100 ng) was incubated with quercetagetin for 10 min at 30 °C. The mixture was then incubated with 20 μL of 0.5 mg/mL phosphatidylinositol (Avanti Polar Lipids, Alabaster, AL) for 5 min at room temperature and then incubated in reaction buffer [100 mM N-2-hydroxyethylpiperazine-N′-2-ethanesulfonic acid (pH 7.6), 50 mM MgCl2, and 250 μM ATP] containing 10 μCi of [γ-32P] ATP for an additional 10 min at 30 °C. The reaction was stopped by adding 15 μL of 4 N HCl and 130 μL of chloroform:methanol (1:1). After vortexing, 30 μL of the lower chloroform phase was spotted onto a 1% potassium-oxalate-coated silica gel plate, which had previously been activated through incubation for 1 h at 110 °C. The resulting 32P-labeled

phosphatidylinositol-3-phosphate was separated by thinlayer chromatography, and the radiolabeled spots were visualized by autoradiography.

2.2.10 Cell culture

JB6 P+ and H-Ras-transformed JB6 P+ mouse epidermal (H-Ras JB6 P+) cells were cultured in monolayers at 37°C in a 5% CO_2 incubator in MEM containing 5% FBS, 2 mM L-glutamine, and 25 μg/mL gentamicin. NIH/3T3 cells were cultured in DMEM supplemented with 10% bovine calf serum in a 37°C, 5% CO_2 incubator. The cells were maintained by splitting at 80% to 90% confluence, and media were changed every 3 days

2.2.11 *In vitro* and *ex vivo* pull-down assay

Recombinant JNK1 (2 μg) or PI3-K (2 μg), or a JB6 P+ cellular supernatant fraction (500 μg protein), was incubated with quercetagetin/Sepharose 4B beads (100 μL, 50% slurry) or Sephar ose 4B beads (as a control) in reaction buffer [50 mM Tris-HCl (pH 7.5), 5 mM EDTA, 150 mM NaCl, 1 mM DTT, 0.01% NP40, 2 μg/mL bovine serum albumin, 0.02 mM phenylmethyl sulfonyl fluoride, 1× protease inhibitor mixture]. After incubation with gentle rocking overnight at 4°C, the beads were washed five times with buffer (50 mM Tris-HCl pH 7.5, 5 mM EDT A, 150 mM NaCl, 1 mM DTT, 0.01% NP40, 0.02 mM phenylmethylsulfonyl fluoride), and pr oteins bound to the beads were analyzed by Western blotting.

2.2.12 ATP competition assay

Recombinant JNK1 (2 μg) or PI3-K (2 μg) was incubated with 100 μL of quercetagetin/Sepha rose 4B or 100 μL of Sepharose 4B in reaction buffer (see *in vitro* and *ex vivo* pull-down as says) for 12 h at 4°C, and ATP was added at a concentration of either 10 or 100 μM to afin al volume of 500 μL. The samples were incubated for 30 min, and then were washed, andpro teins were detected by Western blotting.

2.2.13 Western blot analysis

After the cells (1.5×10^6) were cultured in a 10-cm dish for 48 h, they were starved in serum-free medium for an additional 24 h. The cells were then treated with quercetagetin at concentrations of 0 to 20 μM for the indicated time periods before being exposed to 4 kJ/m^2 UVB and then harvested 30 min later. Cells were disrupted, and the supernatant fractions were boiled for 5 min. The protein concentration was determined using a dye-binding protein assay kit (Bio-Rad Laboratories) as described in the manufacturer's manual. Lysate protein (20 μg) was subjected to 10% SDS-PAGE and then transferred to a polyvinylidene difluoride membrane. After blocking, the membrane was incubated with the appropriate specific primary antibody at 4°C overnight. Protein bands were visualized using a chemiluminescence detection kit after hybridization with the appropriate horseradish peroxidase-conjugated secondary antibody. The relative amounts of proteins associated with specific antibodies were quantified using Scion Image (NIH, Bethesda, MD).

2.2.14 Luciferase assay

AP-1 or NF-κB luciferase reporter-transfected JB6 P+ cells (8×10^3/mL) suspended in 100 μL of 5% FBS/MEM were added to each well of a 96-well plate and incubated at 37°C/5% CO_2. At 80-90% confluence, cells were cultured in 0.1% FBS-MEM for 24 h. Cells were treated for 1 h with quercetagetin (0–20 μM), and then exposed to 4 kJ/m^2 UVB and harvested after 24 h. After treatment, cells were disrupted with 100 μL of lysis buffer (0.1 M potassium phosphate buffer pH 7.8, 1% Triton X-100, 1 mM dithiothreitol (DTT), 2 mM EDTA) and luciferase activity was measured using a luminometer (Luminoskan Ascent; Thermo Electron, Helsinki, Finland).

2.2.15 Focus-forming assay

For the focus-forming assay, the pcDNA3.1-v5-JNK1 plasmid was constructed as previously described (Colburn et al., 1981). Transformation of NIH3T3 cells was conducted according to standard protocols. Cells were transiently transfected with various combinations of H-Ras^{G12V} (50 ng) and pcDNA3-mock (compensation for equal amount of DNA) plasmids as indicated in figures, and then cultured in 5% FBS-DMEM for 2 weeks. Foci were fixed with methanol, stain

ed with 0.5% crystal violet, and then counted under a microscope using the Image-Pro PLUS software program (v. 4, Media Cybernetics).

2.2.16 Anchorage-independent cell transformation assay

The effects of quercetagetin on H-Ras-induced JB6 cells were investigated. Basal medium Eagle agar (0.5%, 3.5 mL) containing 10% FBS with or without quercetagetin was layered onto each well of 6-well plates. H-Ras JB6 cells (8×10^3/mL) treated or not treated with quercetagetin were mixed with 1 mL of 0.33% basal medium Eagle agar containing 10% FBS and layered on top of the 0.5% agar layer. The separate cultures were maintained at 37°C in a 5%CO_2 incubator for 14 days, at which time the cell colonies were counted under a microscopewith the aid of the Image-Pro Plus software program.

2.2.17 Mouse skin tumorigenesis analysis

Skin carcinogenesis in mice was induced using a UVB irradiation system. The UVB radiation source (Bio-Link cross-linker; Vilber Lourmat) emitted at wavelengths of 254, 312, and 365 nm, with peak emission at 312 nm. SKH-1 hairless mice were divided into 4 groups of 15 animals each. In control mice, the dorsal skin was topically treated with 200 μL of acetone only. In the UVB mouse group, the dorsal skin was topically treated with 200 μL of acetone 1 h before UVB irradiation. The mice in the third and fourth groups received topical application of quercetagetin (4 or 20 nmol) in 200 μL of acetone 1 h before UVB irradiation. The UVB dose was 0.18 J/cm^2. Mice were irradiated 3 times per week for 28 weeks. The incidence of skin tumors was recorded weekly, and a tumor was defined as an outgrowth of > 1 mm in diameter that persisted for 2 weeks or more. Tumor incidence, multiplicity, and volume were recorded every week until the end of the experiment.

Part II

Structure of the stapled p53 peptide bound to HDM2

Summary

HDM2 is a major negative regulator of the tumor suppressor p53 protein, a protein that plays a crucial role in maintaining genome integrity. Inactivation of p53 is the most prevalent defect in human cancers. Inhibitors of the HDM2-p53 interaction that restore functional p53 constitute potential nongenotoxic anticancer agents with a novel mode of action. I present here a 2.0 Å resolution structure of HDM2 with a bound stapled p53 peptide (SAH-p53-8). Such peptides, which are conformationally and proteolytically stabilized with all-hydrocarbon staples, are an emerging class of biologics that are capable of disrupting protein-protein interactions and thus have broad therapeutic potential. The structure represents the first crystal structure of an i, i + 7 stapled peptide bound to its target and reveals that SAH-p53-8 uses its Phe19, Trp23, and Leu26 to fill the binding site in a manner similar to the native p53 peptide. This structural analysis of HDM2 in complex with the SAH-p53-8 suggests that acting solely as a passive conformational brace - a staple can intimately interact with the surface of a protein and augment the binding interface.

Teil II

Die Struktur eines gestapelten p53 Peptids im Komplex mit HDM2

Zusammenfassung

HDM2 ist einer der wichtigsten negativen Regulatoren des Tumorsuppressorproteins p53. Die Inaktivierung von p53 stellt den häufigsten Defekt in humanen Krebserkrankungen dar. Als nicht-genotoxische Antikrebsmedikamente zeigen Inhibitoren der HDM2-p53 Interaktion einen neuartigen Wirkmechanismus zur Wiederherstellung der Funktionalität von p53. Im Folgenden beschreibe ich die bei 2.0 Å aufgelöste Kristallstruktur von HDM2 in Komplex mit einem gestapeltem p53 Peptid (SAH-p53-8). Diese neu aufkommende Klasse von konformationell und proteolytisch stabilisierten Peptiden kann Protein-Protein-Interaktionen stören und hat dadurch ein breites therapeutisches Anwendungspotential. Die weltweit erste Kristallstruktur eines an sein Zielmolekül gebundenen i, i + 7 gestapelten Peptids zeigt, dass die Aminosäuren Phe19, Trp23 und Leu26 in SAH-p53-8 die Bindungsstelle in ähnlicher Weise ausfüllen wie das native p53 Peptid. Die strukturelle Analyse von HDM2 in Komplex mit SAH-p53-8 verdeutlicht, dass alleine durch die Aufrechterhaltung einer spezifischen Konformation die Interaktionsfläche zwischen gestapeltem Peptid und Zielmolekül gerichtet vergrößert und die Bindungsaffinität dadurch gesteigert werden kann.

1. Introduction

1.1 The Role of p53 in Cell Cycle Regulation

The cell cycle is a highly ordered and regulated process leading to the division, duplication and transmission of genetic information from one cell generation to the next: DNA replication and chromosome segregation into two separate cells. The cell cycle is divided into distinct phases: G1, S, G2, and M. G1 (Gap1) is also called the growth phase, an interphase between M phase (mitosis) and S phase (DNA synthesis). The cells grow in size in G1 phase and DNA synthesis (replication) occurs during S phase. G2 (Gap2) is the second gap between DNA synthesis and mitosis, the cells continue to grow for the process of division. During M (mitosis) phase which is a relatively short period within the cell cycle, the cells growth stop, the replicated chromosomes are segregated into two daughter cells and cells division occurs. The whole process results in two identical daughter cells. In addition to G1, S, G2, and M, the term G0 refers to a phase where the cells become quiescent (out of the cycle) (Figure 1). The regulation of the cell cycle should ensure that each phase is complete before moving on to the next phase. Thus, several checkpoints are designed to monitor and regulate the progression of the cell cycle (Hartwell and Weinert, 1989; Stephen, 1996). The checkpoints ensure that the cells can't proceed to the next cell cycle phase until the previous step is fully completed. Two important checkpoints have been identified: the G1/S checkpoint placed in late G1 before the cells enter S phase and the G2/M checkpoint placed in the G2/M interface after DNA relplication. p53 plays a prominent role in the quality control of the cell cycle at both G1/S and G2/M checkpoints. The G1/S checkpoint is also known as restriction point (Robbins et al., 2004), a rate-limiting step that arrests the cell cycle to allow time for the inhibition of DNA replication and DNA repair in damaged or mutated cells at the G1/S transition (Kastan et al., 1991; Lin et al., 1992), following the detection of DNA damage. At this point, cell cycle arrest is mediated by p53. Normally, the cellular level of p53 is low but the induction of p53 activity can be increased by DNA damage (Levine, 1997). p53 control of the cell cycle is driven by p53 inhibition of RB phosphorylation and cyclin/CDK complexes which are negatively regulated by CDK inhibitors (Sherr and Roberts, 1995). p53 transcriptionally upregulates the CDK inhibitor, p21 (Agarwal et al., 1998). p21 is one of the well known downstream targets of p53 and a

major mediator of p53-dependent G1 cell cycle arrest in response to DNA damage. Up-regulated p21 binds to the ZRXL motif of cyclin/CDK2 and cyclin/CDK4 complexes and inactivates them which results in hypophosphorylation of Rb, sequestration of E2F and cell cycle arrest preventing the replication of DNA damage (Roberts and Thompson, 1979; Guillot et al., 1997; Zhan et al., 1993). In addition to the G1/S checkpoint, p53 has also been associated with the G2/M checkpoint which can occur by either p53-dependent or -independent mechanisms that lead to G2 arrest (Paules et al., 1995; Agarwal et al., 1995; Cross et al., 1995).

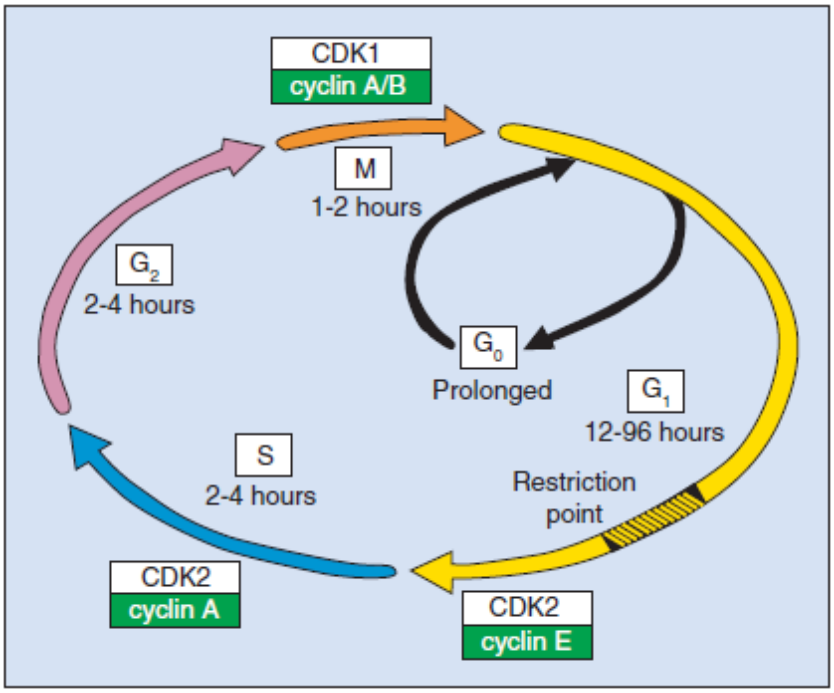

Figure 1 The Cell Cycle - Times are relative. Figure adapted from Israels and Israels, 2000.

1.2 Structural organization of p53

p53 was first identified in 1979 (Lane and Crawford, 1979; DeLeo et al., 1979; Linzer and Levine, 1979). In human, p53 is a ~53 kDa protein encoded by the *TP53* gene, which is located on the short arm of chromosome 17 (Matlashewski et al., 1984; Isobe et al., 1986; Kern et al., 1991; McBride et al,, 1986). The human p53 protein is composed of 393 amino acids with distinct structural and functional domains, each of which exerts its function in the regulation of p53 function. (Figure 2a). The N-terminal domain contains the transactivation domain (subdivided into two subdomains) and a proline-

rich region with the PXXP sequence (where X is any amino acid). The transactivation domain, TAD (residues 1-63) is required for transcriptional transactivation (Fields and Jang, 1990) and interacts with a number of transcriptional factors including acetyltransferase, which regulates p53 through acetylation of its C-terminus as a co-activator (Gu et al., 1997; Grossman, 2001) and the negative regulator MDM2, which inhibits the transactivation of p53 (Momand et al., 2000; Marine et al., 2006; Momand et al., 1992; Oliner et al., 1993).The proline-rich region, PRR (residues 64-92) contains the SH3-domain binding motif (PXXP) which is believed to exhibit a regulatory role and plays an important role in efficient p53-mediated growth suppression dictating the specificity and stability of p53 for the transcriptional activation of downstream gene (Walker and Levine, 1996; Venot et al., 1998). These N-terminal domains are natively unstructured except for the small region which forms a nascent turn or helix (Lee et al., 2000; Bell et al., 2002; Dawson et al., 2003). The nascent helix formation extends into a full amphipathic a-helix (residues 15-29) upon binding to MDM2 (Kussie et al., 1996). A central core domain is the DNA binding domain (residues 94-292) required for sequence-specific DNA binding which contains two copies of the10-bp motif 5'-PuPuPuC(A/T)-(T/A)GPyPyPy-3', separated by up to 13 base pairs (El-Deiry et al., 1992; Pavletich et al., 1993; Bargonetti et al., 1993). It has been reported that most of the cancer mutations are located in this domain as shown in Figure 2a and disrupt the ability of p53 to bind DNA (Nigro et al., 1989; Kern et al., 1991). Moreover, studies of the crystal structure of DNA-bound p53 core domain have revealed that the mutated amino acids in the core domain may alter the structural integrity (Cho et al., 1994; Pietenpol et al., 1994). The DNA binding domain and the tetramerization domain, OD (residues 325-355) near the C-terminus are linked by a flexible linker region (Figure 2b). The tetramerization domain regulates the oligomerization which is essential for p53 function in vivo (Sturzbecher et al., 1992). The negative regulatory domain, CTD (residues 356-393) at the extreme C-terminus binds single stranded DNA nonspecifically (Selivanova et al., 1996) and undergoes posttranslational modifications such as phosphorylation and acetylation (Prives and Manley, 2001; Weinberg et al., 2004; Friedler et al., 2005). Similarly to the N-terminal domain, this regulatory domain is also intrinsically unfolded.

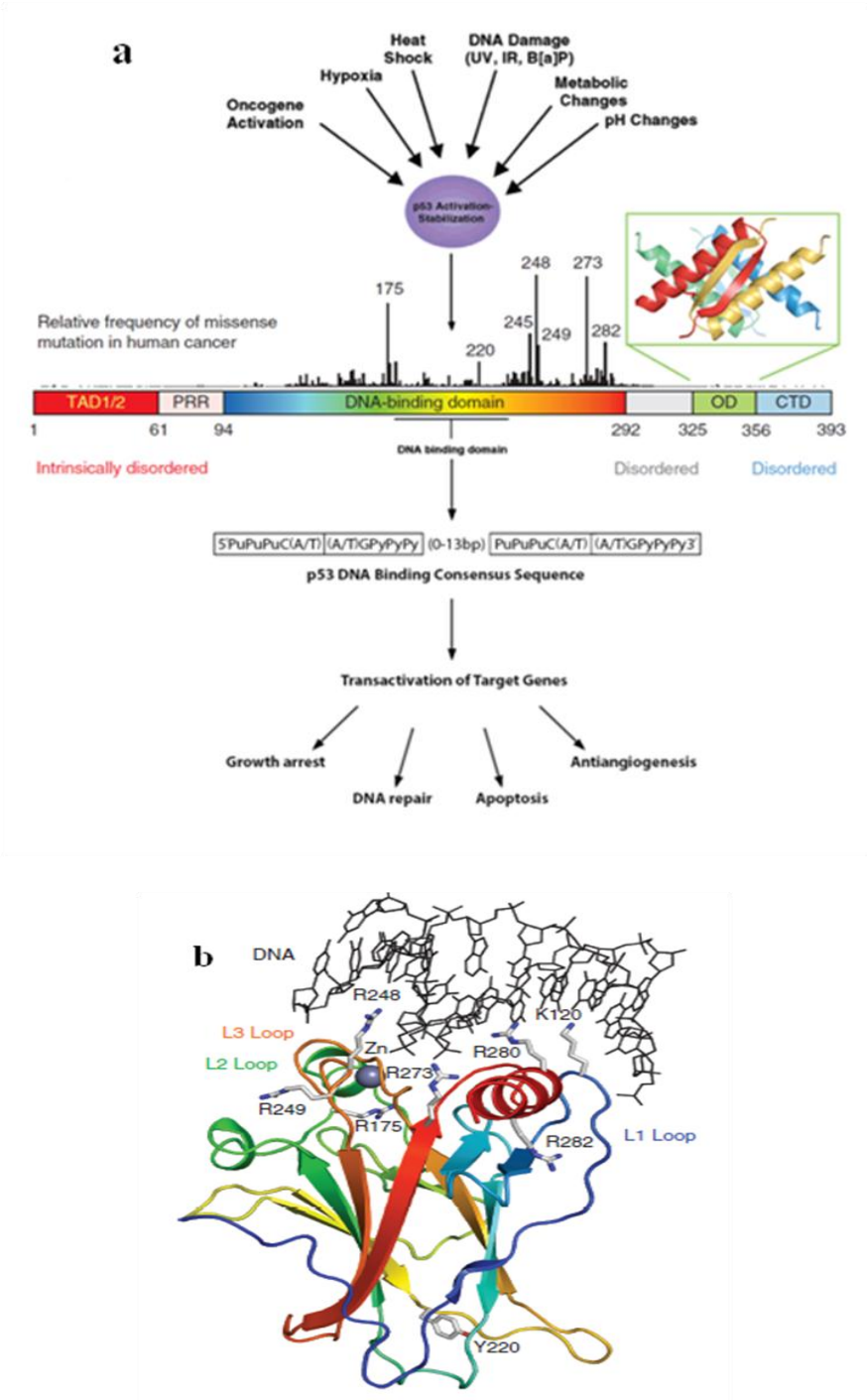

Figure 2 Signaling and domain structure of p53. (a) p53 contains a natively unfolded amino-terminal transactivation domain (TAD), which can be further subdivided into the subdomains TAD1 and TAD2, followed by a proline-rich region (PRR). The structured DNA-binding and tetramerization domains (OD) are connected through a flexible linker region. The DNA binding consensus sequence for p53 is shown. Similarly to the TAD region, the regulatory domain at the extreme carboxyl terminus (CTD) is also intrinsically disordered. The vertical bars indicate the relative missense-mutation frequency in human cancer for each residue based on the TP53 Mutation Database of the International Agency for Research on Cancer (www-p53.iarc.fr) (Petitjean et al.,

2007), showing that most cancer mutations are located in the DNA-binding domain. (b) The structure of the DNA-binding domain (PDB code 1TSR) (Cho et al. 1994) is shown as a ribbon representation and colored with a rainbow gradient from the amino terminus (blue) to the carboxyl terminus (red). Sites of cancer hotspot mutations and essential DNA contacts are shown as stick models. Figures adapted from Stewart and Pietenpol, 2001; Joerger and Fersht, 2010.

1.3 The negative regulator of p53, MDM2

MDM2 (murine double minute 2, HDM2 in human) was first identified in a spontaneously transformed mouse Balb/c cell line called 3T3-DM (Feki and Irminger-Finger, 2004; Momand et al., 1992; Fakharzadeh et al., 1991; Fakharzadeh et al., 1993; Hainaut P, Hollstein, 2000), and MDM2 was later shown to be associated with p53 (Momand et al., 1992).The MDM2-gene encodes a 491 amino acids-long oncoprotein that serves as a master negative regulator of p53 tumor suppressor. The cellular levels of p53 and MDM2 are mutually regulated by autoregulatory feedback loop (Figure 3), in which p53 transcriptionally activate MDM2, and MDM2 inhibits the activity of p53 in several ways: (Barak et al., 1993; Wu et al., 1993) it directly binds to p53 and inhibits p53-mediated transactivation (Fridman JS and Lowe, 2003), further it induces nuclear-cytoplasmic shuttling of p53 (Vousden KH, Lu, 2002) and ubiquitinates p53 at several lysine residues in the p53 C-terminus for proteasomal degradation through its E3 ubiquitin ligase activity (Haupt et al., 1997; Kubbutat and Vousden, 1997). MDM2 contains two different promoters, termed P1 and P2. The upstream P1 promoter is constitutively active in most cells (Mendrysa and Perry, 2000). The second promoter P2 which is located downstream of the p53-binding domain has to two p53-responsive elements (Zauberman et al, 1995) and the transcription from P2 is controlled by p53, forming an auto-regulatory feedback loop. MDM2 also contains evolutionally conserved domains including including an N-terminal p53 binding

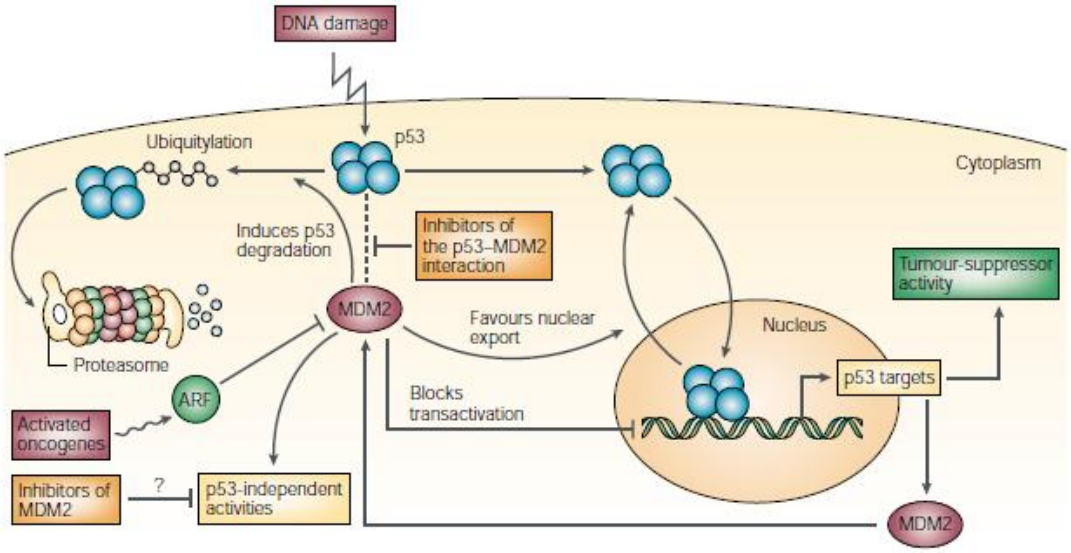

Figure 3 Regulation of p53 by MDM2. p53 and MDM2 form an auto-regulatory feedback loop. p53 stimulates the expression of MDM2; MDM2 inhibits p53 activity because it blocks its transcriptional activity, favours its nuclear export and stimulates its degradation. Different cellular signals, such as DNA-damage or oncogene activation, induce p53 activation. DNA damage favours p53 phosphorylation, preventing its association with MDM2. Activated oncogenes activate the ARF protein, which prevents the MDM2-mediated degradation of p53. Similarly, inhibitors of the p53–MDM2 interaction should activate p53 tumour-suppressor activity in tumour cells that express wild-type p53. These compounds, because they bind to MDM2, could also affect the p53-independent activities of MDM2. Figure adapted from Chène, 2003.

domain that binds to the transactivation domain of p53 suppressing its ability to activate transcription (Kussie et al., 1996). The central acidic domain of MDM2 appears to be important for regulation of its function through the phosphorylation of residues within this domain, and moreover it is necessary for interaction with a number of proteins including p14ARF, p300/ CBP (CREB-binding protein) and YY1 (Bothner et al., 2001; Sui et al., 2004). The nuclear localization signal and the nuclear export signal are located between the p53-binding domain and the acidic domain (Hay and Meek, 2000). Another well-conserved domain is zinc finger domain that plays an important role in the interaction between MDM2 and ribosomal proteins and the degradation of p53 under ribosomal stress condition (Lindstrom et al., 2007). MDM2 also contains a RING-finger domain located at the C-terminus, which is common in E3 ligases and is critical for E3 ligase activity towards p53 as well as itself (Fang et al., 2000). This domain contains a Cys3-His2-Cys3 consensus that coordinates two molecules of zinc

which is essential for proper folding of the RING domain (Boddy et al., 1994). In addition, the RING-finger domain at the C-terminal domain of MDM2 is required to interact and ubiquitinate MDMX (Pan and Chen, 2003) (Figure 4).

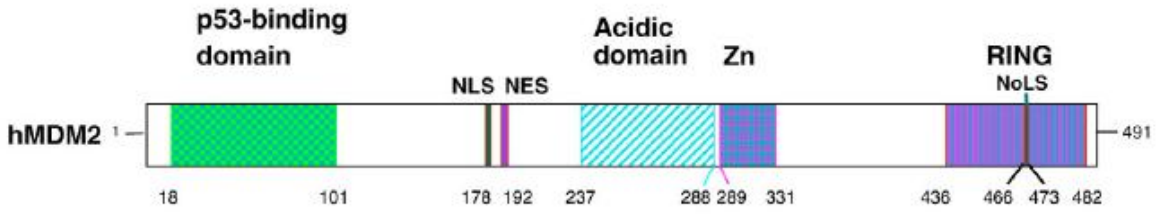

Figure 4 Primary structure of MDM2. The p53-binding domain, zinc (Zn) finger and RING finger [containing the nucleolar location signal (NoLS)] are represented. Figure adapted from Marine et al., 2007.

The crystal structure of the amino terminus of HDM2 (residues 17-125) in complex with the amino terminus of human p53 (residues 15-29) was solved by Kussie, P.H. *et al* (Kussie et al., 1996) (Figure 5), which have provided atomic details of the interaction between these two proteins. This structure revealed that the interaction of HDM2 and p53 is mediated by a well-defined hydrophobic surface pocket in HDM2 and the hydrophobic face of the amphipathic p53 α-helix, in particular, a triad of three key hydrophobic residues in p53: Phe19, Trp23, and Leu26 making contact, which fit into a deep hydrophobic cleft in HDM2. These same p53 residues which are buried deep with the cleft of HDM2 are also involved in transactivation, supporting the hypothesis that HDM2 inactivates p53 by concealing its transactivation domain. Thr18 in the region of direct contact with HDM2 is critical for the stability of a p53 α-helix (Kussie et al., 1996) and a charge-charge repulsion that destabilizes the interaction of p53 and HDM2 is introduced by phosphorylation of Thr18. The crystal structure also showed that an additional interaction is formed by the indole group of Trp23 in p53 and the carbonyl group of Leu54 in HDM2 located deep inside the cleft. The cleft of HDM2 is formed by amino acids 26-108 and comprises two structurally similar portions that fold up into a deep groove lined by 14 hydrophobic and aromatic residues (Kussie et al., 1992). The interactions between p53 and HDM2 are tightly regulated, showing a tight key-lock configuration of the p53-HDM2 interface.

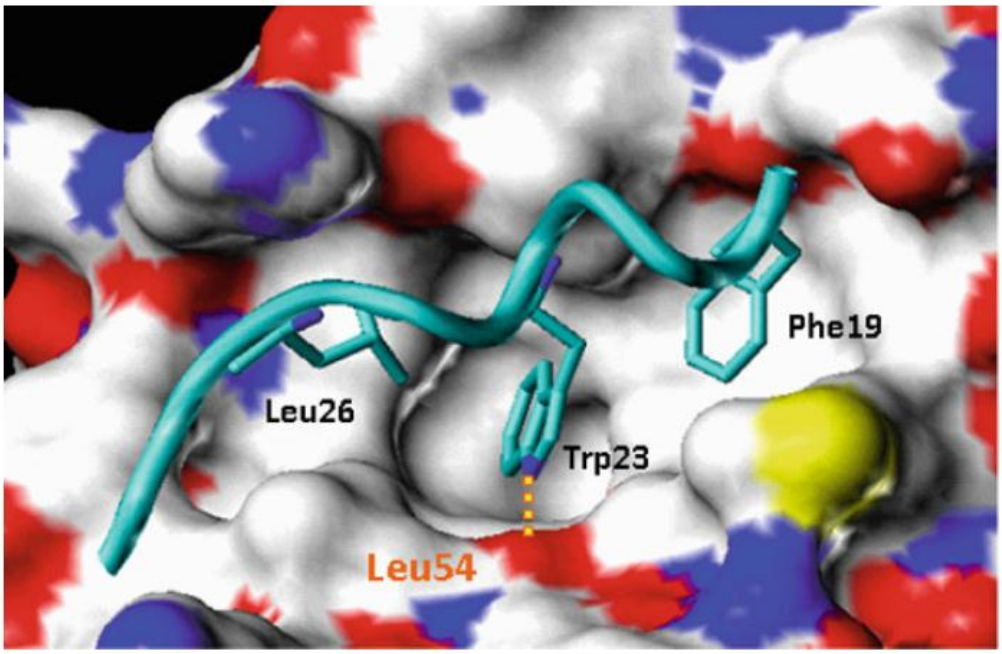

Figure 5 Crystal structure of HDM2 protein complexed with p53 peptide (residues 13–29). Figure adapted from Wang et al., 2012.

1.4 Inhibitors of the p53-HDM2 interaction as a promising therapeutic strategy

The tumor suppressor p53 protein, "the guardian of the genome," plays a central role in maintaining the integrity of the genome and implicates in diverse types of cancers (Lane, 1992).Consistent with its prominent role, p53 is has been found to be inactivated by mutation or deletion in approximately 50% of human cancers (Feki and Irminger-Finger, 2004; Miller and Koeffler, 1993; Greenblatt et al., 1994). Since the function of wild-type p53 is effectively inhibited by HDM2 in cancers, the restoration of the impaired function of p53 by disrupting the interaction of HDM2-p53 provides an attractive therapeutic strategy across a broad spectrum of cancers (Vassilev, 2007; Murray and Gellman, 2007; Dömling, 2008; Bixby et al., 2008; Cheok and Lane, 2008; Shangary and Wang, 2008). The detailed structural analysis of HDM2 bound to p53 revealed that the relatively compact binding pocket in HDM2 makes it possible to design peptides, small molecule inhibitors for aiming to inhibit this interaction as a means to rescue p53. Of note, only HDM2 has structurally well-defined binding sites, whereas p53 undergoes conformational change by phosphorylation, which means that inhibitors should mimic p53 rather than HDM2.

As of today, there are several small molecules and peptidic inhibitors have been designed to sit in the

p53 binding pocket of HDM2, which are able to disrupt the HDM2-p53 interaction with high (nM) affinity and specificity, (Vassilev et al., 2004; Shangary and Wang, 2008; Grasberger BL, et al. 2005) thereby blocking the HDM2-mediated p53 ubiquitination and degradation of p53, leading to the accumulation and the transcriptional activation of p53. The first reported inhibitors have been identified to be chalcone derivatives that broadly have anticancer effects, showing an ability to inhibit the HDM2-p53 interaction (Stoll et al., 2001; Go et al., 2005). In addition to this biological effect, their binding mode was determined by NMR. However, these compounds cannot be considered as drug candidates because of their low potency. In consequence, they do not fully occupy the binding cleft and only interact with Trp23. In 2004, scientists from Hoffmann-La Roche, Inc. described the best-documented, potent and specific small molecule HDM2 inhibitor, Nutlin-3 which is a class of cis-imidazolidine analogues screened by HTS, with a crystallographic structure (Vassilev et al., 2004). Nutlin-3 can bind to HDM2 and inhibit the HDM2-p53 interaction by mimicking the three key hydrophobic residues in p53, by doing so, leads to cell-cycle arrest and apoptosis and activates p53, and exhibits antitumor efficacy in vivo (Vassilev et al., 2004). However, several limitations with Nutlin have been raised. One of them is the high toxicity of inhibiting HDM2 by Nutlin. In case of peptidic inhibitors based on the modified p53 sequence, they suffer from low cell permeability and are proteolytically unstable despite of the very high affinity toward MDM2. A successful attempt to overcome these problems has recently been made by Bernal *et al*. in designing cyclic peptides that are closed by an all-hydrocarbon staple (Bernal et al., 2010; Schafmeister et al., 2000; Walensky et al., 2004). This designed strategy known as ‘‘hydrocarbon stapling’’ installs an all-hydrocarbon cross-link within peptides to restore an α-helical structure with potential therapeutic benefit including protease resistance combined with promoted cellular uptake (Bird et al., 2010; Schafmeister et al., 2000; Walensky et al., 2004). The ‘‘stabilized alpha-helix’’ of p53 (SAH-p53-8) peptide is one of the ‘‘stapled’’ peptides that was derived from the p53 transactivation domain for improving target affinity and proteolytic resistance (Bernal et al. 2007). SAH-p53-8 was shown to contribute to the enhanced affinity for HDM2 relative to the wild-type peptide (Moellering et al., 2009). Importantly, SAH-p53-8 also targets HDMX, thereby can overcome HDMX-mediated cancer resistance. Although SAH-p53-8 exhibits a 25-fold greater binding preference for HDMX over HDM2 in co-immunoprecipitation

experiments, it demonstrates cytotoxicity toward cancer cells overexpressing HDM2, HDMX or both (Bernal et al., 2010) as well as a clue to reactivate p53 pathway in tumors in vitro and in vivo (Joseph et al., 2010a; Popowicz et al., 2010; Joseph et al., 2010b). Taken together, these finding indicate that stapled peptides may afford new therapeutic opportunities for p53 activating cancer therapy.

2. Materials and Methods

2.1 Materials

2.1.1 Chemicals, enzymes, primers and equipments

All chemicals were purchased from Merck, Sigma-Aldrich or Carl Roth unless otherwise stated. (>99% pure) Oligonucleotides for PCR were synthesized by Metabion Enzymes used for PCR and cloning were from Fermentas, New England Biolabs, Stratagene and Takara. All cloning vectors used here were purchased from Novagen. All chromatographic materials and columns were obtained from GE Healthcare (AKTA system).

2.2 Methods

2.2.1 Cloning

The recombinant human HDM2 (residues 25-111) was cloned into the pET-20 vector without an affinity tag and expressed in E. coli BL21-CodonPlus(DE3)-RIL expression cells (Stratagene).

2.2.2 Peptide synthesis

SAH-p53-8 was synthesized as previously described (Kim et al., 2011).

2.2.3 Protein expression and purification

For expression of HDM2, cells were grown at 37 °C and induced at OD600nm of 0.8 with 1 mM IPTG. After 5 h induction at 37 °C the cells were harvested by centrifugation. The harvested cells from 5 liters of E. coli cell culture were re-suspended in PBS at pH 7.4 and ruptured by sonication. After centrifugation the inclusion bodies were washed with PBS containing 0.05% Triton X-100 with subsequent low-speed centrifugation (12000G). The procedure was repeated three times. The inclusion bodies were solubilized with 6 M GuHCl in 100 mM Tris-HCl, pH 8.0 including 1 mM EDTA and 10 mM DTT. The protein was dialyzed at 4 °C, against 4 M GuHCl, pH 3.5 including 10 mM DTT. For

renaturation, the protein was diluted 1:100 in 10 mM Tris- HCl, pH 7.0, containing 1 mM EDTA and 10 mM DTT by adding the denatured protein drop-wise into the refolding buffer. Refolding was carried out for 10 h at 4 °C. Ammonium sulfate was added to a final concentration of 1.5 M and the protein was applied to the Butyl Sepharose 4 Fast Flow and subsequently eluted with 100 mM Tris-HCl, pH 7.2, including 5 mM DTT. The protein was further purified by gel filtration on HiLoad 16/60 Superdex200. The HDM2 containing fractions are mixed with the 2-fold excess of the peptide and concentrated to about 10 mg/mL before the crystallization trial. The purity and folding of the protein was measured by SDS-PAGE and 1D NMR.

2.2.4 X-ray crystallography

Crystallization of the HDM2 with the peptide was achieved at room temperature by sitting drop vapor diffusion and the protein to crystallization solution ratio of 1:1, with the crystallization solution containing 100 mM Sodium acetate trihydrate, pH 4.75 and 2.5 M NaCl. The crystals appeared in several days and grew to a final size of 0.1 mm. They were transferred to cryoprotectant solution containing the crystallization solution supplemented with 25% (v/v) glycerol, then directly plunged frozen in liquid nitrogen. Native dataset to 2.0 Å were collected from a single crystal at 100 K on the SLS PXII beam line at Paul Scherrer Institute, Villigen, Switzerland and processed using XDS and XSCALE (Kabsch, 1993) program. The structure of HDM2 from PDB entry 1YCR was used as a search model after the p53 peptide was removed. The initial Rfactor of the solution was 0.45. The model was subsequently rebuilt using Xfit (McRee, 1999) and refined using Refmac5 from CCP4 suite (Collaborative Computational Project, Number 4., 1994). Data collection and refinement statistics are given in table S1. Each asymmetric unit contains two stapled peptide-HDM2 complexes. Both are virtually identical (RMSD of the main chain atoms 0.7 Å) except for the region between Asp84-Val88 in chain A that is shifted by about 1.2 Å due to crystal contacts. The residues outside 18-27 range in the peptide are generally not visible in electron density (one chain shows additionally Gln28-Asn30 stabilized due to crystal contacts) indicating that this part is flexible and do not take direct part in binding to HDM2. Several solvent-exposed side chains had no interpretable electron density and were removed from the model.

3. References

Adams, J. A. (2003). Activation loop phosphorylation and catalysis in protein kinases: is there functional evidence for the autoinhibitor model? *Biochemistry* **42**, 601-607.

Adler, V., Franklin, C. C. & Kraft, A. S. (1992). Phorbol esters stimulate the phosphorylation of c-Jun but not v-Jun: regulation by the N-terminal delta domain. *Proc. Natl. Acad. Sci. USA* **89**, 5341-5345.

Agarwal, M. L., Taylor, W. R., Chernov, M. V., Chernova, O. B. & Stark, G. R. (1998). The p53 network. *J. Biol. Chem.* **273**, 1-4.

Agarwal, M. L., Agarwal, A., Taylor, W. R. & Stark, G. (1995). p53 controls both the G2/m and G1 cell cycle checkpoints and mediates growth arrest in human fibroblasts. *Proc. Natl. Acad. Sci. USA* **92**, 8493-8497.

Aguirre, V., Werner, E. D., Giraud, J., Lee, Y. H., Shoelson, S. E. & White, M. F. (2002). Phosphorylation of Ser307 in insulin receptor substrate-1 blocks interactions with the insulin receptor and inhibits insulin action. *J. Biol. Chem.* **277**, 1531-1537.

Ahn, N. G., Seger, R., Bratlien, R. L., Diltz, C. D., Tonks, N. K. & Krebs, E. G. (1991). Multiple components in an epidermal growth factor–stimulated protein kinase cascade. *J. Biol. Chem.* **266**, 4220-4227.

Aikin, R., Maysinger, D. & Rosenberg, L. (2004). Cross-talk between phosphatidylinositol 3-kinase/AKT and c-jun NH2-terminal kinase mediates survival of isolated human islets. *Endocrinology* **145**, 4522-4531.

Anderson, N. G., Maller, J. L., Tonks, N. K. & Sturgill, T. W. (1990). Requirement for integration of signals from two distinct phosphory lation pathways for activation of MAP kinase. Nature *343*, 651-653.

Bader, A. G., Kang, S., Zhao, L. & Vogt, P. K. (2005). Oncogenic PI3K deregulates transcription and translation. *Nature Rev. Cancer* **5**, 921-929.

Barak, Y., Juven, T., Haffner, R. & Oren, M. (1993). Mdm2 expression is induced by wild type p53 activity. *EMBO J.* **12**, 461-468.

Bargonetti, J., Manfredi, J. J., Chen, X., Marshak, D. R. & Prives, C. (1993). A proteolytic fragment

from the central region of p53 has marked sequence-specific DNA-binding activity when generated from wild-type but not from oncogenic mutant p53 protein. *Genes Dev.* **7**, 2565-2574.

Barr, R. K. & Bogoyevitch, M. A. (2001). The c-Jun N-terminal protein kinase family of mitogen-activated protein kinases (JNK MAPKs). *Int J. Biochem. Cell. Biol.* **33**, 1047-1063.

Bell, S., Klein, C., Muller, L., Hansen, S. & Buchner, J. (2002). p53 contains large unstructured regions in its native state. *J. Mol. Biol*. **322**, 917-927.

Bennett, B. L., Sasaki, D. T., Murray, B. W., O'Leary, E. C., Sakata, S. T., Xu, W., Leisten, J. C., Motiwala, A., Pierce, S., Satoh, Y., Bhagwat, S. S., Manning, A. M. & Anderson, D. W. (2001). SP600125, an anthrapyrazolone inhibitor of Jun N-terminal kinase. *Proc Natl Acad Sci USA* **98**, 13681-13686.

Bernal, F., Tyler, A. F., Korsmeyer, S. J., Walensky, L. D. & Verdine, G. L. (2007). Reactivation of the p53 tumor suppressor pathway by a stapled p53 peptide. *J. Am. Chem. Soc*. **129**, 2456-2457.

Bernal, F., Wade, M., Godes, M., Davis, T. N., Whitehead, D. G., Kung, A. L., Wahl, G. M. & Walensky, L. D. (2010). A stapled p53 helix overcomes HDMX-mediated suppression of p53. *Cancer Cell*. **18**, 411-422.

Bird, G. H., Madani, N., Perry, A. F., Princiotto, A. M., Supko, J. G., He, X., Gavathiotis, E., Sodroski, J. G. & Walensky, L. D. (2010). Hydrocarbon double-stapling remedies the proteolytic instability of a lengthy peptide therapeutic. *Proc. Natl. Acad. Sci. USA* **107**, 14093-14098.

Bixby, D., Kujawski, L., Wang, S., Sami, N. & Malek, S. N. (2008). The pre-clinical development of MDM2 inhibitors in chronic lymphocytic leukemia uncovers a central role for p53 status in sensitivity to MDM2 inhibitormediated apoptosis. *Cell Cycle* **7**, 971-979.

Blease, K., Lewis, A. & Raymon, H. K. (2003). Emerging treatments for asthma. *Expert Opin. Emerg. Drugs* **8**, 71-81.

Boddy, M. N., Freemont, P. S. & Borden, K. L. (1994). The p53-associated protein MDM2 contains a newly characterized zinc-binding domain called the RING finger. *Trends Biochem. Sci.* **19**, 198-199.

Bode, A. M. & Dong, Z. (2003). Mitogen-activated protein kinase activation in UV-induced signal transduction. *Sci. STKE.* **2003**, RE2.

Bogoyevitch, M. A. & Arthur, P. G. (2008). Inhibitors of c-Jun N-terminal kinases: JuNK no more? *Biochim Biophys Acta*. **1784**, 76-93.

Bogoyevitch, M. A. & Kobe, B. (2006). Uses for JNK: the many and varied substrates of the c-Jun N-terminal kinases. *Microbiol. Mol. Biol. Rev.* **70**, 1061-1095.

Borsello, T. & Forloni, G. (2007). JNK signalling: a possible target to prevent neurodegeneration. *Curr. Pharm.* **13**, 1875-1886.

Bothner, B., Lewis, W. S., DiGiammarino, E. L., Weber, J. D., Bothner, S. J. & Kriwacki, R. W. (2001). Defining the molecular basis of Arf and Hdm2 interactions. *J. Mol. Biol.* **314**, 263-277.

Boulton, T. G. & Cobb, M. H. (1991). Identification of multiple extra- cellular signal-regulated kinases (ERKs) with antipeptide antibodies. *Cell Regulation* **2**, 357-371.

Byun, S., Lee, K. W., Jung, S. K., Lee, E. J., Hwang, M. K., Lim, S. H., Bode, A. M., Lee, H. J. & Dong, Z. (2010). Luteolin inhibits protein kinase C(epsilon) and c-Src activities and UVB-induced skin cancer. *Cancer Res*. **70**, 2415-2423.

Canagarajah, B., Khokhlatchev, A., Cobb, M. H. & Goldsmith, E. J. (1997). Activation mechanism of the MAP kinase ERK2 by dual phos phorylation. *Cell* **90**, 859-869.

Cantley, L. C. (2002). The phosphoinositide 3-kinase pathway. *Science* **296**, 1655-1657.

Cantley, L. C. & Neel, B. G. (1999). New insights into tumor suppression: PTEN suppresses tumor formation by restraining the phosphoinositide 3-kinase/AKT pathway. *Proc. Natl Acad. Sci. USA* **96**, 4240-4245.

Chang, L. & Karin, M. (2001). Mammalian MAP kinase signalling cascades. *Nature* **410,** 37-40.

Charles, L. Sawyers. (2003). Opportunities and challenges in the development of kinase inhibitor therapy for cancer. *Genes Dev.* **17**, 2998-3010.

Chen, N., Nomura, M., She, Q. B., Ma, W. Y., Bode, A. M., Wang, L., Flavell, R. A. & Dong, Z. (2001). Suppression of skin tumorigenesis in c-Jun NH2-terminal kinase-2-deficient mice. *Cancer Res*. **61**, 3908-3912.

Chen, W. S., Lee, Y. J., Yu, Y. C., Hsaio, C. H., Yen, J. H. & Yu, S. H. (2010). Enhancement of p53-mutant human colorectal cancer cells radiosensitivity by flavonoid fisetin. *Int. J. Radiat. Oncol. Biol. Phys.* **77**, 1527-1535.

Cheok, C. F. & Lane, D. P. (2008). New developments in small molecules targeting p53 pathways in anticancer therapy. *Drug Dev. Res.* **69,** 289-296.

Chialda, L., Zhang, M., Brune, K. & Pahl, A. (2005). Inhibitors of mitogen activated protein kinases differentially regulate costimulated T cell cytokine production and mouse airway eosinophilia. *Respir. Res*. **6**, 36-54.

Cho, Y., Gorina, S., Jeffrey, P. D. & Pavletich, N. P. (1994). Crystal structure of a p53 tumor suppressor-DNA complex: understanding tumorigenic mutations. *Science* **265**, 346-355.

Cho, YY., Yao, K., Pugliese, A., Malakhova, M. L., Bode, A. M. & Dong, Z. (2009). A regulatory mechanism for RSK2 NH(2)-terminal kinase activity. *Cancer Res*. **69**, 4398-4406.

Cobb, M. H. & Goldsmith, E. J. (1996). How MAP kinases are regulated. *J. Biol. Chem.* **270**, 14843-14846.

Cohen, P. (1999a). Protein kinases: the major drug targets of the twenty-first century*? Nat Rev Drug Disc*. **1**, 309-315.

Cohen, P. (1999b). The development and therapeutic potential of protein kinase inhibitors. *Curr. Opin. Chem. Biol.* **3**, 459-465.

Colburn, N. H., Wendel, E. J. & Abruzzo, G. (1981). Dissociation of mitogenesis and late-stage promotion of tumor cell phenotype by phorbol esters: mitogen-resistant variants are sensitive to promotion. *Proc. Natl. Acad. Sci. USA* **78**, 6912-6916.

Collaborative Computational Project, Number 4. (1994). The CCP4 suite: programs for protein crystallography. *Acta Crystallogr. D. Biol. Crystallogr.* **50**, 760-763.

Cross, S. M., Sanchez, C. A., Morgan, C. A., Schimke, M. K., Ramel, S., Idzerda, R. L., Rasking, W. H. & Reid, B. J. (1995). A p53-dependent mouse spindle checkpoint. Science **267**, 1353-1356.

Cully, M., You, H., Levine, A. J. & Mak, T. W. (2006). Beyond PTEN mutations: the PI3K pathway as

an integrator of multiple inputs during tumorigenesis. *Nature Rev. Cancer* **6**, 184-192.

Davis, R. J. (2000). Signal transduction by the JNK group of MAP kinases. *Cell* **103**, 239-252.

Dawson, R., Muller, L., Dehner, A., Klein, C., Kessler, H. & Buchner, J. (2003). The N-terminal domain of p53 is natively unfolded. *J. Mol. Biol.* **332**, 1131-1141.

Deleo, A. B., Jay, G., Appella, E., Dubois, G. C., Law, L. W. & Old, L. J. (1979). Detection of a transformation-related antigen in chemically induced sarcomas and other transformed cells of the mouse. *Proc. Natl. Acad. Sci. USA* **76**, 2420-2424.

Demetri, G. D., von Mehren, M., Blanke, C. D., Van den Abbeele, A. D., Eisenberg, B., Roberts, P. J., Heinrich, M. C., Tuveson, D. A., Singer, S., Janicek, M., Fletcher, J. A., Silverman, S. G., Silberman, S. L., Capdeville, R., Kiese, B., Peng, B., Dimitrijevic, S., Druker, B. J., Corless, C., Fletcher, C. D. & Joensuu, H. (2002). Efficacy and safety of imatinib mesylate in advanced gastrointestinal stromal tumors. *N. Engl. J. Med.* **347**, 472-480.

Domling, A. Small molecular weight protein-protein interaction antagonists–an insurmountable challenge? *Curr. Opin. Chem. Biol.* **12**, 281-291.

Druker, B. J., Talpaz, M., Resta, D. J., Peng, B., Buchdunger, E., Ford, J. M., Lydon, N. B., Kantarjian, H., Capdeville, R., Ohno-Jones, S. & Sawyers, C. L. (2001). Efficacy and safety of a specific inhibitor of the BCR-ABL tyrosine kinase in chronic myeloid leukemia. *N. Engl. J. Med.* **344**, 1031-1037.

Edwards, M. L., Stemerick, D. M. & Sunkara, P. S. (1990). Chalcones: a new class of antimitotic agents. *J. Med. Chem.* **33**, 1948-1954.

El-Deiry, W. S., Kern, S. E., Pietenpol, J. A., Kinzler, K. W. & Vogelstein, B. (1992). Definition of a consensus binding site for p53. *Nat. Genet.* **1**, 45-49.

Elledge, S. J. (1996). Cell Cycle Checkpoints: Preventing an Identity Crisis. *Science* 274, 1664-1672.

Engelman, J. A., Luo, J. & Cantley, L. C. (2006). The evolution of phosphatidylinositol 3-kinases as regulators of growth and metabolism. *Nat Rev Genet.* **7**, 606-619.

Fakharzadeh, S. S., Trusko, S. P. & George, D. L. (1991). Tumorigenic potential associated with enhanced expression of a gene that is amplified in a mouse tumor cell line. *EMBO J.* **10**, 1565-1569.

Fakharzadeh, S. S., Rosenblum-Vos, L., Murphy, M., Hoffman, E. K. & George, D. L. (1993). Structure and organization of amplified DNA on double minutes containing the mdm2 oncogene. *Genomics* **15**, 283-290.

Fang, S., Jensen, J. P., Ludwig, R. L., Vousden, K. H. & Weissman, A. M. (2000). Mdm2 is a RING finger-dependent ubiquitin protein ligase for itself and p53. *J. Biol. Chem.* **275**, 8945-8951.

Feki, A. & Irminger-Finger, I. (2004). Mutational spectrum of p53 mutations in primary breast and ovarian tumors. *Crit. Rev. Oncol. Hematol.* **52**, 103-116.

Fields, S. & Jang, S. K. (1990). Presence of a potent transcription activating sequence in the p53 protein. *Science* **249**, 1046-1049.

Freedman, D. A., Wu, L. & Levine, A. J. (1999). Functions of the MDM2 oncoprotein. *Cell. Mol. Life. Sci.* **55**, 96-107.

Fricker, M., Lograsso, P., Ellis, S., Wilkie, N., Hunt, P. & Pollack, S. J. (2005). Substituting c-Jun N-terminal kinase-3 (JNK3) ATP-binding site amino acid residues with their p38 counterparts affects binding of JNK- and p38- selective inhibitors. *Arch. Biochem. Biophys.* **438**, 195-205.

Fridman, J. S. & Lowe, S. W. (2003). Control of apoptosis by p53. *Oncogene* **22**, 9030-9040.

Friedler, A., Veprintsev, D. B., Freund, S. M., von Glos, K. I. & Fersht, A. R. (2005). Modulation of binding of DNA to the C-terminal domain of p53 by acetylation. *Structure* **13**, 629-636.

Fruman, D. A., Meyers, R. E. & Cantley, L. C. (1998). Phosphoinositide kinases. *Annu. Rev. Biochem.* **67**, 481-507.

Futreal, P. A., Coin, L., Marshall, M., Down, T., Hubbard, T., Wooster, R., Rahman, N. & Stratton, M. R. (2004). A census of human cancer genes. *Nature Rev. Cancer* **4**, 177-183.

Gaillard, P., Jeanclaude-Etter, I., Ardissone, V., Arkinstall, S., Cambet, Y., Camps, M., Chabert, C., Church, D., Cirillo, R., Gretener, D., Halazy, S., Nichols, A., Szyndralewiez, C., Vitte, P. A. & Gotteland, J. P. (2005). Design and synthesis of the first generation of novel potent, selective, and in vivo active (benzothiazol-2-yl)acetonitrile inhibitors of the c-Jun N-terminal kinase. *J. Med. Chem.* **48**, 4596-4607.

Go, M. L., Wu, X. & Liu, X. L. (2005). Chalcones: an update on cytotoxic and chemoprotective properties. *Curr. Med. Chem.* **12**, 481-499.

Graczyk, P. P., Khan, A., Bhatia,, G. S., Palmer, V., Medland, D., Numata, H., Oinuma, H., Catchick, J., Dunne, A., Ellis, M., Smales, C., Whitfield, J., Neame, S. J., Shah, B., Wilton, D., Morgan, L., Patel, T., Chung, R., Desmond, H., Staddon, J. M., Sato, N. & Inoue, A. (2005). The neuroprotective action of JNK3 inhibitors based on the 6,7-dihydro-5H-pyrrolo[1,2-a]imidazole scaffold. *Bioorg. Med. Chem. Lett.* **15**, 4666-4670.

Grasberger, B. L., Lu, T., Schubert, C., Parks, D. J., Carver, T. E., Koblish, H. K., Cummings, M. D., LaFrance, L. V., Milkiewicz, K. L., Calvo, R. R., Maguire, D., Lattanze, J., Franks, C. F., Zhao, S., Ramachandren, K., Bylebyl, G. R., Zhang, M., Manthey, C. L., Petrella, E. C., Pantoliano, M. W., Deckman, I. C., Spurlino, J. C., Maroney, A. C., Tomczuk, B. E., Molloy, C. J. & Bone, R. F. (2005). Discovery and cocrystal structure of benzodiazepinedione HDM2 antagonists that activate p53 in cells. *J. Med. Chem*. **48**, 909-912.

Greenblatt, M. S., Bennett, W. P., Hollstein, M. & Harris, C. C. (1994). Mutations in the p53 tumor suppressor gene: clues to cancer etiology and molecular pathogenesis. *Cancer Res*. **54**, 4855-4878.

Grossman, S. R. (2001). p300/CBP/p53 interaction and regulation of the p53 response. *Eur. J. Biochem.* **268**, 2773-2778.

Guillot, C., Falette, N., Paperin, M. P., Courtois, S., Gentil-Perret A., Treilleux, I., Ozturk, M. & Puisieux, A. (1997). p21(WAF1/CIP1) response to genotoxic agents in wild-type TP53 expressing breast primary tumours. *Oncogene* **14**, 45-52.

Gupta, S., Barrett, T., Whitmarsh, A. J., Cavanagh, J., Sluss, H. K., Dérijard, B. & Davis, R. J. (1996). Selective interaction of JNK protein kinase isoforms with transcription factors. *EMBO J.* **15**, 2760-2770.

Gu, W., Shi, X. L. & Roeder, R. G. (1997). Synergisticac tivation of transcription by CBP and p53. *Nature* **387**, 819-823.

Hainaut, P. & Hollstein, M. (2000). p53 and human cancer: the first ten thousand mutations. *Adv. Cancer Res*. **77**, 81-137.

Han, Z., Chang, L., Yamanishi, Y., Karin, M. & Firestein, G. S. (2002). Joint damage and

inflammation in c-Jun N-terminal kinase 2 knockout mice with passive murine collagen-induced arthritis. *Arthritis Rheum.* **46**, 818-823.

Hartwell, L. H. & Weinert, T. A. (1989). Checkpoints: Controls that ensure the order of cell cycle events. *Science* **246**, 629-634.

Haupt, Y., Maya, R., Kazaz, A. & Oren, M. (1997). MDM2 promotes the rapid degradation of p53. *Nature* **387**, 296 -299.

Hay, T. J. & Meek, D. W. (2000). Multiple sites of in vivo phosphorylation in the MDM2 oncoprotein cluster within two important functional domains. *FEBS Lett* **478**, 183-186.

Hibi, M., Lin, A., Smeal, T., Minden, A. & Karin, M. (1993). Identification of an oncoprotein- and UV-responsive protein kinase that binds and potentiates the c-Jun activation domain. *Genes Dev*. **7,** 2135-2148.

Hirosumi, J., Tuncman, G., Chang, L., Görgün, C. Z., Uysal, K. T., Maeda, K., Karin, M. & Hotamisligil, G. S. (2002). A central role for JNK in obesity and insulin resistance. *Nature* **420**, 333-336.

Holder, S., Zemskova, M., Zhang, C., Tabrizizad, M., Bremer, R., Neidigh, J. W. & Lilly, M. B. (2007). Characterization of a potent and selective small molecule inhibitor of the PIM1 kinase. *Mol. Cancer Ther*. **6**, 163-172.

Hubbard, S. R. (1997). Crystal structure of the activated insulin recep tor tyrosine kinase in complex with peptide substrate and ATP ana log. *EMBO J*. **16**, 5572-5581.

Hunot, S., Vila, M., Teismann, P., Davis, R. J., Hirsch, E. C., Przedborski, S., Rakic, P. & Flavell, R. A. (2004). JNK-mediated induction of cyclooxygenase 2 is required for neurodegeneration in a mouse model of Parkinson's disease. *Proc. Natl. Acad. Sci. USA* **101**, 665-670.

Huse, M. & Kuriyan, J. (2002). The conformational plasticity of protein kinases. *Cell* **109**, 275-282.

Hwang, M. K., Song, N. R., Kang, N. J., Lee, K. W. & Lee, H. J. (2009). Activation of phosphatidylinositol 3-kinase is required for tumor necrosis factor-alpha-induced upregulation of matrix metalloproteinase-9: Its direct inhibition by quercetin. *Int. J. Biochem. Cell. Biol.* **41**, 1592-1600.

Ip, Y. T. & Davis, R. J. (1998). Signal transduction by the c-Jun N-terminal kinase (JNK)–from inflammation to development. *Curr. Opin. Cell. Biol*. **10**, 205-219.

Isobe, M., Emanuel, B. S., Givol, D., Oren, M. & Croce, C. M. (1986). Localization of gene for human p53 tumour antigen to band 17p13. *Nature* **320**, 84-85.

Israels, E. D. & Israels, L. G. (2000). The cell cycle. *Oncologist* **5**, 510-513.

Iwakuma, T. & Lozano, G.(2003). MDM2, an introduction. *Mol. Cancer Res*. **1**, 993-1000.

Joerger, A. C. & Fersht, A. R. (2010). The tumor suppressor p53: from structures to drug discovery. *Cold Spring Harb Perspect Biol.* **2**(6):a000919.

Johnson, L. N., Noble, M. E. & Owen, D. J. (1996). Active and inactive protein kinases: structural basis for regulation. *Cell* **85**, 149-158.

Joseph, T. L., Lane, D. & Verma, C. S. (2010b). Stapled peptides in the p53 pathway: computer simulations reveal novel interactions of the staples with the target protein. *Cell Cycle* **9**, 4560-4568.

Joseph, T. L., Madhumalar, A., Brown, C. J., Lane, D. P. & Verma, C. S. (2010a) Differential binding of p53 and nutlin to MDM2 and MDMX: computational studies. *Cell Cycle* **9**, 1167-1181.

Jung, S. K., Lee, K. W., Byun, S., Kang, N. J., Lim, S. H., Heo, Y. S., Bode, A. M., Bowden, G. T., Lee, H. J. & Dong, Z. (2008). Myricetin suppresses UVB-induced skin cancer by targeting Fyn. *Cancer Res*. **68**, 6021-6029.

Jung, S. K., Lee, K. W., Byun, S., Lee, E. J., Kim, J. E., Bode, A. M., Dong, Z. & Lee, H. J. (2010a). Myricetin inhibits UVB-induced angiogenesis by regulating PI-3 kinase in vivo. *Carcinogenesis* **31**, 911-917.

Jung, S. K., Lee, K. W., Kim, H. Y., Oh, M. H., Byun, S., Lim, S. H., Heo, Y. S., Kang, N. J., Bode, A. M., Dong, Z. & Lee, H. J. (2010b). Myricetin suppresses UVB-induced wrinkle formation and MMP-9 expression by inhibiting Raf. *Biochem Pharmacol*. **79**, 1455-1461.

Juven-Gershon, T. & Oren, M. (1999). Mdm2: the ups and downs. *Mol. Med.* **5**, 71-83.

Kabsch, W. J. (1993). Automatic processing of rotation diffraction data from crystals of initially

unknown symmetry and cell constants. *Appl. Cryst*. **26**, 795-800.

Kallunki, T., Deng, T., Hibi, M. & Karin, M. (1886). c-Jun can recruit JNK to phosphorylate dimerization partners via specific docking interactions. *Cell* **87**, 929-939.

Kaneto, H., Matsuoka, T. A., Nakatani, Y., Kawamori, D., Matsuhisa, M. & Yamasaki, Y. (2005). Oxidative stress and the JNK pathway in diabetes. *Curr. Diabetes Rev.* **1**, 65-72.

Kang, N. J., Shin, S. H., Lee, H. J. & Lee, K. W. (2011). Polyphenols as small molecular inhibitors of signaling cascades in carcinogenesis. *Pharmacol Ther*. 130, 310-324.

Karin, M. (1995). The regulation of AP-1 activity by mitogen-activated protein kinases. *J. Biol. Chem.* **270,** 16483-16486.

Karin, M. & Gallagher, E. (2005). From JNK to pay dirt: jun kinases, their biochemistry, physiology and clinical importance. *IUBMB Life* **57**, 283-295.

Kastan, M. B., Onyekwere, O., Sidransky, D., Vogelstein, B. & Craig, R. W. (1991). Participation of p53 protein in the cellular response to DNA damage. *Cancer Res*. **51**, 6304-6311.

Katso, R., Okkenhaug, K., Ahmadi, K., White, S., Timms, J. & Waterfield, M. D. (2001). Cellular function of phosphoinositide 3-kinases: implications for development, homeostasis, and cancer. *Annu. Rev. Cell Dev. Biol.* **17**, 615-675.

Kennedy, N. J. & Davis, R. J. (2003). Role of JNK in tumor development. *Cell Cycle* **2**, 199-201.

Kern, S. E., Kinzler, K. W., Bruskin, A., Jarosz, D., Friedman, P., Prives, C. & Vogelstein, B. (1991). Identification of p53 as a sequence-specific DNA-binding protein. *Science* **252**, 1708-1711.

Kern, S. E., Kinzler, K. W., Baker, S. J., Nigro, J. M., Rotter, V., Levine, A. J., Friedman, P., Prives, C. & Vogelstein, B. (1991). Mutant p53 proteins bind DNA abnormally *in vitro. Oncogene* **6**, 131-136.

Kim, J. E., Kwon, J. Y., Lee, D. E., Kang, N. J., Heo, Y. S., Lee, K. W. & Lee, H. J. (2009). MKK4 is a novel target for the inhibition of tumor necrosis factor-alpha-induced vascular endothelial growth factor expression by myricetin. *Biochem Pharmacol.* **77**, 412-421.

Kim, Y. W., Grossmann, T. N. & Verdine, G. L. (2011). Synthesis of all-hydrocarbon stapled α-helical

peptides by ring-closing olefin metathesis. *Nat. Protoc*. **6**, 761-771.

Kontzias, A., Laurence, A., Gadina, M. & O'Shea, J. J. (2012). Kinase inhibitors in the treatment of immune-mediated disease. F1000 *Med Rep*. 4:5.

Kubbutat, M. H. & Vousden, K. H. (1997). Proteolytic cleavage of human p53 by calpain: a potential regulator of protein stability. *Mol. Cell. Biol*. **17**, 460-468.

Kumamoto, T., Fujii, M. & Hou, D. X. (2009). Myricetin directly targets JAK1 to inhibit cell transformation. *Cancer Lett* **275**, 17-26.

Kumar, V., Abbas, A. K. & Fausto, N. (2004). Robbins and Cotran Pathological Basis of Disease. Elsevier. ISBN 81-8147-528-3.

Kussie, P. H., Gorina, S., Marechal, V., Elenbaas, B., Moreau, J., Levine, A. J. & Pavletich, N. P. (1996). Structure of the MDM2 oncoprotein bound to the p53 tumor suppressor transactivation domain. *Science* **274**, 948-953.

Kyriakis, J. M. & Avruch, J. (2001). Mammalian mitogen-activated protein kinase signal transduction pathways activated by stress and inflammation. *Physiol. Rev.* **81**, 807-869.

Lane, D. P. & Crawford, L. V. (1979). T antigen is bound to a host protein in SV40-transformed cells. *Nature* **278**, 261-263.

Lee, H., Mok, K. H., Muhandiram, R., Park, K. H., Suk, J. E., Kim, D. H., Chang, J., Sung, Y. C., Choi, K. Y. & Han, K. H. (2000). Local structural elements in the mostly unstructured transcriptional activation domain of human p53. *J. Biol. Chem.* **275**, 29426-29432.

Lee, K. M., Lee, K. W., Byun, S., Jung, S. K., Seo, S. K., Heo, Y. S., Bode, A. M., Lee, H. J. & Dong, Z. (2010e). 5-deoxykaempferol plays a potential therapeutic role by targeting multiple signaling pathways in skin cancer. *Cancer Prev. Res.* (Phila Pa) **3**, 454-465.

Lee, K. M., Lee, K. W., Jung, S. K., Lee, E. J., Heo, Y. S., Bode, A. M., Lubet, R. A., Lee, H. J. & Dong, Z. (2010f). Kaempferol inhibits UVB-induced COX-2 expression by suppressing Src kinase activity. *Biochem Pharmacol* **80**, 2042-2049.

Lee, K. M., Lee, D. E., Seo, S. K., Hwang, M. K., Heo, Y. S., Lee, K. W. & Lee, H. J. (2010d).

Phosphatidylinositol 3-kinase, a novel target molecule for the inhibitory effects of kaempferol on neoplastic cell transformation. *Carcinogenesis* **31**, 1338-1343.

Lee, K. W., Kang, N. J., Rogozin, E. A., Kim, H. G., Cho, Y. Y., Bode, A. M., Lee, H. J., Surh, Y. J., Bowden, G. T. & Dong, Z. (2007). Myricetin is a novel natural inhibitor of neoplastic cell transformation and MEK1. *Carcinogenesis* **28**, 1918-1927.

Lee, K. W., Kang, N. J., Heo, Y. S., Rogozin, E. A., Pugliese, A., Hwang, M. K., Bowden, G. T., Bode, A. M., Lee, H. J. & Dong, Z. (2008b). Raf and MEK protein kinases are direct molecular targets for the chemopreventive effect of quercetin, a major flavonol in red wine. *Cancer Res*. **68**, 946-955.

Lee, T., Hoofnagle, A. N., Resing, K. A. & Ahn, N. G. (2005). Hydrogen exchange solvent protection by an ATP analogue reveals conformational changes in ERK2 upon activation. *J Mol Biol.* **353**, 600-612.

Leevers, S. J., Vanhaesebroeck, B. & Waterfield, M. D. (1999). Signalling through phosphoinositide 3-kinases: the lipids take centre stage. *Curr. Opin. Cell. Biol*. **11**, 219-225.

Levine, A. J. (1997). p53, the cellular gatekeeper for growth and division. *Cell* **88**, 323-331.

Lew, J. (2003). MAP kinases and CDKs: kinetic basis for catalytic activation. *Biochemistry* **42**, 849-856.

Lin, A. (2003). Activation of the JNK signaling pathway: breaking the break on apoptosis. *Bioessays* **25,** 1-8.

Lin, D., Shields, M. T., Ullrich, S. J., Appella, E. & Mercer, W. E. (1992). Growth arrest induced by wild-type p53 protein blocks cells prior to or near the restriction point in late G1 phase. *Proc. Natl. Acad. Sci. USA* **89**,9210-9214.

Lindstrom, M. S., Jin, A., Deisenroth, C., White Wolf, G. & Zhang, Y. (2007). Cancer-associated mutations in the MDM2 zinc finger domain disrupt ribosomal protein interaction and attenuate MDM2-induced p53 degradation. *Mol. Cell. Biol.* **27**, 1056-1068.

Linzer, D. I. & Levine, A. J. (1979). Characterization of a 54 K Dalton cellular SV40 tumor antigen present in SV40-transformed cells and uninfected embryonal carcinoma cells. *Cell* **17**, 43-52.

Liu, G., Zhao, H., Liu, B., Xin, Z., Liu, M., Kosogof, C., Szczepankiewicz, B. G., Wang, S., Clampit, J. E., Gum, R. J., Haasch, D. L., Trevillyan, J. M. & Sham, H. L. (2006). Aminopyridine carboxamides as c-Jun Nterminal kinase inhibitors: targeting the gatekeeper residue and beyond. *Bioorg. Med. Chem. Lett.* **16**, 5723-5730.

Liu, M., Xin, Z., Clampit, J. E., Wang, S., Gum, R. J., Haasch, D. L., Trevillyan, J. M., Abad-Zapatero, C., Fry, E. H., Sham, H. L. & Liu, G. (2006). Synthesis and SAR of 1,9-dihydro-9-hydroxypyrazolo[3,4-b]quinolin-4-ones as novel, selective c-Jun N-terminal kinase inhibitors. *Bioorg. Med. Chem. Lett.* **16**, 2590-2594.

Liu, M., Wang, S., Clampit, J. E., Gum, R. J., Haasch, D. L., Rondinone, C. M., Trevillyan, J. M., Abad-Zapatero, C., Fry, E. H., Sham, H. L. & Liu, G. (2007). Discovery of a new class of 4-anilinopyrimidines as potent c-Jun N-terminal kinase inhibitors: synthesis and SAR studies. *Bioorg. Med. Chem. Lett*. **17**, 668-672.

Lu, H., Chang, D. J., Baratte, B., Meijer, L. & Schulze-Gahmen, U. (2005). Crystal structure of a human cyclin-dependent kinase 6 complex with a flavonol inhibitor, fisetin. *J. Med. Chem.* **48**, 737-743.

Manning, G., Whyte, D. B., Martinez, R., Hunter, T. & Sudarsanam, S. (2002). The protein kinase complement of the human genome. *Science* **298**, 1912-1934.

Marine, J. C., Dyer, M. A. & Jochemsen, A. G. (2007). MDMX: from bench to bedside. *J. Cell Sci.* **120**, 371-378.

Maroney, A. C., Finn, J. P., Connors, T. J., Durkin, J. T., Angeles, T., Gessner, G., Xu, Z., Meyer, S. L., Savage, M. J., Greene, L. A., Scott, R. W. & Vaught, J. L. (2001). Cep-1347 (KT7515), a semisynthetic inhibitor of the mixed lineage kinase family. *J Biol Chem.* **276**, 25302-25308.

Marshall, C. J. (1994). MAP kinase kinase kinase, MAP kinase kinase and MAP kinase. *Curr. Opin. Gene.t Dev.* **4**, 82-89.

Noble, M. E., Endicott, J. A. & Johnson, L. N. (2004). Protein Kinase Inhibitors: Insights into Drug Design from Structure. *Science* **303**, 1800-1805.

Martin, J. H., Mohit, A. A. & Miller, C. A. (1996). Developmental expression in the mouse nervous system of the p493F12 SAP kinase. *Mol. Brain Res*. **35**, 47-57.

Martin, T. F. (1998). Phosphoinositide lipids as signaling molecules: common themes for signal transduction, cytoskeletal regulation, and membrane trafficking. *Annu. Rev. Cell. Dev. Biol.* **14**, 231-264.

Matlashewski, G., Lamb, P., Pim, D., Peacock, J., Crawford, L. & Benchimol, S. (1984). Isolation and characterization of a human p53 cDNA clone: expression of the human p53 gene. *EMBO J.* **3**, 3257-3262.

Maundrell, K., Antonsson, B., Magnenat, E., Camps, M., Muda, M., Chabert, C., Gillieron, C., Boschert, U., Vial-Knecht, E., Martinou, J. C. & Arkinstall, S. (1997). Bcl-2 undergoes phosphorylation by c-Jun N-terminal kinase/stress- activated protein kinases in the presence of the constitutively active GTP binding protein Rac1. *J. Biol. Chem.* **272,** 25238-25242.

McBride, O. W., Merry, D. & Givol, D. (1986). The gene for human p53 cellular tumor antigen is located on chromosome 17 short arm (17p13). Proc. Natl. Acad. Sci. U.S.A. **83**, 130-134.

McRee, D. E. (1999). XtalView/Xfit--A versatile program for manipulating atomic coordinates and electron density. *J. Struct. Biol*. **125**, 156-165.

Mendrysa, S. M. & Perry, M. E. (2000). The p53 tumor suppressor protein does not regulate expression of its own inhibitor, MDM2, except under conditions of stress. *Mol. Cell. Biol.* **20**, 2023-2030.

Miller, C. & Koeffler, H. P. (1993). P53 mutations in human cancer. *Leukemia* **7**, S18.

Moellering, R. E., Cornejo, M., Davis, T. N., Del Bianco, C., Aster, J. C., Blacklow, S. C., Kung, A. L., Gilliland, D. G., Verdine, G. L. & Bradner JE. (2009). Direct inhibition of the NOTCH transcription factor complex. *Nature* **462**, 182-188.

Momand, J., Zambetti, G. P., Olson, D. C., George, D. & Levine, A. J. (1992). The mdm-2 oncogene product forms a complex with the p53 protein and inhibits p53-mediated transactivation. *Cell* **69**, 1237-1245.

Murray, J. K. & Gellman, S. H. (2007). Targeting protein-protein interactions: Lessons from p53/MDM2. *Biopolymers* **88,** 657-686.

Nagar, B., Bornmann, W. G., Pellicena, P., Schindler, T., Veach, D. R., Miller, W. T., Clarkson, B. &

Kuriyan, J. (2002). Crystal structures of the kinase domain of c-Abl in complex with the small molecule inhibitors PD173955 and imatinib (STI-571). *Cancer Res* **62**, 4236-4243.

Newman, D. J. (2008). Natural Products as Leads to Potential Drugs: An Old Process or the New Hope for Drug Discovery? *J. Med. Chem.* **51**, 2589-2599.

Newman, D. J., Cragg, G. M. & Snader, K. M. (2003). Natural Products as Sources of New Drugs over the Period 1981-2002. *J. Nat. Prod.* **66**, 1022-1037.

Nigro, J. M., Baker, S. J., Preisinger, A. C., Jessup, J. M., Hostetter, R., Cleary, K., Bigner, S. H., Davidson, N., Baylin, S., Devilee, P., Glover, T., Collins, F. S., Weston, A., Modali, R., Harris, C. C. & Vogelstein, B. (1989). Mutations in the p53 gene occur in diverse human tumour types. *Nature* **342**, 705-708.

Oliner, J. D., Pietenpol, J. A., Thiagalingam, S., Gyuris, J., Kinzler, K. W. & Vogelstein, B. (1993). Oncoprotein MDM2 conceals the activation domain of tumour suppressor p53. *Nature* **362**, 857-860.

Pan, Y. & Chen, J. (2003). MDM2 promotes ubiquitination and degradation of MDMX. *Mol. Cell. Biol.* **23**, 5113-5121.

Patrick, Chène. (2003). Inhibiting the p53–MDM2 interaction: an important target for cancer therapy. *Nature Reviews Cancer* **3**, 102-109.

Paules, R. S., Levedakou, E. N., Wilson, S. J., Innes, C. L., Rhodes, N., Tlsty, T. D., Galloway, D. A., Donehower, L. A., Tainsky, M. A. & Kaufmann, W. K. (1995). Defective G2 checkpoint function in cells from individuals with familial cancer syndromes. *Cancer Res.* **55**, 1763-1773.

Pavletich, N. P., Chambers, K. A. & Pabo, C. O. (1993). The DNA-binding domain of p53 contains the four conserved regions and the major mutation hot spots. *Genes Dev.* **7**, 2556-2564.

Payne, D. M., Rossomando, A. J., Martino, P., Erickson, A. K., Her, J.-H., Shabanowitz, J., Hunt, D. F., Weber, M. J. & Sturgill, T. W. (1991). Identification of the regulatory phosphorylation sites in pp42/ mitogen-activated protein kinase (MAP kinase). *EMBO J.* **10**, 885-892.

Pelaia, G., Cuda, G., Vatrella, A., Gallelli, L., Caraglia, M., Marra, M., Abbruzzese, A., Caputi, M., Maselli, R., Costanzo, F. S. & Marsico, S. A. (2005). Mitogen-activated protein kinases and asthma. *J. Cell. Physiol.* **202**, 642-653.

Petitjean, A., Mathe, E., Kato, S., Ishioka, C., Tavtigian, S. V., Hainaut, P. & Olivier, M. (2007). Impact of mutant p53 functional properties on TP53 mutation patterns and tumor phenotype: Lessons from recent developments in the IARC TP53 database. *Hum. Mutat.* **28**, 622-629.

Pietenpol, J. A., Tokino, T., Thiagalingam, S., el-Deiry, W. S., Kinzler, K. W. & Vogelstein, B. (1994). Sequence-specific transcriptional activation is essential for growth suppression by p53. Proc. Natl. Acad. Sci. USA **91**, 1998-2002.

Popowicz, G. M., Czarna, A., Wolf, S., Wang, K., Wang, W., Domling, A. & Holak, T. A. (2010). Structures of low molecular weight inhibitors bound to MDMX and MDM2 reveal new approaches for p53-MDMX/MDM2 antagonist drug discovery. *Cell Cycle* **9**, 1104-1111.

Prives, C. & Manley, J. L. (2001). Why is p53 acetylated? *Cell* **107**, 815-818.

Robbins, D. J. & Cobb, M. H. (1992). ERK2 autophosphorylates on a subset of peptides phosphorylated in intact cells in response to insulin and nerve growth factor: analysis by peptide mapping. *Mol. Biol. Cell* **3**, 299-308.

Robbins, D. J., Zhen, E., Owaki, H., Vanderbilt, C. A., Ebert, D., Geppert, T. D. & Cobb, M. H. (1993). Regulation and properties of extracellular signal-regulated protein kinases 1 and 2 in vitro. *J. Biol. Chem.* **268**, 5097-5106.

Roberts, J. J. & Thompson, A. J. (1979). The mechanism of action of anti-tumor platinum compounds. *Prog. Nucleic Acid Res. Mol. Biol.* **22**, 71-133.

Rubin, G. M., Yandell, M. D., Wortman, J. R., Gabor Miklos, G. L., Nelson, C. R., Hariharan, I. K., Fortini, M. E., Li, P. W., Apweiler, R., Fleischmann, W., Cherry, J. M., Henikoff, S., Skupski, M. P., Misra, S., Ashburner, M., Birney, E., Boguski, M. S., Brody, T., Brokstein, P., Celniker, S. E., Chervitz, S. A., Coates, D., Cravchik, A., Gabrielian, A., Galle, R. F., Gelbart, W. M., George, R. A., Goldstein, L. S., Gong, F., Guan, P., Harris, N. L., Hay, B. A., Hoskins, R. A., Li, J., Li, Z., Hynes, R. O., Jones, S. J., Kuehl, P. M., Lemaitre, B., Littleton, J. T., Morrison, D. K., Mungall, C., O'Farrell, P. H., Pickeral, O. K., Shue, C., Vosshall, L. B., Zhang, J., Zhao, Q., Zheng, X. H. & Lewis, S. (2000) Comparative genomics of the eukaryotes. *Science* **287**, 2204-2215.

Ruckle, T., Biamonte, M., Grippi-Vallotton, T., Arkinstall, S., Cambet, Y., Camps, M., Chabert, C., Church, D. J., Halazy, S., Jiang, X., Martinou, I., Nichols, A., Sauer, W. & Gotteland, J. P. (2004). Design, synthesis, and biological activity of novel, potent, and selective (benzoylaminomethyl)

thiophene sulfonamide inhibitors of c-Jun–N-terminal kinase. *J. Med. Chem*. **47**, 6921-6934.

Sabio, G. & Davis, R. J. (2010). cJun NH2-terminal kinase 1 (JNK1): roles in metabolic regulation of insulin resistance. *Trends Biochem. Sci*. **35**, 490-496.

Scapin, G., Patel, S. B., Lisnock, J., Becker, J. W. & LoGrasso, P. V. (2003). The structure of JNK3 in complex with small molecule inhibitors: structural basis for potency and selectivity. *Chem. Biol*. **10**, 705-712.

Schafmeister, C., Po, J. & Verdine, G. L. (2000). An all-hydrocarbon cross-linking system for enhancing the helicity and metabolic stability of peptides. *J. Am. Chem. Soc*. **122**, 5891-5892.

Selivanova, G., Iotsova, V., Kiseleva, E., Ström, M., Bakalkin, G., Grafström, R. C. & Wiman, K. G. (1996). The single-stranded DNA end binding site of p53 coincides with the C-terminal regulatory region. *Nucleic Acids Res.* **24**, 3560-3567.

Selivanova, G., Iotsova, V., Kiseleva, E., Ström, M., Bakalkin, G., Grafström, R. C., Wiman, K. G. & Lane, D. P. (1992). p53, guardian of the genome. *Nature* **358**, 15-16.

Shangary, S. & Wang, S. M. (2008). Small-molecule inhibitors of the MDM2-p53 protein-protein interaction to reactivate p53 function: a novel approach for cancer therapy. *Annu. Rev. Pharmacol. Toxicol*. **49**, 223-241.

Shaulian, E. & Karin, M. (2002). AP-1 as a regulator of cell life and death. *Nat. Cell. Biol.* **4,** E131-136.

Sherr, C. J. & Roberts, J. M. (1995). Inhibitors of mammalian G1 cyclin-dependent kinases. *Genes Dev.* **9**, 1149-1163.

Smeal, T., Binetruy, B., Mercola, D. A., Birrer, M. & Karin, M. (1991). Oncogenic and transcriptional cooperation with Ha-Ras requires phosphorylation of c-Jun on serines 63 and 73. *Nature* **354**, 494-496.

Stewart, Z. A. & Pietenpol, J. A. (2001). p53 Signaling and cell cycle checkpoints. *Chem. Res. Toxicol.* **14**, 243-263

Stoll, R., Renner, C., Hansen, S., Palme, S., Klein, C., Belling, A., Zeslawski, W., Kamionka, M., Rehm, T., Mühlhahn, P., Schumacher, R., Hesse, F., Kaluza, B., Voelter, W., Engh, R. A. & Holak, T.

A. (2001). Chalcone derivatives antagonize interactions between the human oncoprotein MDM2 and p53. *Biochemistry* **40**, 336-344.

Stürzbecher, H. W., Brain, R., Addison, C., Rudge, K., Remm, M., Grimaldi, M., Keenan, E. & Jenkins, J. R. (1992). A C-terminal alpha-helix plus basic region motif is the major structural determinant of p53 tetramerization. *Oncogene* **7**, 1513-1523.

Sui, G., Affar el, B., Shi, Y., Brignone, C., Wall, N. R., Yin, P., Donohoe, M., Luke, M. P., Calvo, D., Grossman, S. R. & Shi, Y. (2004). Yin Yang 1 is a negative regulator of p53. *Cell* **117**, 859-872.

Sun, H., Charles, C. H., Lau, L. F. & Tonks, N. K. (1993). MKP-1 (3CH1–34), an immediate early gene product, is a dual specificity phosphatase that dephosphorylates MAP kinase in vivo. *Cell* **75**, 487-493.

Swahn, B. M., Huerta, F., Kallin, E., Malmström, J., Weigelt, T., Viklund, J., Womack, P., Xue, Y. & Ohberg, L. (2005). Design and synthesis of 6-anilinoindazoles as selective inhibitors of c-Jun N-terminal kinase-3, *Bioorg. Med. Chem. Lett.* **15**, 5095-5099.

Swahn, B. M., Xue, Y., Arzel, E., Kallin, E., Magnus, A., Plobeck, N. & Viklund, J. (2006). Design and synthesis of 2'-anilino-4,4'-bipyridines as selective inhibitors of c-JunN-terminal kinase-3. *Bioorg.Med.Chem. Lett.* **16**, 1397-1401.

Szczepankiewicz, B. G., Kosogof, C., Nelson, L. T., Liu, G., Liu, B., Zhao, H., Serby, M. D., Xin, Z., Liu, M., Gum, R. J., Haasch, D. L., Wang, S., Clampit, J. E., Johnson, E. F., Lubben, T. H., Stashko, M. A., Olejniczak, E. T., Sun, C., Dorwin, S. A., Haskins, K., Abad-Zapatero, C., Fry, E. H., Hutchins, C. W., Sham, H. L., Rondinone, C. M. & Trevillyan, J. M. (2006). Aminopyridinebased c-Jun N-terminal kinase inhibitors with cellular activity and minimal cross-kinase activity. *J. Med. Chem.* **49**, 3563-3580.

Thalhamer, T., McGrath, M. A. & Harnett, M. M. (2008). MAPKs and their relevance to arthritis and inflammation. *Rheumatology* (Oxford) **47**, 409-414.

Tokino, T., Thiagalingam, S., El-Deiry, W. S., Waldmann, T., Kinzler, K. W. & Vogelstein, B. (1994). p53 tagged sites from human genomic DNA. *Hum. Mol. Genet.* **3**, 1537-1542.

Tournier, C., Hess, P., Yang, D. D., Xu, J., Turner, T. K., Nimnual, A., Bar-Sagi, D., Jones, S. N., Flavell, R. A. & Davis, R. J. (2000). Requirement of JNK for stress-induced activation of the

cytochrome c-mediated death pathway. *Science* **288**, 870-874.

Vanhaesebroeck, B., Guillermet-Guibert, J., Graupera, M. & Bilanges, B. (2010). The emerging mechanisms of isoform-specific PI3K signalling. *Nat. Rev. Mol. Cell. Biol.* **11**, 329-341.

Vassilev, L. T. (2007). MDM2 inhibitors for cancer therapy. *Trends Mol. Med.* **13**, 23-31.

Vassilev, L. T., Vu, B. T., Graves, B., Carvajal, D., Podlaski, F., Filipovic, Z., Kong, N., Kammlott, U., Lukacs, C., Klein, C., Fotouhi, N. & Liu, E. A. (2004). In vivo activation of the p53 pathway by small molecule antagonists of MDM2. *Science* **303**, 844-848.

Venot, C., Maratrat, M., Dureuil, C., Conseiller, E., Bracco, L. & Debussche, L. (1998). The requirement for the p53 prolinerich functional domain for mediation of apoptosis is correlated with specific PIG3 gene transactivation and with transcriptional repression. *EMBO J.* **17**, 4668-4679.

Vivanco, I. & Sawyers, C. L. (2002). The phosphatidylinositol 3 kinase AKT pathway in human cancer. *Nature Rev. Cancer* **2**, 489-501.

Vivanco, I., Palaskas, N., Tran, C., Finn, S. P., Getz, G. & Kennedy, N. J. (2007). Identification of the JNK signaling pathway as a functional target of the tumor suppressor PTEN. *Cancer Cell*, **11**, 555-569.

Vousden, K. H. & Lu, X. (2002). Live or let die: the cell's response to p53. *Nat. Rev. Cancer* **2**,594-604.

Wagner, E. F. & Nebreda, A. R. (2009). Signal integration by JNK and p38 MAPK pathways in cancer development. *Nat. Rev. Cancer* **9**, 537-549.

Walensky, L. D., Kung, A. L., Escher, I., Malia, T. J., Barbuto, S., Wright, R. D., Wagner, G., Verdine, G. L. & Korsmeyer, S. J. (2004). Activation of apoptosis in vivo by a hydrocarbon-stapled BH3 helix. *Science* **305**, 1466-1470.

Walker, K. K. & Levine, A. J. (1996). Identification of a novel p53 functional domain that is necessary for efficient growth suppression. *Proc. Natl. Acad. Sci. U.S.A.* **93**, 15335-15340.

Wang, S., Zhao, Y., Bernard, D., Aguilar, A. & Kumar, S. (2012). Targeting the MDM2-p53 Protein-Protein Interaction for New Cancer Therapeutics. *Top. Med. Chem.* **8**, 57-80.

Waskiewicz, A. J. & Cooper, J. A. (1995). Mitogen and stress response pathways: MAP kinase cascades and phosphatase regulation in mammals and yeast. *Curr. Opin. Cell. Biol*. **7**, 798-805.

Weinberg, R. L., Freund, S. M., Veprintsev, D. B., Bycroft, M. & Fersht, A. R. (2004). Regulation of DNA binding of p53 by its C-terminal domain. *J. Mol. Biol.* **342**, 801-811.

Weston, C. R. & Davis, R. J. (2002). The JNK signal transduction pathway. *Curr. Opin. Genet. Dev*. **12,** 14-21.

Widmann, C., Gibson, S., Jarpe, M. B. & Johnson, G. L. (1999). Mitogen-activated protein kinase: conservation of a three-kinase module from yeast to human. *Physiol Rev*. **79**, 143-180.

Wong, W. S. (2005). Inhibitors of the tyrosine kinase signaling cascade for asthma. *Curr. Opin. Pharmacol.* **5**, 264-271.

Wu, G. S. (2004). The functional interactions between the p53 and MAPK signaling pathways. *Cancer. Biol. Ther.* **3**, 156-161.

Wu, X., Bayle, J. H., Olson, D. & Levine, A. J. (1993). The p53–mdm-2 autoregulatory feedback loop. *Genes Dev*. **7**, 1126-1132.

Yamamoto, K., Ichijo, H. & Korsmeyer, S. J. (1999). BCL-2 is phosphorylated and inactivated by an ASK1/Jun N-terminal protein kinase pathway normally activated at G(2)/M. *Mol. Cell. Biol.* **19,** 8469-8478.

Yu, C., Minemoto, Y., Zhang, J., Liu, J., Tang, F., Bui, T. N., Xiang, J. & Lin, A. (2004). JNK suppresses apoptosis via phosphorylation of the proapoptotic Bcl-2 family protein BAD. *Molecular Cell* **13,** 329-340.

Zauberman, A., Flusberg, D., Haupt, Y., Barak, Y. & Oren, M. (1995). A functional p53-responsive intronic promoter is contained within the human mdm2 gene. *Nucleic Acids Res.* **23**, 2584-2592.

Zhan, Q., Carrier, F. & Fornace, A. J. Jr. (1993). Induction of cellular p53 activity by DNA-damaging agents and growth arrest. *Mol. Cell. Biol.* **13**,4242-4250.

Zhang, G. Y. & Zhang, Q. G. (2005). Agents targeting c-Jun N-terminal kinase pathway as potential neuroprotectants. *Expert Opin. Investig. Drugs* **14**, 1373-1383.

Zhang, J., Strand, A., Robbins, D., Cobb, M. H. & Goldsmith, E. J. (1994). Atomic structure of the MAP kinase ERK2 at 2.3A° resolution. *Nature* **367**, 704-711.

Zhang, J., Yang, P. L. & Gray, N. S. (2009). Targeting cancer with small molecule kinase inhibitors. *Nature Rev.Cancer* **9**, 28-39.

Zhao, H., Serby, M. D., Xin, Z., Szczepankiewicz, B. G., Liu, M., Kosogof, C., Liu, B., Nelson, L. T., Johnson, E. F., Wang, S., Pederson, T., Gum, R. J., Clampit, J. E., Haasch, D. L., Abad-Zapatero, C., Fry, E. H., Rondinone, C., Trevillyan, J. M., Sham, H. L. & Liu, G. (2006). Discovery of potent, highly selective, and orally bioavailable pyridine carboxamide c-Jun NH2-terminal kinase inhibitors. *J. Med. Chem.* **49**, 4455-4458.

Zheng, C-F. & Guan, K-L. (1993). Dephosphorylation and inacti vation of the mitogen-activated protein kinase by a mitogen-induced Thr/Tyr protein phosphatase. *J. Biol. Chem.* **268**, 16116-16119.

Zheng, J., Knighton, D. R., TenEyck, L. F., Karlsson, R., Xuong, N-H., Taylor, S. S. & Sowadski, J. M. (1993). Crystal structure of the catalytic subunit of c-AMP-dependent protein kinase complexed with Mg/ATP and peptide inhibitor. *Biochemistry* **32**, 2154-2161.

jmb Article

Structural and Functional Analysis of the Natural JNK1 Inhibitor Quercetagetin

Sohee Baek[1,2,3†], Nam Joo Kang[4,5†], Grzegorz M. Popowicz[1], Marcelino Arciniega[1,2], Sung Keun Jung[5], Sanguine Byun[5,6], Nu Ry Song[5,6], Yong-Seok Heo[7], Bo Yeon Kim[8], Hyong Joo Lee[6], Tad A. Holak[1,9], Martin Augustin[10], Ann M. Bode[5], Robert Huber[1,2,11,12], Zigang Dong[5] and Ki Won Lee[3,6]

1 - Max Planck Institute for Biochemistry, *Am Klopferspitz 18, 82152 Martinsried, Germany*
2 - Department of Chemistry, *Technical University of Munich, Lichtenbergstraße 4, 85748 Garching, Germany*
3 - Advanced Institutes of Convergence Technology, *Seoul National University, Suwon 443-270, Republic of Korea*
4 - School of Applied Biosciences, *Kyungpook National University, Daegu 702-701, Republic of Korea*
5 - The Hormel Institute, *University of Minnesota, Austin, MN 55912, USA*
6 - WCU Biomodulation Major, *Department of Agricultural Biotechnology, Seoul National University, Seoul 151-921, Republic of Korea*
7 - Department of Chemistry, *Konkuk University, Seoul 143-701, Republic of Korea*
8 - Chemical Biology Research Center, *Korea Research Institute of Bioscience and Biotechnology, Cheongwongun 363-883, Republic of Korea*
9 - Department of Chemistry, *Jagiellonian University, Ul. Ingardena 3, 30-060 Krakow, Poland*
10 - Proteros Biostructures GmbH, *Bunsenstr. 7a, 82152 Martinsried, Germany*
11 - School of Biosciences, *Cardiff University, Cardiff CF10 3US, Wales, UK*
12 - Center for Medical Biotechnology, *University of Duisburg-Essen, 45117 Essen, Germany*

Correspondence to Zigang Dong and Ki Won W. Lee: *K. W. Lee, Advanced Institutes of Convergence Technology, Seoul National University, Suwon 443-270, Republic of Korea. zgdong@hi.umn.edu; kiwon@snu.ac.kr*
http://dx.doi.org/10.1016/j.jmb.2012.10.019
Edited by M. Guss

Abstract

c-Jun NH2-terminal kinases (JNKs) and phosphatidylinositol 3-kinase (PI3-K) play critical roles in chronic diseases such as cancer, type II diabetes, and obesity. We describe here the binding of quercetagetin (3,3′,4′,5,6,7-hydroxyflavone), related flavonoids, and SP600125 to JNK1 and PI3-K by ATP-competitive and immobilized metal ion affinity-based fluorescence polarization assays and measure the effect of quercetagetin on JNK1 and PI3-K activities. Quercetagetin attenuated the phosphorylation of c-Jun and AKT, suppressed AP-1 and NF-κB promoter activities, and also reduced cell transformation. It attenuated tumor incidence and reduced tumor volumes in a two-stage skin carcinogenesis mouse model.

Our crystallographic structure determination data show that quercetagetin binds to the ATP-binding site of JNK1. Notably, the interaction between Lys55, Asp169, and Glu73 of JNK1 and the catechol moiety of quercetagetin reorients the N-terminal lobe of JNK1, thereby improving compatibility of the ligand with its binding site. The results of a theoretical docking study suggest a binding mode of PI3-K with the hydroxyl groups of the catechol moiety forming hydrogen bonds with the side chains of Asp964 and Asp841 in the p110γ catalytic subunit. These interactions could contribute to the high inhibitory activity of quercetagetin against PI3-K. Our study suggests the potential use of quercetagetin in the prevention or therapy of cancer and other chronic diseases.

Introduction

The c-Jun NH_2-terminal kinases (JNKs) are a group of serine/threonine protein kinases that are members of the mitogen-activated protein kinase family, which also includes the extracellular signal-regulated kinases (ERKs) and p38 kinases. JNK1 and JNK2 have a broad tissue distribution, whereas JNK3 appears primarily to be localized to neuronal tissues and cardiac myocytes.[1] JNKs are potently

activated by various inflammatory signals and stressors, and expression of JNK proteins is frequently altered in human tumors and cancer cells.[2] Although some debate exists regarding the roles of JNKs in cancer, they are up-regulated in several types of cancer, such as liver and prostate cancers.[3–5] JNKs are best known for their role in the activation of the c-Jun/activator protein-1 (AP-1) transcription–factor complex. AP-1 activation is required for neoplastic transformation[6] and for skin tumor formation in mice.[7] Tumor formation is inhibited in c-Jun-knockout mice.[8] A recent study suggested that the interaction of the tumor suppressor $p16^{INK4a}$ with JNK1 can occur at the same site where c-Jun binds, and it interferes with the phosphorylation and activation of c-Jun in response to UV exposure.[9] Additionally, JNKs are crucial mediators of obesity and insulin resistance and potential targets in type II diabetes.[10] Therefore, inhibition of JNKs might provide clinical benefits in chronic disease.

The phosphatidylinositol 3-kinase (PI3-K)/AKT signaling pathway has been identified as a key player in human cancer, including skin cancer,[11] and is considered an attractive target for cancer prevention or treatment. This pathway can also regulate JNKs. Vivanco *et al.* recently showed, using an elegant screening technique, that JNK pathway activation is a major consequence of PTEN loss, suggesting that PI3-K promotes cancer progression by inducing the parallel activation of AKT and JNKs.[12] PTEN deficiency sensitizes cells to JNK inhibition. Moreover, negative feedback regulation of PI3-K was impaired in PTEN-null cells. Thus, dual JNKs and PI3-K inhibition might be a novel and effective therapeutic approach in patients, preventing feedback and cross talk.

Flavonoids have been known for some time for their general chemopreventive effects in human health, which might be explained partially by the identification of the molecular targets and their mechanism of action.[13,14] An earlier, small-scale study examined the effects of 24 flavonoids on AP-1 transactivation and c-Jun phosphorylation in cell-based systems.[15] To identify a novel natural inhibitor of JNK1, we examined the activity of four representative flavonoids (quercetagetin, quercetin, myricetin, and kaempferol) using an *in vitro* kinase screening system. Only quercetagetin strongly suppressed JNK1 activity. Here, we report the crystal structure of JNK1 bound to quercetagetin and the effects of quercetagetin in *in vitro* and *in vivo* models. The results of a docking study suggest that PI3-K is also a molecular target of quercetagetin.

Results

Crystal structure of the ternary JNK1–pepJIP1–quercetagetin complex

To investigate the molecular basis of the inhibition of JNK1 by quercetagetin (Fig. 1a), we determined the crystal structure of the JNK1–pepJIP1–quercetagetin ternary complex, where pepJIP1 is a docking site peptide fragment of the scaffold protein JIP1. JNK1 consists of N- and C-terminal lobes linked through a loop, the "hinge region." Interestingly, the N-terminal lobe of JNK1 underwent substantial structural changes in our structure when compared with the apo form.[16] The whole N-terminal lobe region is rotated toward the C-terminal lobe, causing shifts of approximately 2.5 Å in peripheral segments (Fig. 1b). A similar rearrangement was observed in the structure of the JNK1-α1 isoform in complex with a biaryl tetrazol inhibitor [A-82118; Protein Data Bank (PDB) ID: 3O2M],[17] which does not utilize the ATP-binding site. Quercetagetin is located in the ATP-binding site and forms hydrogen bonds with the protein (Fig. 1c and d). The side chains of Lys55, Asp169, and Glu73 form a network of hydrogen bonds with the 4-hydroxy group of the 3,4-dihydroxyphenyl part (the catechol moiety) of the ligand, while the benzopyran portion forms hydrogen bonds with the protein main chain of Glu109 and Met111 (in the hinge loop). The ligand forms additional hydrophobic interactions with both nonpolar faces of the binding cleft (Ile32, Val40, Ala53, Met108, Val158, and Leu168 from the N- and C-terminal lobes). A water molecule in the hydrogen-bonding network connects the 3,4-dihydroxyphenyl part of quercetagetin with the Asp169 main-chain amide nitrogen and the Glu73 side-chain carboxy group. The movement of the N-terminal lobe narrows the binding site, which allows the Lys55–NH_2 group to form a hydrogen bond with quercetagetin and moves Val158 and Leu168 approximately 2 Å closer to the ligand. Additionally, the Lys30–Ala42 region of the N-terminal lobe folds over and caps the binding site. The glycine-rich loop Gly33–Gly38 is substantially shifted in this region, with the Gly35 C^{α} atom moving 6 Å toward the C-terminal lobe from its position in the apo structure (Fig. 1e). The adaptability of this region is a feature of many kinase structures.[18] All changes in the N-terminal lobe of JNK1 seem to improve the compatibility of the ligand with the binding site and must be taken into account when designing JNK1-specific inhibitors based on the apo structure.

Determination of IC_{50} values for JNK1 with the inhibitors quercetagetin and SP600125 using the IMAP system

Next, we examined the effect of quercetagetin and other flavonoids on JNK1 activity. *In vitro* JNK1 kinase assays revealed that quercetagetin inhibited JNK1 activity more potently than did SP600125 (a pharmacological JNK1 inhibitor). Quercetin, myricetin, and kaempferol had no effect on JNK1 activity *in vitro* (Fig. 2a). We next calculated IC_{50} values for quercetagetin and SP600125 using the immobilized metal ion affinity-based fluorescence

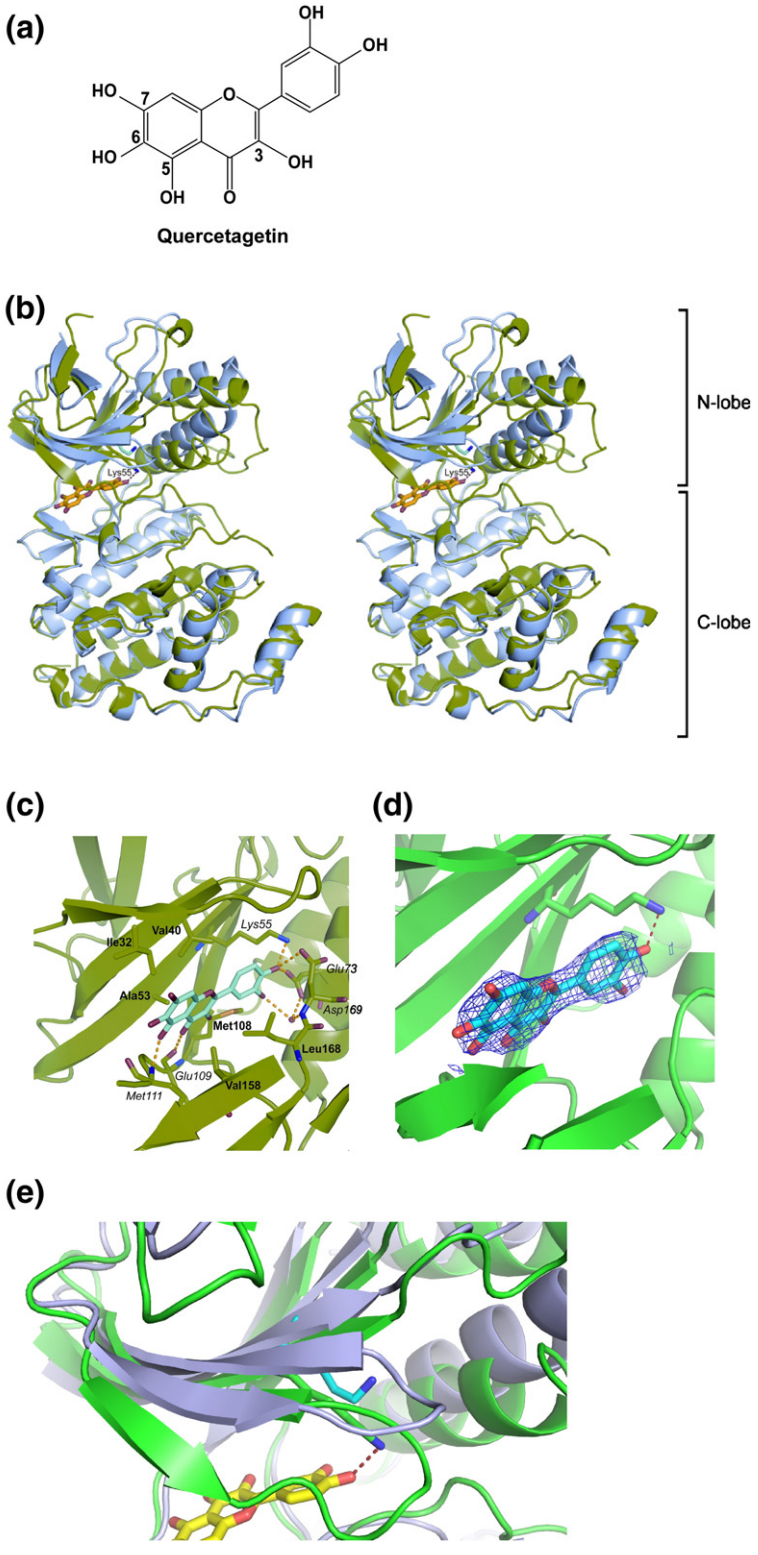

Fig. 1. Crystal structure of the ternary JNK1–pepJIP1–quercetagetin complex. (a) Chemical structure of quercetagetin. (b) Structures of apo-JNK1 alone (blue) and in complex with quercetagetin (green), presented as stereo ribbon plots. In the complex, the N-terminal lobe is shifted substantially toward the C-terminal lobe and Lys55 assumes a different conformation to form a hydrogen bond with the ligand. The glycine-rich loop (Gly33–Gly38) relocates to cover the binding site. (c) Molecular interactions between quercetagetin and JNK1. Residues involved in hydrophobic interactions are highlighted in bold, and those involved in hydrogen bonding are in italics. All hydrogen bonds are marked as yellow broken lines. (d) $2F_o - F_c$ omit map of quercetagetin electron density contoured at 1 σ. The map was created without quercetagetin in the starting model. The density data allowed unambiguous building of the ligand molecule. The hydrogen bond formed with Lys55 is shown. (e) Enlarged view of the Lys30–Ala42 region of the N-terminal lobe. Apo-JNK1 is shown in blue, and the complex with quercetagetin is in green. The region loses its β-strand configuration upon binding and folds over and caps the binding site. The glycine-rich loop Gly33–Gly38 is substantially shifted in this region, with the Gly35 moving by 6 Å toward the C-terminal lobe from its position in the apo structure.

polarization (IMAP) assay system.[19] The IC_{50} values for quercetagetin and SP600125 were 4.6 μM and 5.2 μM, respectively (Fig. 2b). These values are in accord with the *in vitro* JNK1 kinase assay results.

Quercetagetin competes with ATP for binding to JNK1

Pull-down assays showed that active JNK1 binds to quercetagetin-conjugated Sepharose 4B beads

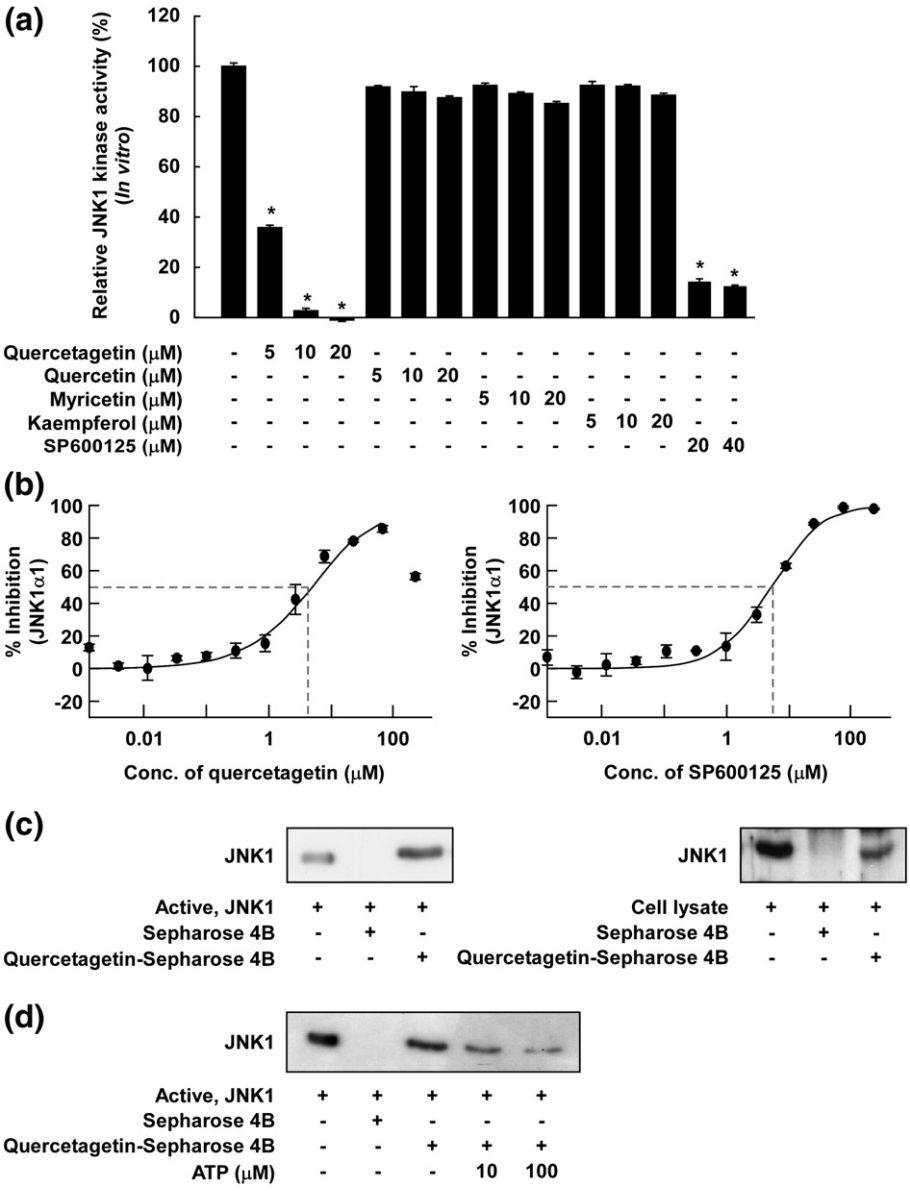

Fig. 2. Effects of quercetagetin on JNK1 activity. (a) Comparison of the effects of various flavonoids and SP600125 on JNK1 activity. JNK1 kinase assays were performed as described in Materials and Methods. Kinase activity is presented as percentage of inhibition relative to the corresponding untreated control. Average ^{32}P count was determined from the results of three independent experiments. Data are presented as means ± SD. Asterisks (*) indicate significant differences in kinase activity between active JNK1 and individual compounds and active JNK1 alone (kinase assays; $p<0.05$). (b) Inhibition of JNK1 by quercetagetin and SP600125 and comparison of the IC_{50} values in an IMAP assay. An IMAP assay was performed as described in Materials and Methods. Each experiment was performed in triplicate. The data point for quercetagetin titration above 100 μM is affected by limited solubility and not included in the calculation and curve fitting. (c) JNK1–quercetagetin binding *in vitro* and *ex vivo* was confirmed by Western blotting using an antibody against JNK1. Lane 1 (input control), JNK1 protein standard or lysate; lane 2 (control), JNK1 or lysate pulled down using Sepharose 4B beads; lane 3, JNK1 or lysate pulled down using quercetagetin-Sepharose 4B affinity beads. (d) Quercetagetin competes with ATP for binding to JNK1. Lane 1, input control; lane 2, negative control, indicating that JNK1 cannot bind to Sepharose 4B; lane 3, positive control, indicating that JNK1 can bind to quercetagetin-Sepharose 4B. Each experiment was performed three times.

(Fig. 2c, left panel, lane 3) but not to unconjugated Sepharose 4B beads (Fig. 2c, left panel, lane 2). The input lane (Fig. 2c, left panel, lane 1), to which 50 ng of active JNK1 was loaded (as a marker), verified that the detected band represented JNK1. Cell-based pull-down assays further revealed that

quercetagetin strongly binds to UVB-induced JNK1 in JB6 P+ cells (Fig. 2c, right panel). Furthermore, the ability of quercetagetin to bind to JNK1 varied according to ATP levels (Fig. 2d), suggesting that, as expected from its location in the ATP-binding site in the crystal structure, quercetagetin competes with ATP.

Evaluation of the binding affinity of quercetagetin for JNK1 by docking analysis

The results of the docking procedure (Supplemental Table 1) are represented as Glide docking scores.[20,21] The Glide docking score is a semi-quantitative measure of binding energy. The lower the value, the higher the binding affinity. The goal of the docking procedure is to explain the preference of JNK1 for quercetagetin over the other flavonoids and SP600125. The results indicate that quercetagetin had the lowest docking score, and thus the highest binding affinity, under both sets of docking conditions (Supplemental Table 1). This can be explained by consideration of the entropic terms in the docking score. Although the interaction energy for the binding of SP600125 to JNK1 was lower than that for the tested flavonoids, SP600125 has a lower loss of entropy upon binding. The Glide scoring function applied higher entropic penalties to the flavonoids. Consequently, their predicted binding affinities were reduced. Considering this penalization, quercetagetin was predicted to have the highest binding affinity, followed by SP600125, in agreement with the results of the kinase assays. But it is clear that the differences in the flavonoid series are small, perhaps not surprising in view of their related chemistry. Detailed ranking on the basis of these calculations must obviously be viewed with caution.

Quercetagetin inhibits PI3-K activity through direct ATP-competitive binding

A previous study suggested that quercetin binds to PI3-K.[22] Because the chemical structure of quercetin is very similar to that of quercetagetin, we tested the interaction of quercetagetin with PI3-K in a modeling study using the crystal structure of PI3-K in complex with quercetin[22] and found that quercetagetin docked well to the ATP-binding site of PI3-K (Fig. 3a). The hydroxyl groups at the 3-, 5-, and 6-positions and the carbonyl group at the 4-position can form hydrogen bonds with the backbone atoms of the hinge region (amino acids 880–885). The hydroxyl groups at the 3′- and 4′-positions can form hydrogen bonds with the side chains of Asp964 and Asp841, respectively. Additionally, quercetagetin would be sandwiched by the side chains of the hydrophobic residues in the ATP-binding site, including Met804, Trp812, Ile831, Leu838, Tyr867, and Ile879 from the N-terminal lobe and Ala885, Met953, Phe961, and Ile963 from the C-terminal lobe. To confirm that the interaction between PI3-K and quercetagetin leads to the suppression of PI3-K activity, we tested PI3-K activity *in vitro*. At a concentration of 20 μM, quercetagetin almost completely blocked PI3-K activity, the inhibitory effect being greater than that observed with the specific PI3-K inhibitor LY294002 (Fig. 3b). We performed a binding assay and verified that quercetagetin directly interacts with PI3-K and competes with ATP (Fig. 3c and d). These findings suggest that PI3-K, like JNK1, is an important target of quercetagetin.

Quercetagetin suppresses UVB-induced AP-1 and NF-κB transactivation and Ras^{G12V}- and H-ras-induced cell transformation in JB6 P+ cells by targeting JNK1 and PI3-K

Consistent with the JNK1 and PI3-K kinase assay data, quercetagetin strongly suppressed UVB-induced phosphorylation of c-Jun, AKT, and GSK3β, but not JNKs, ERKs, p90RSK, p38, or MSK1 (Fig. 4a and b). Quercetagetin inhibited UVB-induced transactivation of AP-1 and NF-κB in a dose-dependent manner (Fig. 4c). Previous studies showed that H-Ras acts as a potent activator of the JNKs and PI3-K signaling pathways that lead to neoplastic transformation. To examine the effects of quercetagetin on cell transformation, we introduced Ras (Ras^{G12V}) expression vectors into NIH3T3 cells and conducted a focus-forming assay. As expected, quercetagetin inhibited H-Ras-induced cell transformation and Ras^{G12V}-induced focus formation in a dose-dependent manner (Fig. 4d and e). At a concentration of 5 μM, quercetagetin inhibited H-Ras-induced neoplastic cell transformation by 73%. These findings suggest that quercetagetin suppresses cell transformation by targeting JNK1 and PI3-K.

Quercetagetin inhibits UVB-induced skin tumorigenesis in an SKH-1 hairless mouse model

To investigate the pharmaceutical effect of quercetagetin, we used a two-stage mouse skin tumorigenesis model. We found that quercetagetin significantly inhibited UVB-induced skin cancer development (Fig. 5a). Topical application of 4 or 20 nmol of quercetagetin to mouse skin reduced tumor incidence by 32.0% and 46.7%, respectively ($p<0.001$ *versus* the UVB irradiation group, $n=10$; Fig. 5b). The volumes of the skin tumors that developed in UVB-exposed mice were significantly reduced by quercetagetin treatment (Fig. 5c). Overall, these results indicate that quercetagetin might serve as an effective chemopreventive agent against UVB-mediated skin cancer.

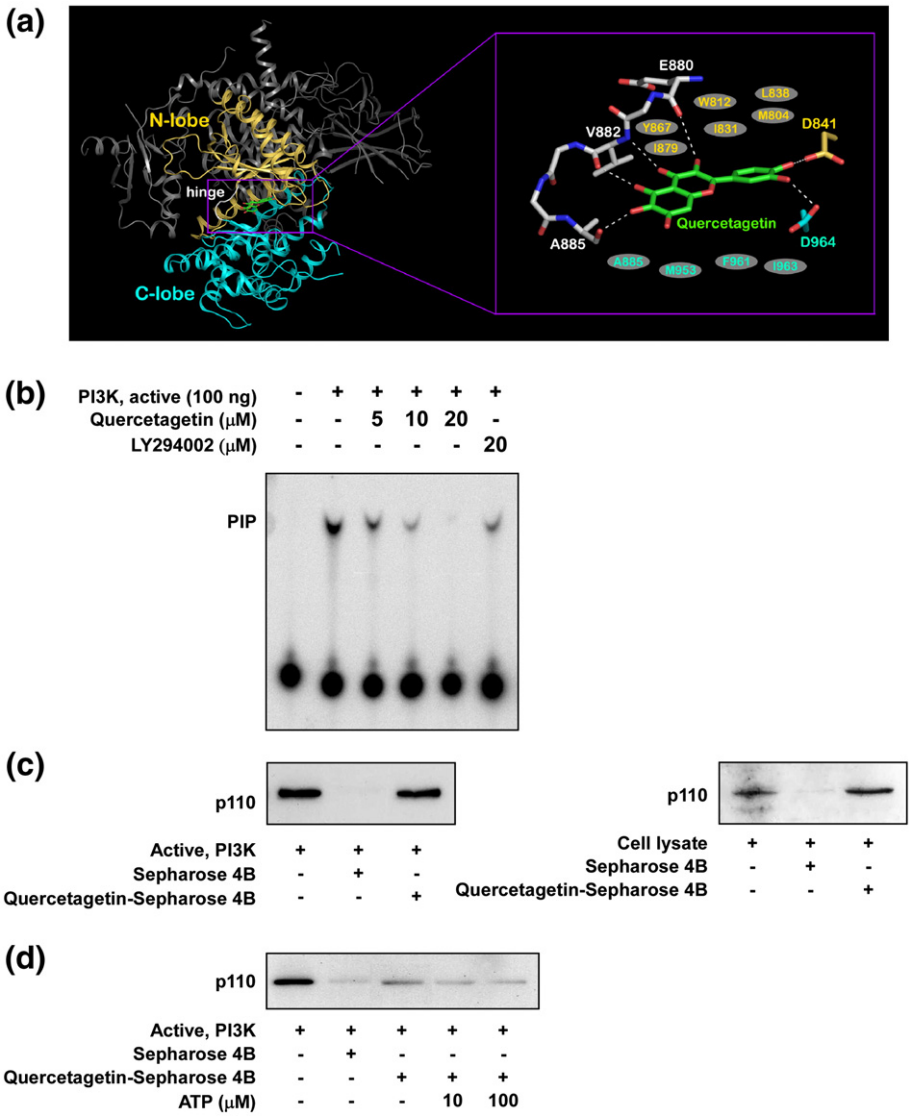

Fig. 3. Effects of quercetagetin on PI3-K activity. (a) Hypothetical model of PI3-K in complex with quercetagetin. The N-terminal lobe, C-terminal lobe, and hinge region of the catalytic domain are shown in yellow, cyan, and white, respectively. Quercetagetin (atomic color) binds to the ATP-binding site in the catalytic domain of PI3-K. In the close-up view, the hydrogen bonds are depicted as broken lines, and the residues in gray ellipses are hydrophobic residues interacting with quercetagetin. (b) Quercetagetin inhibits PI3-K activity *in vitro*. The resulting ^{32}P-labeled phosphatidylinositol-3-phosphate was measured as described in Materials and Methods. (c) Quercetagetin specifically binds to the p110 subunit of PI3-K *in vitro* and *ex vivo*, as confirmed by Western blotting with an antibody directed against the p110 subunit. Lane 1, PI3-K protein standard or whole-cell lysate (input control); lane 2, PI3-K or lysate precipitated with Sepharose 4B beads (control); lane 3, PI3-K or whole-cell lysate pulled down using quercetagetin-Sepharose 4B affinity beads. (d) Quercetagetin binds to PI3-K in an ATP-competitive manner. Lane 1, input control; lane 2, negative control showing lack of binding of PI3-K to Sepharose 4B beads; lane 3, binding of PI3-K to quercetagetin-Sepharose 4B (positive control); lanes 4 and 5, increasing concentrations of ATP alter the binding of quercetagetin to PI3-K. Each experiment was performed three times.

Discussion

The development of clinically useful small-molecule kinase inhibitors has been a seminal event in the world of chronic disease. Although many natural compounds have been shown to regulate the activity of kinases in cell-based assays, fewer data exist to show that these molecules can directly bind to and inhibit specific target proteins *in vitro*. In the present study, we have shown, by X-ray crystallography, that JNK1 crystallizes as the apo form in the more open configuration.[16] We observed the same crystal form without bound ligand, even when ligand was present in the

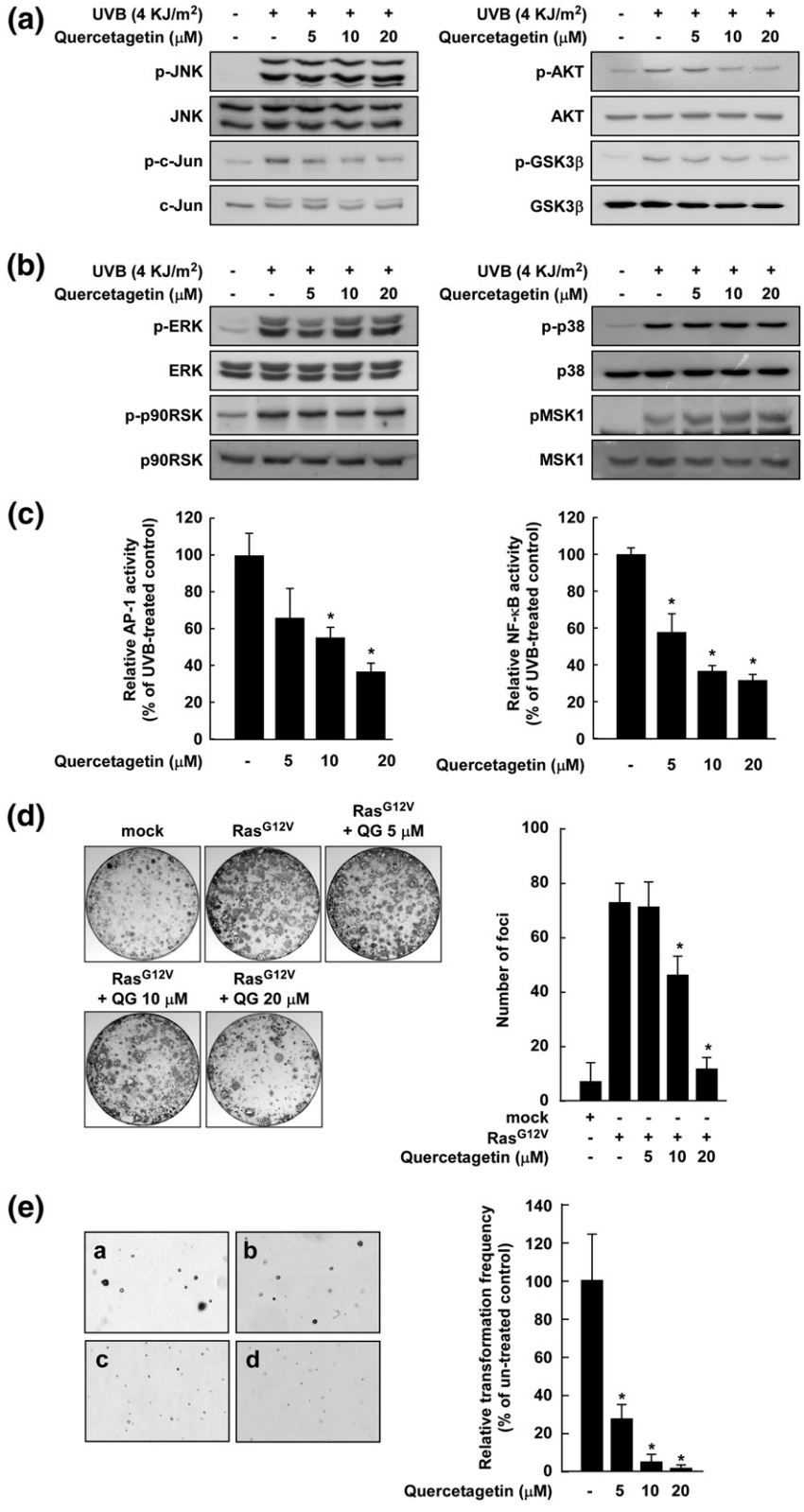

Fig. 4. Effects of quercetagetin on UVB-induced JNKs and PI3-K signaling. (a and b) Quercetagetin inhibits UVB-induced phosphorylation of c-Jun, AKT, and GSK3β, but not JNKs, ERKs, p90RSK, p38, or MSK1. The data are representative of three independent experiments that gave similar results. (c) Quercetagetin inhibits UVB-induced AP-1 and NF-κB transactivation. Luciferase activity was assayed and AP-1 and NF-κB activities were calculated relative to the values for control cells (without UVB). Data are presented as means ± SD of AP-1 and NF-κB luciferase activities obtained from three independent experiments. (d) Quercetagetin inhibits Ras^{G12V}-induced focus formation. The data are representative of three independent experiments that gave similar results. The graph shows the average number of foci. (e) Effects of quercetagetin on H-Ras-induced cell transformation in untreated control cells (a), and cells treated with quercetagetin at a concentration of 5 μM (b), 10 μM (c), or 20 μM (d). Data are presented as means ± SD of three independent experiments. The asterisk (*) indicates a significant difference ($p<0.05$) between groups untreated or treated with quercetagetin. For (d) and (e), cell colonies were counted under a microscope with the aid of Image-Pro Plus software (v. 4).

crystallization medium. The closed conformation, however, only crystallizes in the presence of ligand, which has a well-defined electron density. Figure 1b is an overlay of the two experimental structures, the apo form[16] and the complex described, and documents the pronounced relative

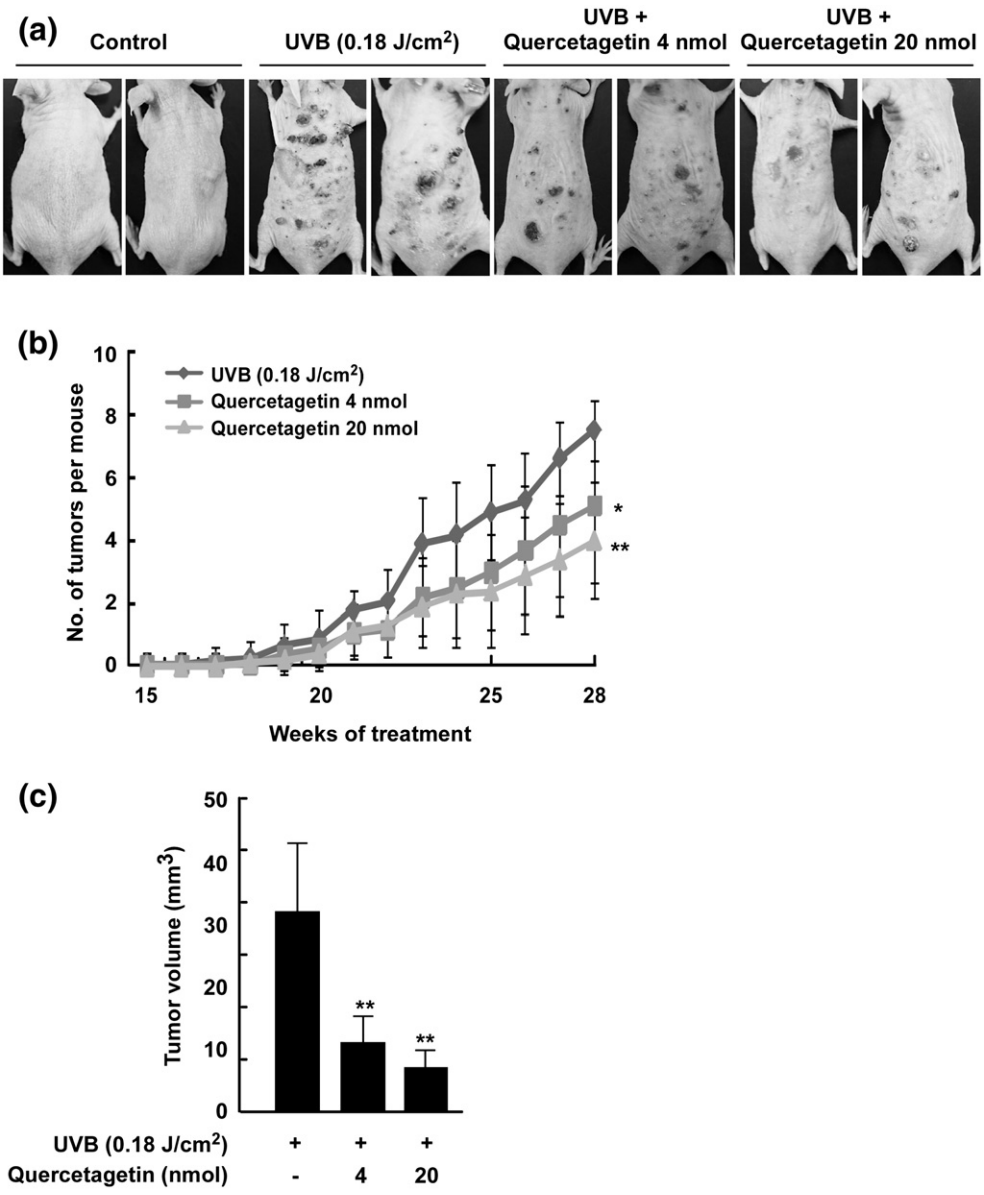

Fig. 5. Effect of quercetagetin on UVB-induced skin carcinogenesis in SKH-1 hairless mice. (a) External appearance of UVB-induced tumors. (b) Quercetagetin strongly reduces the incidence of UVB-induced tumors in SKH-1 hairless mice. A tumor was defined as an outgrowth of >1 mm in diameter that persisted for 2 weeks or longer. Tumor incidence and multiplicity were recorded each week until the end of the experiment. (c) Quercetagetin strongly reduces UVB-induced tumor volume in mice. At the end of the study, the dimensions of each tumor in each mouse were recorded. Tumor volume was calculated using the hemiellipsoid model formula: tumor volume = 1/2 (4π/3) (*l*/2) (*w*/2) *h*, where *l* is the length, *w* is the width, and *h* is the height. The data were analyzed using SAS software (SAS Institute, Cary, NC).

movement of the N- and C-terminal domains upon ligand binding. Hinge bending in kinases is indeed well known and has been seen already in the first cAMP-dependent protein kinase structures.[18] The mechanism by which ligand binding induces hinge bending, however, is unclear. A distinction between the two limiting cases, induced fit or conformational selection, requires kinetic data for different ligand concentrations with a sufficient time resolution to identify the initial reaction step, which would be unimolecular for conformational selection and bimolecular for induced fit. We are not aware of any kinase system where these experiments have been performed.

Quercetagetin is a direct ligand for the ATP-binding pocket of JNK1 (Fig. 1). Interestingly, the interaction between the Lys55–NH_2 group and quercetagetin allows movement and changes in

the N-terminal lobe of JNK1. This feature improves compatibility of the ligand with the binding site of JNK1 and is a unique binding mode. Quercetagetin reaches much deeper into the ATP-binding pocket with its catechol side group than the JNK1 inhibitor SP600125, making prominent contacts with Lys55 and Glu73 through their hydroxyl groups, which may trigger the aforementioned N-terminal lobe movement. SP600152 binds to the $P2_12_12_1$ crystal form (apo form) of JNK1 without causing substantial structural rearrangements.[16] Quercetagetin binds to JNK1 similar to quercetin–PIM1 kinase (PDB ID: 2O3P[14]). However, the catechol moiety with its meta-hydroxyl pointing inside the binding cleft in our JNK1–quercetagetin complex is rotated by 180° to that observed by Holder *et al*. (PDB ID: 2O64[14]) in the quercetagetin–PIM1 kinase complex. This difference might be caused by different environments of the catechol group. That quercetagetin can "adjust" to bind both PIM1 and JNK1 kinases by rotation of its only rotatable bond is interesting. As a note of caution, the electron density of the quercetagetin ligand is best interpreted as shown (meta-hydroxyl group "in") (Fig. 1d), but we cannot exclude partial occupation by the alternative conformer (meta-hydroxyl group "out"). The interaction mode in JNK1–quercetagetin is also similar to that shown in the structure of quercetin with PI3-K γ (PDB ID: 1E8W[22]). Thus, the 4-hydroxy group of the catechol forms the majority of the hydrogen bonding, whereas in other structures, the hydrogen bonds are formed by the 3-hydroxy group. Another unique feature of our structure is the presence of a water molecule trapped below the ligand. Its presence suggests that increasing ligand selectivity and affinity might be realized by introducing a polar group to replace the water molecule. This was tested by changing the catechol moiety *in silico* to pyrogallol, whereby the additional hydroxyl group occupies approximately the space of the observed water molecule. The calculation of the glide score indicates a decrease (affinity improvement) of 0.7 (Glide score −13.2) compared to quercetagetin. A hydroxymethyl group would be even a closer mimic of the bound water, and the corresponding quercetagetin derivative indeed has a glide score of −14.1, the highest in the series.

Quercetagetin inhibited JNK1 activity more strongly than did quercetin, myricetin, kaempferol, or SP600125. The IC_{50} value of quercetagetin, as determined by IMAP assay, was 4.6 μM in agreement with the *in vitro* JNK1 kinase assay. The binding of JNK1 and quercetagetin in an ATP-competitive manner was confirmed in a pull-down assay (Fig. 2c and d). To further evaluate the binding affinity of quercetagetin, quercetin, myricetin, kaempferol, and SP600125, we created a series of docking simulations (Supplemental Table 1). The docking confirmed the unusually deep placement of the quercetagetin molecule in the pocket, which agreed with the observed structural and kinetic data. In the predicted binding conformation of quercetagetin, however, the catechol ring was flipped by 180° compared with the X-ray crystal structure. Obviously, the complicated nature of the H-bond pattern in this region, which is also influenced by the structural water molecule, is difficult to model. Nevertheless, quercetagetin is predicted to have the highest binding affinity for JNK1, followed by SP600126. Walker *et al.* presented X-ray crystallographic structures of the PI3-K γ–quercetin complex, which binds in the ATP-binding pocket.[22] According to their structure, quercetin binds to PI3-K very differently from the JNK1 and PIM1 kinase complexes. Because the chemical structures of quercetagetin and quercetin have a high degree of similarity, we hypothesized that quercetagetin could also interact with PI3-K. The results of a docking study indicated that quercetagetin is an ATP-competitive inhibitor of PI3-K. Several hydrogen bonds and hydrophobic interactions are involved in the binding of quercetagetin. Notably, the hydroxyl groups at the 3′ and 4′ positions form hydrogen bonds with the side chains of Asp964 and Asp841 (Fig. 3a). As shown experimentally (Fig. 3b–d), quercetagetin strongly inhibits PI3-K activity through ATP-competitive binding, consistent with the above docking results.

In cell-based systems and an animal model, we examined the functional significance of the binding of quercetagetin to JNK1 and PI3-K. In these studies, quercetagetin inhibited UVB-induced phosphorylation of c-Jun and AKT in JB6 P+ cells, but had no effect on the phosphorylation of ERKs or p38. Inhibition of JNKs and PI3-K signaling led to the suppression of neoplastic transformation through inhibition of AP-1 and NF-κB (Fig. 4). Quercetagetin delayed the development of tumors and reduced tumor volumes in an SKH-1 hairless mice model (Fig. 5). These cancer chemopreventive effects of quercetagetin might be explained by its inhibitory effects on JNK1 and PI3-K activities. Overall, our crystallographic findings, the accompanying biochemical data, and the cell-based and animal model data show that quercetagetin is a strong inhibitor of JNK1 and PI3-K and might have practical implications for the prevention or therapy of cancer and other chronic diseases.

Materials and Methods

Protein expression and purification

To express JNK1 for structural analysis, we amplified the C-terminal truncated form of human JNK1α1 (residues

1–364) by a standard PCR-based cloning strategy. The PCR product was inserted into the pET21b expression vector (Novagen) with a 6His-tag at the C-terminus and this plasmid was transformed into BL21(DE3) *Escherichia coli* cells. The transformant cells were grown in LB medium at 37 °C up to an $A_{600\ nm}$ of 0.6. Protein expression was induced by adding 1 mM IPTG, and the cells were grown for 15 h. Cells were then harvested by centrifugation; resuspended in buffer A containing 50 mM Hepes (pH 7.2), 10% glycerol, 100 mM NaCl, 2 mM β-mercaptoethanol, and protease inhibitors (0.1 mM phenylmethylsulfonyl fluoride, 1 μg/mL leupeptin, and 1 μg/mL pepstatin); and frozen quickly by immersion in liquid nitrogen. Then, JNK1 was purified. Briefly, cells were thawed, sonicated, and centrifuged. The supernatant fraction was passed through a 10-mL Ni-NTA Superflow Column. The column was washed with resuspension buffer A and washed again with buffer A plus 10 mM imidazole. The protein was then eluted with buffer A plus 250 mM imidazole. The eluted protein was dialyzed against buffer B (20 mM Hepes, pH 7.0, 10% glycerol, 50 mM NaCl, and 2 mM DTT) and applied to an SP-Sepharose cation-exchange column. The column was washed with seven column volumes of buffer B, and bound protein was then eluted with a 10-column-volume linear gradient of 50–400 mM NaCl. The eluted protein from the SP-Sepharose column was concentrated and passed over a gel-filtration column (Superdex 200) pre-equilibrated with buffer C (25 mM Hepes, pH 7.0, 5% glycerol, 50 mM NaCl, and 10 mM DTT). Peak fractions were concentrated to 10 mg/mL as measured by the Bradford method. Purity was judged to be >98% by Coomassie Blue-stained SDS-PAGE.

Crystallization and data collection

Before the crystallization trial, the purified protein was mixed with a peptide fragment of JIP1 (pepJIP1) with the sequence RPKRPTTLNLF at a molar ratio of 1:5 and incubated on ice for 3 h to allow complex formation. To obtain the JNK1–pepJIP1–quercetagetin ternary complex, we mixed the JNK1–pepJIP1 complex with a 10-fold excess of quercetagetin and concentrated it to approximately 10 mg/mL. Crystallization was achieved at 4 °C by vapor diffusion using the sitting drop method and a protein-to-well solution ratio of 1:1 with well solution containing 2.1 M $(NH_4)_2SO_4$ and 0.1 M 2-[bis(2-hydroxyethyl)amino]-2-(hydroxymethyl)propane-1,3-diol (pH 5.5). Single crystals grew within 1 week to an average size of 0.3 mm×0.1 mm×0.1 mm. Crystals were transferred to cryoprotectant solution containing well solution plus 25% (v/v) ethylene glycol for a few seconds and then flash-frozen in liquid nitrogen. Data sets to 2.60 Å resolution were collected at 100 K on the PXII beamline at the Swiss Light Source synchrotron (Paul Scherrer Institute, Switzerland) and processed using XDS and XSCALE software.[23] Two different crystal forms were measured, one of which belonged to space group $P2_12_12_1$. The unit cell parameters were a=61.24 Å, b=80.31 Å, and c=83.36 Å. The second belonged to space group $I422$, and its cell parameters were $a=b$=172.37 and c=86.04. Both crystal types contained one complex per asymmetric unit. Table 1 summarizes the statistics for data collection and refinement.

Table 1. Data collection and refinement statistics

Data collection	
Space group	$I422$
Cell constants (Å)	$a=b$=172.37 c=86.04
Resolution range (Å)	50–2.7
Wavelength (Å)	1.0
Observed reflections	138,356
Unique reflections	13,950
Whole range	
Completeness (%)	77.0[a]
R_{merge}	3.9
$I/\sigma(I)$	26.33
Last shell	
Resolution range (Å)	2.7–2.8
Completeness (%)	43.6
R_{merge}	15.5
$I/\sigma(I)$	2.98
Refinement	
No. of reflections	13,278
Resolution (Å)	20–2.7
R-factor (%)	22.6
R_{free} (%)	26.5
Average B (A^2)	63.6
r.m.s. bond length (Å)	0.013
r.m.s. angle (°)	1.458
Content of asymmetric unit	
No. of protein–ligand complexes	1
No. of protein residues/atoms	362/2898
No. of solvent molecules	27

[a] The data statistics are reported with signal-to-noise cutoff equal to 2. Using this cutoff, the data are 77% complete. Without cutoff, the data are 99% complete.

Structure determination and refinement

The structures of the JNK1–pepJIP1–quercetagetin ternary complex were solved with the molecular replacement program Phaser[24] using the N- and C-terminal domains of the structure of the binary complex JNK1–pepJIP1 separately[16] (PDB ID: 1UKH). The crystals, which belonged to space group $P2_12_12_1$, were isomorphous to the 1UKH unit cells and did not contain interpretable ligand density. The other space group, $I422$, contained an interpretable ligand density in the ATP-binding site. The model was subsequently improved by rigid-body refinement of the individual domains and restrained refinement using Refmac software[25] and rebuilt using the Coot and X-fit programs.[26] Water molecules were added by ARP/wARP.[27] The refinement statistics are summarized in Table 1.

IMAP assay

An IMAP assay was carried out in accordance with the instructions provided by Molecular Devices. The IMAP reaction was carried out with recombinant JNK1 in 384-well black plates containing serially diluted test compounds. The reaction contained 7.46 μM ATP, 100 nM JNK1, 400 nM fluorescein-isothiocyanate-labeled JNK1 substrate peptide (LVEPLTPSGEAPNQK-5FAM-COOH), 20 mM Mops (pH 6.5), 1 mM DTT, 10 mM $MgCl_2$, and

0.01% Brij35. It was incubated for 1 h at room temperature with the addition of IMAP Binding Buffer (a 1:1200 dilution of IMAP Progressive Binding Reagent in 65% IMAP Progressive Binding Buffer A/45% IMAP Progressive Binding Buffer B). Then, the plate was read using a PHERAstar Plus microplate reader from BMG Labtech. The excitation and emission wavelengths were 485 nm with a bandwidth of 20 nm and 530 nm with a bandwidth of 25 nm, respectively.

Docking simulations

To further evaluate the binding affinity of quercetagetin in comparison with other flavonoids, we performed a series of docking simulations. A set of five inhibitors (the flavonoids quercetagetin, quercetin, myricetin, and kaempferol and the commercially available inhibitor SP600126) was docked in the ATP-binding sites of two JNK1 structures: (1) JNK1 in complex with quercetagetin (reported in this article) and (2) the apoprotein structure (PDB ID 1UKH). A 25-Å simulation box was defined around the binding pocket. The geometric center of the docking box was chosen to coincide with the molecule's center of mass. The docking procedure consisted of three stages: (1) inhibitor–receptor pose generation, (2) pose minimization, and (3) scoring of the final pose. After the first stage, 400 poses were selected for energy minimization (100 steps of Steepest Descent). The XP-scoring function of Glide version 5.6 was used to evaluate the final pose. No constraints were imposed on the system.

Molecular modeling and docking

Insight II (Accelrys, Inc., San Diego, CA) was used for docking studies and structure analysis with the crystal coordinates of PI3-K in complex with quercetin (PDB ID: 1E8W), available from the PDB‡. Docking was subsequently performed using the XP-scoring function of Glide version 5.6 (Schrödinger, LLC, New York, NY, 2010). No constraints were imposed on the system. For each ligand, 400 poses were selected for energy minimization (100 steps Steepest Descent) and scoring.

In vitro JNK1 kinase assays

The *in vitro* kinase assay was conducted in accordance with the instructions provided by Upstate Biotechnology. Briefly, each reaction contained 20 µL of assay dilution buffer [20 mmol/L Mops (pH 7.2), 25 mM β-glycerophosphate, 5 mM ethylene glycol bis(β-aminoethyl ether) *N*, *N*′-tetraacetic acid, 1 mM sodium orthovanadate (Na_3VO_4), and 1 mM DTT] and a magnesium-ATP cocktail buffer. For JNK1, the activating transcription factor 2 substrate peptide was included at a concentration of 3 µM. Active JNK1 protein (20 ng) and 10 µL of diluted [γ-^{32}P] ATP solution were incubated at 30 °C for 10 min with the above assay buffer and substrate peptide, and then 15-µL aliquots were transferred onto p81 paper and washed three times with 0.75% phosphoric acid (5 min per wash) and once with acetone (5 min). The incorporation of radioactivity was determined using a scintillation counter (LS6500, Beckman Coulter). Each experiment was performed in triplicate.

In vitro PI3-K kinase assay

Active PI3-K protein (100 ng) was incubated with quercetagetin for 10 min at 30 °C. The mixture was then incubated with 20 µL of 0.5 mg/mL phosphatidylinositol (Avanti Polar Lipids, Alabaster, AL) for 5 min at room temperature and then incubated in reaction buffer [100 mM *N*-2-hydroxyethylpiperazine-*N*′-2-ethanesulfonic acid (pH 7.6), 50 mM $MgCl_2$, and 250 µM ATP] containing 10 µCi of [γ-^{32}P]ATP for an additional 10 min at 30 °C. The reaction was stopped by adding 15 µL of 4 N HCl and 130 µL of chloroform:methanol (1:1). After vortexing, 30 µL of the lower chloroform phase was spotted onto a 1% potassium-oxalate-coated silica gel plate, which had previously been activated through incubation for 1 h at 110 °C. The resulting ^{32}P-labeled phosphatidylinositol-3-phosphate was separated by thin-layer chromatography, and the radiolabeled spots were visualized by autoradiography.

Statistical analysis

As necessary, data are expressed as means ± SD or SE, and significant differences were determined using one-way ANOVA. A probability value of $p<0.05$ was used as the criterion for statistical significance. All analyses were performed using Statistical Analysis Software (SAS, Inc.).

Accession numbers

The coordinates of the crystal structure of the ternary complex JNK1–pepJIP1–quercetagetin have been deposited in the PDB under accession code 3V3V.

Acknowledgements

This work was supported by The Hormel Foundation and grants from the National Institutes of Health (CA027502, CA120388, R37 CA081064, and ES016548), USA; by the World Class Institute Program (2009-002), World Class University Program (R31-2008-00-10056-0), and Leap Research Program (2010-0029233), the Ministry of Education, Science and Technology, and by the Next-Generation BioGreen 21 Program (Plant Molecular Breeding Center No. PJ008187-02-2011), Rural Development Administration, Republic of Korea; and by a Deutsche Krebshilfe Grant (108354) and the CONACYT-DAAD, Germany (M.A.). We thank Tonya M. Poorman at The Hormel Institute, University of Minnesota, USA, for help in submitting our manuscript.

Supplementary Data

Supplementary data to this article can be found online at http://dx.doi.org/10.1016/j.jmb.2012.10.019

Received 30 May 2012;
Received in revised form 26 October 2012;
Accepted 29 October 2012
Available online 8 November 2012

Keywords:
JNK1;
quercetagetin;
PI3-K

† S.B. and N.J.K. are joint first authors.
‡ http://www.rcsb.org/pdb/

Abbreviations used:
JNK, c-Jun NH_2-terminal kinase; PI3-K, phosphatidylinositol 3-kinase; IMAP, immobilized metal ion affinity-based fluorescence polarization; ERK, extracellular signal-regulated kinase; AP-1, activator protein-1; PDB, Protein Data Bank.

References

1. Martin, J. H., Mohit, A. A. & Miller, C. A. (1996). Developmental expression in the mouse nervous system of the p493F12 SAP kinase. *Brain Res. Mol. Brain Res.* **35**, 47–57.
2. Wagner, E. F. & Nebreda, A. R. (2009). Signal integration by JNK and p38 MAPK pathways in cancer development. *Nat. Rev. Cancer*, **9**, 537–549.
3. Chang, Q., Zhang, Y., Beezhold, K. J., Bhatia, D., Zhao, H., Chen, J. *et al.* (2009). Sustained JNK1 activation is associated with altered histone H3 methylations in human liver cancer. *J. Hepatol.* **50**, 323–333.
4. Ouyang, X., Jessen, W. J., Al-Ahmadie, H., Serio, A. M., Lin, Y., Shih, W. J. *et al.* (2008). Activator protein-1 transcription factors are associated with progression and recurrence of prostate cancer. *Cancer Res.* **68**, 2132–2144.
5. Sakurai, T., Maeda, S., Chang, L. & Karin, M. (2006). Loss of hepatic NF-kappa B activity enhances chemical hepatocarcinogenesis through sustained c-Jun N-terminal kinase 1 activation. *Proc. Natl Acad. Sci. USA*, **103**, 10544–10551.
6. Dong, Z., Birrer, M. J., Watts, R. G., Matrisian, L. M. & Colburn, N. H. (1994). Blocking of tumor promoter-induced AP-1 activity inhibits induced transformation in JB6 mouse epidermal cells. *Proc. Natl Acad. Sci. USA*, **91**, 609–613.
7. Young, M. R., Li, J. J., Rincon, M., Flavell, R. A., Sathyanarayana, B. K., Hunziker, R. & Colburn, N. (1999). Transgenic mice demonstrate AP-1 (activator protein-1) transactivation is required for tumor promotion. *Proc. Natl Acad. Sci. USA*, **96**, 9827–9832.
8. Zenz, R., Scheuch, H., Martin, P., Frank, C., Eferl, R., Kenner, L. *et al.* (2003). c-Jun regulates eyelid closure and skin tumor development through EGFR signaling. *Dev. Cell*, **4**, 879–889.
9. Choi, B. Y., Choi, H. S., Ko, K., Cho, Y. Y., Zhu, F., Kang, B. S. *et al.* (2005). The tumor suppressor p16(INK4a) prevents cell transformation through inhibition of c-Jun phosphorylation and AP-1 activity. *Nat. Struct. Mol. Biol.* **12**, 699–707.
10. Hirosumi, J., Tuncman, G., Chang, L., Gorgun, C. Z., Uysal, K. T., Maeda, K. *et al.* (2002). A central role for JNK in obesity and insulin resistance. *Nature*, **420**, 333–336.
11. Cantley, L. C. (2002). The phosphoinositide 3-kinase pathway. *Science*, **296**, 1655–1657.
12. Vivanco, I., Palaskas, N., Tran, C., Finn, S. P., Getz, G., Kennedy, N. J. *et al.* (2007). Identification of the JNK signaling pathway as a functional target of the tumor suppressor PTEN. *Cancer Cell*, **11**, 555–569.
13. Edwards, M. L., Stemerick, D. M. & Sunkara, P. S. (1990). Chalcones: a new class of antimitotic agents. *J. Med. Chem.* **33**, 1948–1954.
14. Holder, S., Zemskova, M., Zhang, C., Tabrizizad, M., Bremer, R., Neidigh, J. W. & Lilly, M. B. (2007). Characterization of a potent and selective small-molecule inhibitor of the PIM1 kinase. *Mol. Cancer Ther.* **6**, 163–172.
15. Ichimatsu, D., Nomura, M., Nakamura, S., Moritani, S., Yokogawa, K., Kobayashi, S. *et al.* (2007). Structure–activity relationship of flavonoids for inhibition of epidermal growth factor-induced transformation of JB6 Cl 41 cells. *Mol. Carcinog.* **46**, 436–445.
16. Heo, Y. S., Kim, S. K., Seo, C. I., Kim, Y. K., Sung, B. J., Lee, H. S. *et al.* (2004). Structural basis for the selective inhibition of JNK1 by the scaffolding protein JIP1 and SP600125. *EMBO J.* **23**, 2185–2195.
17. Comess, K. M., Sun, C., Abad-Zapatero, C., Goedken, E. R., Gum, R. J., Borhani, D. W. *et al.* (2011). Discovery and characterization of non-ATP site inhibitors of the mitogen activated protein (MAP) kinases. *ACS Chem. Biol.* **6**, 234–244.
18. Bossemeyer, D., Engh, R. A., Kinzel, V., Ponstingl, H. & Huber, R. (1993). Phosphotransferase and substrate binding mechanism of the cAMP-dependent protein kinase catalytic subunit from porcine heart as deduced from the 2.0 Å structure of the complex with Mn^{2+} adenylyl imidodiphosphate and inhibitor peptide PKI(5–24). *EMBO J.* **12**, 849–859.
19. Sportsman, J. R., Gaudet, E. A. & Boge, A. (2004). Immobilized metal ion affinity-based fluorescence polarization (IMAP): advances in kinase screening. *Assay Drug Dev. Technol.* **2**, 205–214.
20. Friesner, R. A., Banks, J. L., Murphy, R. B., Halgren, T. A., Klicic, J. J., Mainz, D. T. *et al.* (2004). Glide: a new approach for rapid, accurate docking and scoring. 1. Method and assessment of docking accuracy. *J. Med. Chem.* **47**, 1739–1749.
21. Friesner, R. A., Murphy, R. B., Repasky, M. P., Frye, L. L., Greenwood, J. R., Halgren, T. A. *et al.* (2006). Extra precision glide: docking and scoring incorporating a model of hydrophobic enclosure for protein–ligand complexes. *J. Med. Chem.* **49**, 6177–6196.
22. Walker, E. H., Pacold, M. E., Perisic, O., Stephens, L., Hawkins, P. T., Wymann, M. P. & Williams, R. L. (2000). Structural determinants of phosphoinositide

3-kinase inhibition by wortmannin, LY294002, quercetin, myricetin, and staurosporine. *Mol. Cell*, **6**, 909–919.
23. Kabsch, W. (1993). Automatic processing of rotation diffraction data from crystals of initially unknown symmetry and cell constants. *J. Appl. Crystallogr.* **26**, 795–800.
24. The CCP4 suite: programs for protein crystallography. (1994). *Acta Crystallogr., Sect. D: Biol. Crystallogr.* **50**, 760–763.
25. Lamzin, V. S. & Wilson, K. S. (1993). Automated refinement of protein models. *Acta Crystallogr., Sect. D: Biol. Crystallogr.* **49**, 129–147.
26. McRee, D. E. (1999). XtalView/Xfit—a versatile program for manipulating atomic coordinates and electron density. *J. Struct. Biol.* **125**, 156–165.
27. Murshudov, G. N., Vagin, A. A. & Dodson, E. J. (1997). Refinement of macromolecular structures by the maximum-likelihood method. *Acta Crystallogr., Sect. D: Biol. Crystallogr.* **53**, 240–255.

Supplementary data_ *J. Mol. Biol.* **425**, 411–423

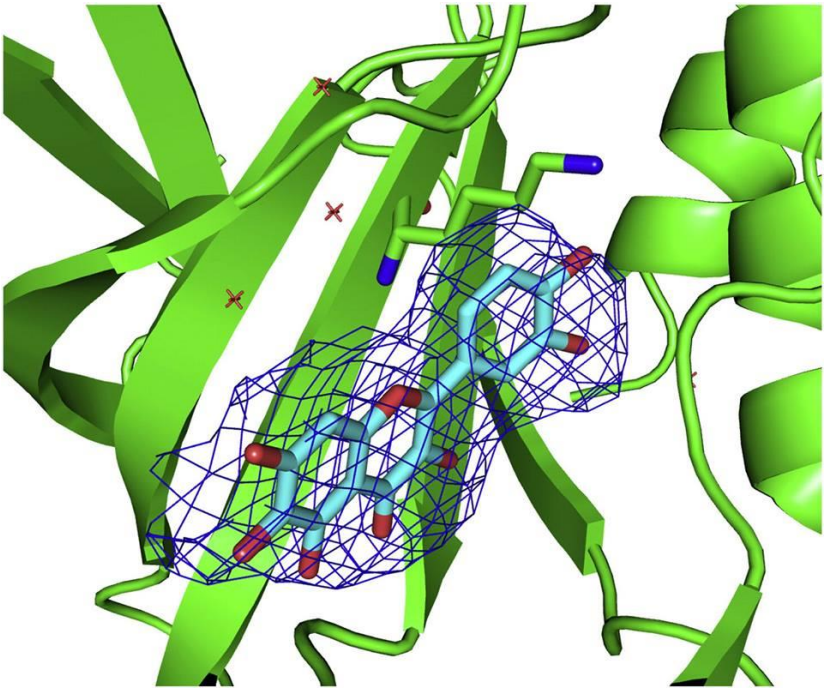

Supplemental Methods

Chemicals

The IMAP assay kit for JNK1, which includes the lyophilized fluorescein-labeled JNK1 substrate (LVEPLTPSGEAPNQK-5FAM-COOH), IMAP kinase reaction buffer, IMAP binding buffer, and IMAP binding reagent, was from Molecular Devices Corp. (Sunnyvale, CA). The black 384-well plate used in the IMAP assay was obtained from Corning, Inc. (Corning, NY). Residues 14-327 of recombinant human JNK1 used in this kit were obtained from Millipore Corp. (Billerica, MA). Quercetagetin and all other chemicals used were analytical-grade products purchased from Sigma (St. Louis, MO). Eagle's minimal essential medium (MEM), Dulbecco's Modified Eagle's Medium (DMEM), basal medium Eagle (BME), gentamicin, and L-glutamine were from Gibco-BRL (Grand Island, NY). Fetal bovine serum (FBS) was from Gemini Bio-Products (Calabasas, CA). JetPEI transfection reagent for NIH3T3 cells was from Q-Biogene. Antibodies against phosphorylated JNKs (Thr183/Tyr185), total JNKs, phosphorylated c-Jun (Ser63), phosphorylated AKT (Ser473), phosphorylated GSK3β (Ser9), phosphorylated ERKs (Thr202/Tyr204), total ERKs, phosphorylated p90RSK (Thr359/Ser363), total p90RSK, phosphorylated p38 (Thr180/Tyr182), total p38, and phosphorylated MSK1 (Thr581) were purchased from Cell Signaling Biotechnology (Beverly, MA). Antibodies against total c-Jun, total MSK1, and PI3-K p110 α were from Santa Cruz Biotechnology (Santa Cruz, CA). Recombinant human active PI3-K (p110α/p85α) and a JNK1 kinase assay kit were obtained from Upstate Biotechnology (Lake Placid, NY). CNBr-Sepharose 4B and glutathione-Sepharose 4B beads and [γ-^{32}P] ATP were from Amersham Pharmacia Biotech (Piscataway, NJ). The protein assay kit was from Bio-Rad Laboratories (Hercules, CA).

Cell culture

JB6 P+ and H-Ras-transformed JB6 P+ mouse epidermal (H-Ras JB6 P+) cells were cultured in monolayers at 37°C in a 5% CO_2 incubator in MEM containing 5% FBS, 2 mM L-glutamine, and 25 μg/mL gentamicin. NIH/3T3 cells were cultured in DMEM supplemented with 10% bovine calf

serum in a 37°C, 5% CO_2 incubator. The cells were maintained by splitting at 80% to 90% confluence, and media were changed every 3 days.

In vitro and ex vivo pull-down assays

Recombinant JNK1 (2 μg) or PI3-K (2 μg), or a JB6 P+ cellular supernatant fraction (500 μg protein), was incubated with quercetagetin/Sepharose 4B beads (100 μL, 50% slurry) or Sepharose 4B beads (as a control) in reaction buffer [50 mM Tris-HCl (pH 7.5), 5 mM EDTA, 150 mM NaCl, 1 mM DTT, 0.01% NP40, 2 μg/mL bovine serum albumin, 0.02 mM phenylmethylsulfonyl fluoride, 1× protease inhibitor mixture]. After incubation with gentle rocking overnight at 4°C, the beads were washed five times with buffer (50 mM Tris-HCl pH 7.5, 5 mM EDTA, 150 mM NaCl, 1 mM DTT, 0.01% NP40, 0.02 mM phenylmethylsulfonyl fluoride), and proteins bound to the beads were analyzed by Western blotting.

ATP competition assay

Recombinant JNK1 (2 μg) or PI3-K (2 μg) was incubated with 100 μL of quercetagetin/Sepharose 4B or 100 μL of Sepharose 4B in reaction buffer (see *in vitro* and *ex vivo* pull-down assays) for 12 h at 4°C, and ATP was added at a concentration of either 10 or 100 μM to a final volume of 500 μL. The samples were incubated for 30 min, and then were washed, and proteins were detected by Western blotting.

Western blot analysis

After the cells (1.5×10^6) were cultured in a 10-cm dish for 48 h, they were starved in serum-free medium for an additional 24 h. The cells were then treated with quercetagetin at concentrations of 0 to 20 μM for the indicated time periods before being exposed to 4 kJ/m^2 UVB and then harvested 30 min later. Cells were disrupted, and the supernatant fractions were boiled for 5 min. The protein concentration was determined using a dye-binding protein assay kit (Bio-Rad Laboratories) as described in the manufacturer's manual. Lysate protein (20 μg) was subjected to 10% SDS-PAGE and

then transferred to a polyvinylidene difluoride membrane. After blocking, the membrane was incubated with the appropriate specific primary antibody at 4°C overnight. Protein bands were visualized using a chemiluminescence detection kit after hybridization with the appropriate horseradish peroxidase-conjugated secondary antibody. The relative amounts of proteins associated with specific antibodies were quantified using Scion Image (NIH, Bethesda, MD).

Luciferase assay

AP-1 or *NF-κB* luciferase reporter-transfected JB6 P+ cells (8×10^3/mL) suspended in 100 μL of 5% FBS/MEM were added to each well of a 96-well plate and incubated at 37°C/5% CO_2. At 80-90% confluence, cells were cultured in 0.1% FBS-MEM for 24 h. Cells were treated for 1 h with quercetagetin (0–20 μM), and then exposed to 4 kJ/m^2 UVB and harvested after 24 h. After treatment, cells were disrupted with 100 μL of lysis buffer (0.1 M potassium phosphate buffer pH 7.8, 1% Triton X-100, 1 mM dithiothreitol (DTT), 2 mM EDTA) and luciferase activity was measured using a luminometer (Luminoskan Ascent; Thermo Electron, Helsinki, Finland).

Focus-forming assay

For the focus-forming assay, the pcDNA3.1-v5-JNK1 plasmid was constructed as previously described (1). Transformation of NIH3T3 cells was conducted according to standard protocols. Cells were transiently transfected with various combinations of H-Ras^{G12V} (50 ng) and pcDNA3-mock (compensation for equal amount of DNA) plasmids as indicated in figures, and then cultured in 5% FBS-DMEM for 2 weeks. Foci were fixed with methanol, stained with 0.5% crystal violet, and then counted under a microscope using the Image-Pro PLUS software program (v. 4, Media Cybernetics).

Anchorage-independent cell transformation assay

The effects of quercetagetin on H-Ras-induced JB6 cells were investigated. Basal medium Eagle agar (0.5%, 3.5 mL) containing 10% FBS with or without quercetagetin was layered onto each well of 6-well plates. H-Ras JB6 cells (8×10^3/mL) treated or not treated with quercetagetin were

mixed with 1 mL of 0.33% basal medium Eagle agar containing 10% FBS and layered on top of the 0.5% agar layer. The separate cultures were maintained at 37°C in a 5% CO_2 incubator for 14 days, at which time the cell colonies were counted under a microscope with the aid of the Image-Pro Plus software program.

Mouse skin tumorigenesis analysis

Skin carcinogenesis in mice was induced using a UVB irradiation system. The UVB radiation source (Bio-Link cross-linker; Vilber Lourmat) emitted at wavelengths of 254, 312, and 365 nm, with peak emission at 312 nm. SKH-1 hairless mice were divided into 4 groups of 15 animals each. In control mice, the dorsal skin was topically treated with 200 μL of acetone only. In the UVB mouse group, the dorsal skin was topically treated with 200 μL of acetone 1 h before UVB irradiation. The mice in the third and fourth groups received topical application of quercetagetin (4 or 20 nmol) in 200 μL of acetone 1 h before UVB irradiation. The UVB dose was 0.18 J/cm^2. Mice were irradiated 3 times per week for 28 weeks. The incidence of skin tumors was recorded weekly, and a tumor was defined as an outgrowth of > 1 mm in diameter that persisted for 2 weeks or more. Tumor incidence, multiplicity, and volume were recorded every week until the end of the experiment.

Supplemental Table 1. Glide Score of 4 flavonoids and the JNK inhibitor SP600125 after docking into two different JNK1 structural conformations.

	Receptor	
Ligand	**JNK1-Quercetagetin**	**JNK1-Apo structure**
Quercetagetin	-12.5	-11.0
SP600125	-12.1	-10.8
Myricetin	-12.1	-10.1
Quercetin	-11.8	-9.3
Kaempferol	-10.8	-8.4

Supplemental Table 1. Docking results for 5 inhibitors (the flavonoids quercetagetin, quercetin, myricetin, and kaempferol and the commercially available JNK inhibitor SP600126) docked in the

ATP-binding sites of two JNK1 structures: JNK1 in complex with quercetagetin (reported in this manuscript) and the apo-protein structure (PDB ID 1UKH). The lower the docking score, the higher is the predicted affinity. Quercetagetin is predicted to have the highest binding affinity for both JNK1 structures.

Supplemental References

1. Colburn NH, Wendel EJ, Abruzzo G. Dissociation of mitogenesis and late-stage promotion of tumor cell phenotype by phorbol esters: mitogen-resistant variants are sensitive to promotion. *Proc Natl Acad Sci U S A* 1981;78:6912-6916.

JACS
JOURNAL OF THE AMERICAN CHEMICAL SOCIETY
Communication
pubs.acs.org/JACS

Structure of the Stapled p53 Peptide Bound to Mdm2

Sohee Baek,[†,#] Peter S. Kutchukian,[‡] Gregory L. Verdine,[‡] Robert Huber,[†,§,∥,⊥] Tad A. Holak,[†,∇] Ki Won Lee,[#] and Grzegorz M. Popowicz*[,†]

[†]Max Planck Institute for Biochemistry, Am Klopferspitz 18, 82152 Martinsried, Germany
[‡]Department of Chemistry and Chemical Biology, Harvard University, Cambridge, Massachusetts 02138, United States
[§]Department of Chemistry, Technical University of Munich, Lichtenbergstraße 4, 85748 Garching, Germany
[∥]School of Biosciences, Cardiff University, Cardiff CF10 3US, Wales, U.K.
[⊥]Center for Medical Biotechnology, University of Duisburg-Essen, 45117 Essen, Germany
[#]Department of Agricultural Biotechnology, Seoul National University, Seoul 151-921, Republic of Korea
[∇]Faculty of Chemistry, Jagiellonian University, Ingardena 3, 30-060 Cracow, Poland

Supporting Information

ABSTRACT: Mdm2 is a major negative regulator of the tumor suppressor p53 protein, a protein that plays a crucial role in maintaining genome integrity. Inactivation of p53 is the most prevalent defect in human cancers. Inhibitors of the Mdm2−p53 interaction that restore the functional p53 constitute potential nongenotoxic anticancer agents with a novel mode of action. We present here a 2.0 Å resolution structure of the Mdm2 protein with a bound stapled p53 peptide. Such peptides, which are conformationally and proteolytically stabilized with all-hydrocarbon staples, are an emerging class of biologics that are capable of disrupting protein−protein interactions and thus have broad therapeutic potential. The structure represents the first crystal structure of an *i*, *i* + 7 stapled peptide bound to its target and reveals that rather than acting solely as a passive conformational brace, a staple can intimately interact with the surface of a protein and augment the binding interface.

In tumors where the p53 protein is not mutated (ca. 50% of all cancers), its function is often impaired by increased levels of its negative regulators.[1] One of the principal p53 modulators, the E3 ubiquitin ligase Mdm2, binds directly to the p53 transactivation domain and targets p53 for proteasomal degradation.[2] Reactivation of p53 by inhibiting its binding to Mdm2 is therefore a promising and confirmed approach to cancer therapy.[3] Several small molecules[4,5] and peptidic inhibitors have been developed for this purpose.[6,7] While peptidic inhibitors based on the modified p53 sequence offer very high affinity toward Mdm2, they suffer from low cell permeability and are proteolytically unstable. A successful attempt to overcome these problems has recently been made by designing cyclic peptides that are closed by an all-hydrocarbon "staple".[8−12] The staple stabilizes the helical structure of the peptide,[8,13] a feature which likely contributes to the enhanced affinity of the peptide for Mdm2 relative to the wild-type peptide.[10] Importantly, the most effective stapled-peptide Mdm2 inhibitor, SAH-p53-8, also targets MdmX and demonstrates cytotoxicity toward cancer cells overexpressing Mdm2, MdmX, or both.[14] Here we report the X-ray structure of SAH-p53-8 in complex with the human Mdm2 protein.

The bound SAH-p53-8 forms a compact, short, two-turn α-helix (Figure 1). The peptide is cyclized by an all-hydrocarbon staple introduced before Asn20 (residue numbering as in the native p53 sequence is used) and after Leu26 (Figure 2A). Circular dichroism studies demonstrated that the staple stabilizes the helical state of the unbound peptide.[10] Crystallographic studies of high-affinity p53 analogue peptides revealed extended helicity in the bound state relative to the wild-type peptide.[15] Furthermore, molecular dynamics (MD) simulations of the stapled p53 peptides anticipated elongation of the helical fold relative to the wild-type peptide.[16] Our present structure confirms this prediction and reveals that SAH-p53-8 is the only peptide with a known crystallographic structure that extends its helicity from residue 19 to 27 in the bound state (Figure 2A). None of the other peptides, including those with higher reported affinities toward Mdm2, forms the helix beyond position 24. In the native p53 peptide, Leu26 has Φ/Ψ angles in the β-strand region (−94°/148°, respectively).[17] Stapling of the peptide imposes perfectly helical angles (−58°/−45°) on Leu26 in the structure of SAH-p53-8. The structures of other peptides fall somewhere between these two extremes (Figure 2).[15,18,19] The residues outside the stapled part of the sequence are not visible in the electron density map, indicating that they are conformationally flexible in the bound state. This feature is shared by non-cross-linked peptides, where residues outside Phe19−Leu26 range are either flexible or acquire conformations determined by crystal packing. Mdm2 retains its native fold observed in other structures and undergoes only minor ligand-induced changes upon binding SAH-p53-8. Namely, the Met62 side chain folds away from the p53 binding pocket to make room for the aliphatic staple, Val93 shifts toward the inside of the binding pocket by 1.0 Å, and the Tyr100 side chain is in the so-called "closed" conformation.[20] These features are observed in most of the Mdm2 structures.[15,18,19]

The stapled peptide helix is located over the p53 binding pocket and positions in the "correct" orientation the three p53

Received: October 4, 2011
Published: December 8, 2011

dx.doi.org/10.1021/ja2090367 | J. Am. Chem.Soc. 2012, 134, 103−106

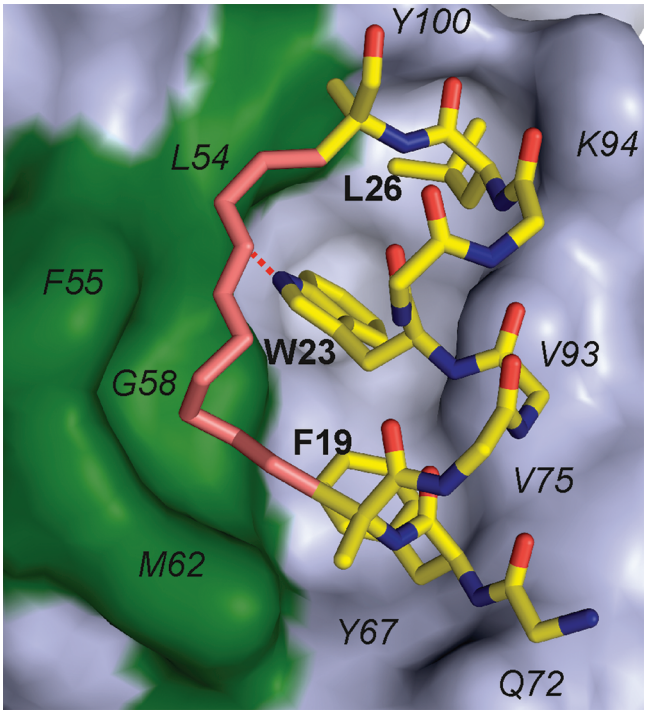

Figure 1. Structure of the complex between Mdm2 and the stapled peptide SAH-p53-8. The Mdm2 molecule is shown in the surface representation. Residues of Mdm2 forming the rim of the binding pocket are labeled in italics. SAH-p53-8 uses its Phe19, Trp23, and Leu26 to fill the binding site in a manner similar to the native p53 peptide. The Trp23 indole ring is bound to Leu54 by a hydrogen bond (red dashed line). The aliphatic staple (salmon) protects this hydrogen bond and forms extended hydrophobic contacts with Leu54, Phe55, Gly58, and Met62 of Mdm2 (green surface).

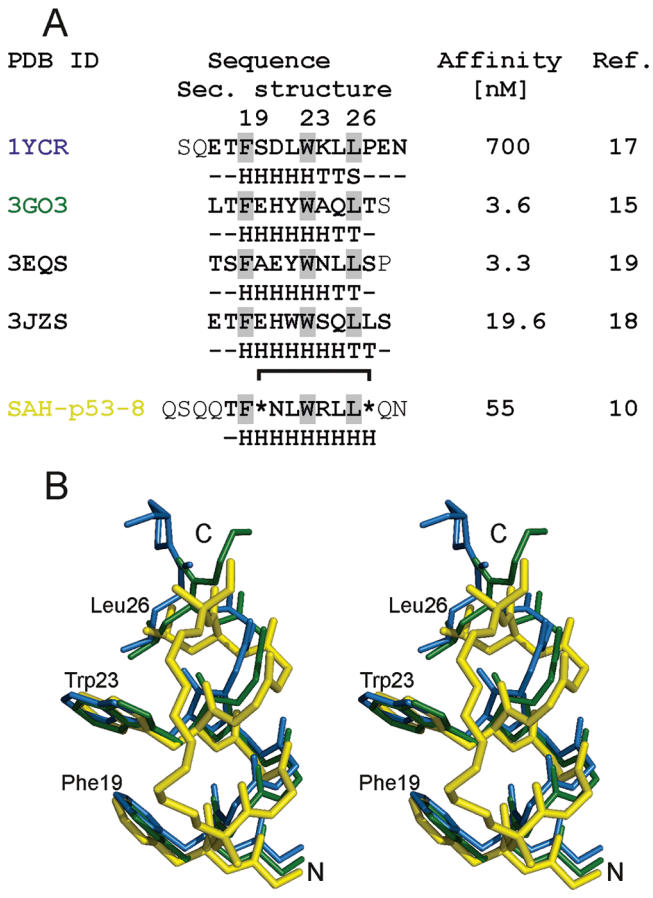

Figure 2. Architecture of different p53 peptide analogues. (A) Sequence alignment of the native p53 peptide (PDB entry 1YCR), high-affinity peptides using natural amino acids (PDB entries 3JZS and 3EQS), and the stapled peptide SAH-p53-8. The p53 residues Phe19, Trp23, and Leu26 (highlighted in gray) are critical for binding to Mdm2. The structured residues are presented in bold. A high helical content correlates with increased affinity toward Mdm2. Only the stapled peptide maintains the helical pattern up to Leu26 and beyond. (B) Comparison of the structures of the native p53 peptide (blue), a high-affinity peptide (PDB entry 3G02, green), and the stapled peptide (yellow). The aliphatic staple encompasses two helical turns, effectively "compressing" and strengthening the helix. Leu26 has to assume a different conformation to fill its pocket correctly. The other peptides gradually lose their helical pattern after Trp23. The staple stabilizes the peptide structure, thereby reducing the entropic cost of binding and thus improving the affinity.

residues that are critical for the binding (Phe19, Trp23, and Leu26). In comparison with the native p53 structure,[17] the whole helix is moved by ca. 1 Å along its long axis toward its N-terminus of p53 (Figure 2B). It is also rotated by 18° counterclockwise around the long axis when looking from the N-terminus toward the C-terminus. This is a unique feature of the stapled peptide, as most of the high-affinity p53 analogue peptides retain an orientation virtually identical to that of the native peptide. Phe19 is located in its Mdm2 pocket in a similar position as the p53 phenylalanine. The plane of its aromatic ring is shifted by 0.6 Å, following the shift of the helix. The Trp23 indole ring plane is identical to the native one but is again rotated to follow the different helix orientation. The hydrogen bond between the indole nitrogen of Trp 23 and the carbonyl oxygen of Leu54 in Mdm2 is preserved in this structure and is 2.82 Å in length. Interestingly, Leu26 fills its pocket in a way that is completely different from the native one. The native p53 lacks helical structure at this residue, while the stapled peptide maintains it (Figure 2A). The position of the Leu26 Cα in SAH-p53-8 is therefore moved by 2.7 Å toward the N-terminus of the peptide. Therefore, the side chain of Leu26 is flipped by nearly 180° to fill the same pocket space. No other known structure shares this feature.

The aliphatic staple intimately interacts with the protein, as predicted by MD simulations.[16] It is located directly over the Met50–Lys64 helix that forms the rim of the p53 binding pocket. The staple contributes ca. 10% of the total surface contact area between the peptide and Mdm2. It protects the hydrogen bond between Trp23 and Leu54 from solvent competition, likely improving its binding contribution. A unique feature of the structure is an extended hydrophobic interface of the staple linker with Leu54, Phe55, Gly58, and Met62 of Mdm2 (Figure 1). Furthermore, in most known Mdm2 structures, a water molecule is hydrogen-bonded to the Gln59 N and Phe55 O atoms, competing with their direct, α-helix-forming bond. The staple displaces this water molecule, which likely entropically stabilizes the complex,[21] and also shields the direct Gln59 N–Phe55 O bond. Taken together, these results indicate that the staple-Mdm2 interaction undoubtedly contributes to the tight binding of the SAH-p53-8 peptide.

In addition to SAH-p53-8, several stapled peptides were experimentally investigated (Table 1),[10] and molecular modeling studies suggested that the placement of the staple was one of the dominating factors in the structure–affinity

dx.doi.org/10.1021/ja2090367 | J. Am. Chem.Soc. 2012, 134, 103–106

Table 1. Staple Attachment, Helicity, and Mdm2 Affinity of SAH Peptides[10]

peptide	sequence[a]	α helicity	K_d (nM)
WT p53	LSQETFSDLWKLLPEN	11%	410
SAH-p53-1	LSQETFSD*WKLLPE*	25%	100
SAH-p53-2	LSQE*FSDLWK*LPEN	10%	400
SAH-p53-3	LSQ*TFSDLWKLL*EN	12%	1200
SAH-p53-4	LSQETF*DLWKLL*EN	59%	0.92
SAH-p53-5	LSQETF*NLWKLL*QN	20%	0.8
SAH-p53-6	LSQQTF*NLWRLL*QN	14%	56
SAH-p53-7	QSQQTF*NLWKLL*QN	36%	50
SAH-p53-8	QSQQTF*NLWRLL*QN	85%	55

[a]Staple attachment positions are indicated by *.

relationships (SARs) displayed by these peptides.[16] Indeed, modeled peptides with staples that "drape" over the protein (e.g., SAH-p53-4−8) experimentally bind Mdm2 with high affinity, while modeled peptides with staples that point out into the solvent (e.g., SAH-p53-1−3) experimentally bind with low affinity. Our structure affirms this interaction for SAH-p53-8 and suggests that if staples are incorporated into future peptide designs, such as reverse[22] or retro-inverso peptides[23,24] aimed at targeting Mdm2, such peptides might profit from placing the staple in such a way that it preserves this beneficial interaction.

One goal of stapling the p53 peptide was to increase its helical content in the unbound state, thereby enhancing its affinity for Mdm2.[10] Our study reveals two accompanying outcomes of stapling. First, the staple makes hydrophobic contacts with the rim of the Mdm2 binding site, likely enhancing the binding affinity. This may also contribute to the 18° rotation observed for the stapled peptide relative to the wild-type peptide. This type of intimate staple-protein hydrophobic−hydrophobic interaction was also observed in the crystal structure of the stapled MCL-1 BH3 helix (MCL-1 $SAHB_D$) in complex with MCL-1.[25] In addition, hydrophobic interactions between the staple of the stapled NR box peptides (SP1 and SP2) and the estrogen receptor have been observed, and in the case of SP1, these interactions resulted in a ca. 90° rotation of the helix and a shift in register of 1 position of residues relative to the wild-type peptide.[26] Second, the staple constrains the peptide to a more helical state in the bound conformation in comparison with non-cross-linked peptides, resulting in a conformational change in Leu26, a residue that plays a critical role in binding Mdm2. This suggests that future stapled p53 peptide designs might benefit from incorporating a less restrictive staple. A longer *i*, *i* + 7 staple, perhaps 1−2 methylene units longer, might still enhance the peptide's affinity for Mdm2 through preorganization of the folded state while allowing Leu26 to bind in its native rotameric state. Indeed, previous experimental studies suggest that longer *i*, *i* + 7 staples increase the helical content relative to the wild-type peptide.[8] Our study supports the notion that in addition to enhancing a peptide's affinity for a protein by preorganizing the unbound state as an α-helix, a staple can confer enhanced affinity for a target through hydrophobic contacts with a protein and can perturb the structure of the bound peptide relative to the wild-type structure.

■ ASSOCIATED CONTENT

Supporting Information

Protein production, peptide synthesis, and crystallographic analysis. This material is available free of charge via the Internet at http://pubs.acs.org. The structure has been deposited in the Protein Data Bank as PDB entry 3V3B.

■ AUTHOR INFORMATION

Corresponding Author

popowicz@biochem.mpg.de

■ ACKNOWLEDGMENTS

This work was supported by the Deutsche Krebshilfe (Grant 108354) and by the High-Tech Industry Multidisciplinary Research Fund from Dana-Farber Cancer Institute.

■ REFERENCES

(1) Vousden, K. H.; Lane, D. P. *Nat. Rev. Mol. Cell Biol.* **2007**, *8*, 275−283.
(2) Wade, M.; Wang, Y. V.; Wahl, G. M. *Trends Cell Biol.* **2010**, *20*, 299−309.
(3) Brown, C. J.; Lain, S.; Verma, C. S.; Fersht, A. R.; Lane, D. P. *Nat. Rev. Cancer* **2009**, *9*, 862−873.
(4) Vassilev, L. T. *Trends Mol. Med.* **2007**, *13*, 23−31.
(5) Shangary, S.; Wang, S. *Annu. Rev. Pharmacol. Toxicol.* **2009**, *49*, 223−241.
(6) Brown, C. J.; Cheok, C. F.; Verma, C. S.; Lane, D. P. *Trends Pharmacol. Sci.* **2011**, *32*, 53−62.
(7) Popowicz, G. M.; Dömling, A.; Holak, T. A. *Angew. Chem., Int. Ed.* **2011**, *50*, 2680−2688.
(8) Schafmeister, C. E.; Po, J.; Verdine, G. L. *J. Am. Chem. Soc.* **2000**, *122*, 5891−5892.
(9) Walensky, L. D.; Kung, A. L.; Escher, I.; Malia, T. J.; Barbuto, S.; Wright, R. D.; Wagner, G.; Verdine, G. L.; Korsmeyer, S. J. *Science* **2004**, *305*, 1466−1470.
(10) Bernal, F.; Tyler, A. F.; Korsmeyer, S. J.; Walensky, L. D.; Verdine, G. L. *J. Am. Chem. Soc.* **2007**, *129*, 2456−2457.
(11) Verdine, G. L.; Walensky, L. D. *Clin. Cancer Res.* **2007**, *13*, 7264−7270.
(12) Verdine, G. L.; Hilinski, G. J. *Methods Enzymol.* **2012**, in press.
(13) Kutchukian, P. S.; Yang, J. S.; Verdine, G. L.; Shakhnovich, E. I. *J. Am. Chem. Soc.* **2009**, *131*, 4622−4627.
(14) Bernal, F.; Wade, M.; Godes, M.; Davis, T. N.; Whitehead, D. G.; Kung, A. L.; Wahl, G. M.; Walensky, L. D. *Cancer Cell* **2010**, *18*, 411−422.
(15) Czarna, A.; Popowicz, G. M.; Pecak, A.; Wolf, S.; Dubin, G.; Holak, T. A. *Cell Cycle* **2009**, *8*, 1176−1184.
(16) Joseph, T. L.; Lane, D.; Verma, C. S. *Cell Cycle* **2010**, *9*, 4560−4568.
(17) Kussie, P. H.; Gorina, S.; Marechal, V.; Elenbaas, B.; Moreau, J.; Levine, A. J.; Pavletich, N. P. *Science* **1996**, *274*, 948−953.
(18) Phan, J.; Li, Z.; Kasprzak, A.; Li, B.; Sebti, S.; Guida, W.; Schönbrunn, E.; Chen, J. *J. Biol. Chem.* **2010**, *285*, 2174−2183.
(19) Pazgier, M.; Liu, M.; Zou, G.; Yuan, W.; Li, C.; Li, C.; Li, J.; Monbo, J.; Zella, D.; Tarasov, S. G.; Lu, W. *Proc. Natl. Acad. Sci. U.S.A.* **2009**, *106*, 4665−4670.
(20) Popowicz, G. M.; Czarna, A.; Rothweiler, U.; Szwagierczak, A.; Krajewski, M.; Weber, L.; Holak, T. A. *Cell Cycle* **2007**, *6*, 2386−2392.
(21) (a) Connelly, P. R.; Aldape, R. A.; Bruzzese, F. J.; Chambers, S. P.; Fitzgibbon, M. J.; Fleming, M. A.; Itoh, S.; Livingston, D. J.; Navia, M. A.; Thomson, J. A.; Wilson, K. P. *Proc. Natl. Acad. Sci. U.S.A.* **1994**, *91*, 1964−1968. (b) Dunitz, J. D. *Science* **1994**, *264*, 670−670.
(22) Placzek, W. J.; Sturlese, M.; Wu, B.; Cellitti, J. F.; Wei, J.; Pellecchia, M. *J. Biol. Chem.* **2011**, *286*, 39829−39835.
(23) Sakurai, K.; Chung, H. S.; Kahne, D. *J. Am. Chem. Soc.* **2004**, *126*, 16288−16289.
(24) Li, C.; Pazgier, M.; Li, J.; Li, C.; Liu, M.; Zou, G.; Li, Z.; Chen, J.; Tarasov, S. G.; Lu, W.-Y.; Lu, W. *J. Biol. Chem.* **2010**, *285*, 19572−19581.
(25) Stewart, M. L.; Fire, E.; Keating, A. E.; Walensky, L. D. *Nat. Chem. Biol.* **2010**, *6*, 595−601.

(26) Phillips, C.; Roberts, L. R.; Schade, M.; Bazin, R.; Bent, A.; Davies, N. L.; Moore, R.; Pannifer, A. D.; Pickford, A. R.; Prior, S. H.; Read, C. M.; Scott, A.; Brown, D. G.; Xu, B.; Irving, S. L. *J. Am. Chem. Soc.* **2011**, *133*, 9696−9699.

Supporting Information

Structure of the stapled p53 peptide bound to Mdm2

Sohee Baek,[†,§] Peter S. Kutchukian,[‡] Gregory L. Verdine,[‡] Robert Huber,[†,‖,**, ††] Tad A. Holak,[†, §§] Ki Won Lee,[§] and Grzegorz M. Popowicz*[,†]

[†] Max Planck Institute for Biochemistry, Am Klopferspitz 18, 82152 Martinsried, Germany

[‡] Department of Chemistry and Chemical Biology, Harvard University, Cambridge MA 02138, United States

[‖] Department of Chemistry, Technical University of Munich, Lichtenbergstraße 4, 85748 Garching, Germany

** School of Biosciences, Cardiff University, Cardiff CF10 3US, Wales, U.K.

[††] Center for Medical Biotechnology, University of Duisburg-Essen, 45117 Essen, Germany

[§] Department of Agricultural Biotechnology, Seoul National University, Seoul 151-921, Republic of Korea

§§ Faculty of Chemistry, Jagiellonian University, Ingardena 3, 30-060 Cracow, Poland

Peptide synthesis

SAH-p53-8 was synthesized as previously described.[1]

Protein expression and purification

The recombinant human Mdm2 (residues 25-111) was cloned into the pET-20 vector (Novagen) without an affinity tag and expressed in *E. coli* BL21-CodonPlus(DE3)-RIL expression cells (Stratagene). Cells were grown at 37 °C and induced at OD_{600nm} of 0.8 with 1 mM IPTG. After 5 h induction at 37 °C the cells were harvested by centrifugation. The harvested cells from 5 liters of *E. coli* cell culture were re-suspended in PBS at pH 7.4 and ruptured by sonication. After centrifugation the inclusion bodies were washed with PBS containing 0.05% Triton X-100 with subsequent low-speed centrifugation (12000G). The procedure was repeated three times. The inclusion bodies were solubilized with 6 M GuHCl in 100 mM Tris-HCl, pH 8.0 including 1 mM EDTA and 10 mM DTT. The protein was dialyzed at 4 °C, against 4 M GuHCl, pH 3.5 including 10 mM DTT. For renaturation, the protein was diluted 1:100 in 10 mM Tris- HCl, pH 7.0, containing 1 mM EDTA and 10 mM DTT by adding the denatured protein drop-wise into the refolding buffer. Refolding was carried out

for 10 h at 4 °C. Ammonium sulfate was added to a final concentration of 1.5M and the protein was applied to the Butyl Sepharose 4 Fast Flow (GE Healthcare) and subsequently eluted with 100 mM Tris-HCl, pH 7.2, including 5 mM DTT. The protein was further purified by gel filtration on HiLoad 16/60 Superdex200 (Pharmacia). The Mdm2 containing fractions are mixed with the 2-fold excess of the peptide and concentrated to about 10 mg/ml before the crystallization trial. The purity and folding of the protein was measured by SDS-PAGE and 1D NMR.

X-ray crystallography

Crystallization of the Mdm2 with the peptide was achieved at room temperature by sitting drop vapor diffusion and the protein to crystallization solution ratio of 1:1, with the crystallization solution containing 100 mM Sodium acetate trihydrate, pH 4.75 and 2.5 M NaCl. The crystals appeared in several days and grew to a final size of 0.1 mm. They were transferred to cryoprotectant solution containing the crystallization solution supplemented with 25% (v/v) glycerol, then directly plunged frozen in liquid nitrogen. Native dataset to 2.0 Å were collected from a single crystal at 100 K on the SLS PXII beam line at Paul Scherrer Institute, Villigen, Switzerland and processed using XDS and XSCALE[2] program. The structure of Mdm2 from PDB entry 1YCR was used as a search model after the p53 peptide was removed. The initial Rfactor of the solution was 0.45. The model was subsequently rebuilt using Xfit[3] and refined using Refmac5 from CCP4 suite[4]. Data collection and refinement statistics are given in table S1. Each asymmetric unit contains two stapled peptide – Mdm2 complexes. Both are virtually identical (RMSD of the main chain atoms 0.7 A) except region between Asp84-Val88 in chain A that is shifted by about 1.2 A due to crystal contacts. The residues outside 18-27 range in the peptide are generally not visible in electron density (one chain shows additionally Gln28-Asn30 stabilized due

to crystal contacts) indicating that this part is flexible and do not take direct part in binding to Mdm2. Several solvent-exposed sidechains had no interpretable electron density and were removed from the model.

Table S1. Data collection and refinement statistics

Data collection	
Space group	$P2_1$
Cell constants (Å)	a = 45.4
	b = 42.41
	c= 50.5
	β = 90.86
Resolution range (Å)	50 – 2.0
Wavelength (Å)	0.999
Observed reflections	48 879
Unique reflections	13 254
Whole range	
Completeness (%)	99.5
R_{merge}	13.6
$I/\sigma(I)$	12.45
Last shell	
Resolution range (Å)	2.0 – 2.1
Completeness (%)	99.8
R_{merge}	60.6
$I/\sigma(I)$	3.14
Refinement	
No. of reflections	11 550
Resolution (Å)	20 – 2.0
R-factor (%)	16.8
R_{free} (%)	21.6
Average B ($Å^2$)	13.42
R.m.s bond lenght (Å)	0.009
R.m.s. angles (°)	1.05
Content of asymmetric unit	
No. of protein complexes	2
No. of protein residues/atoms	197/1660
No. of solvent atoms	146

References

(1) Kim, Y-W.; Grossmann, T. N.; Verdine, G. L, Nat. Protocols. 2011, 6, 761-771.

(2) Kabsch, W. *J. Appl. Cryst.* **1993,** 26, 795-800.

(3) McRee, D.E. *J. Struc. Biol.* **1999,** 125, 156-65.

(4) Collaborative Computational Project, Number 4. *Acta Crystallogr. D. Biol. Crystallogr.* **1994,** 50, 760-3.